Simulation of Sea Level Variations in The Tropical Pacific Using A Linear Multi-mode Model with Application to The Emergence of Central Pacific ENSO

Dissertation
zur Erlangung des Doktorgrades
der Mathematisch-Naturwissenshaftlichen Fakultät
der Christian-Albrechts-Universität zu Kiel

vorgelegt von

Xiaoting Zhu

Kiel, 2018

Erster Gutachter: Prof. Dr. Richard J. Greatbatch
Zweiter Gutachter: Prof. Dr. Joke Lübbecke

Tag der mündlichen Prüfung: 16.05.2018
Zum Druck genehmigt: 16.05.2018

gez. Prof. Dr. Natascha Oppelt, Dekan

Contents

Abstract

The interannual sea level variability in the tropical Pacific is dominated by El Niño-Southern Oscillation (ENSO). In recent two decades, the increasing occurrence of Central Pacific ENSO (CP ENSO) contrasting with the classical Eastern Pacific ENSO (EP ENSO), termed with respect to the locations of maximum Sea Surface Temperature anomalies (SSTa) during the mature phase, post new challenges to the prediction of ENSO. In this thesis, the interannual sea level variations in the tropical Pacific over the time span 1961-2014 are simulated to investigate the dynamics of ENSO, especially of CP ENSO, using a linear multi-mode model, given the good agreement of the ENSO-related sea level variations with the linear wave dynamics.

The linear, multi-mode model for the tropical Pacific is derived by fitting the modelled sea level for multiple vertical modes driven by ERA-Interim monthly wind stress anomalies (named ERA-I exp.) to satellite measurements along the equator in the satellite era (1993-2014) to (i) assess the relative importance of the different vertical modes for ENSO-related variability, and (ii) simulate the sea level throughout the thesis. The results show that the mode 2 is dominant, although with some role for mode 1 in the western basin, mode 5 in eastern basin and mode 3 for both regions. The model readily captures the observed ENSO events as well as the pivot point associated with the so-called "tilt" mode. The pivot point is shifted westward from the center of the basin because most of the wind stress variance is in the western basin. A sensitivity experiment only driven by spatially uniform zonal wind stress suggests that the Sverdrup transport is not fundamental to the recharge/discharge mechanism for EP ENSO, although the spatial structure of the wind forcing does play a role in setting the amplitude of the warm water volume.

Sea level anomalies for the period 1961-2002 reconstructed with the NCEP/NCAR and ERA-40 wind forcing (named NCEP/NCAR exp. and ERA-40 exp.) compare well to tide gauge records. The sensitivity experiments driven by only the zonal component of the two wind stress products suggest that a large increasing trend in sea level found in the NCEP/NCAR exp. rather than in ERA-40 exp. is related to a spurious eastward trend in NCEP/NCAR zonal wind stress in the eastern-central Pacific. The westward shift of pivot point from the period 1961-2002 to the period 1993-2014 is attributed to a persistent upward trend in the zonal

stress variance along the equator west of 160°W throughout the period 1961-2014.

The regression of the modelled sea level onto the principal components (PC) of EOFs of SSTa and the lead/lag correlation between PC1 and PC2 before and after the 1976/77 climate shift support the view that EOF1 and EOF2 can represent EP ENSO and CP ENSO after the climate shift. However, little evidence for the occurrence of Central Pacific (CP) events before the 1976/77 climate shift is found. After the climate shift, the thermocline feedback is found to increase strongly in the CP (Nino4 region) concurrent with the increasing occurrence of CP ENSO. This is associated with the increasing Bjerknes feedback there through the westward shift of pivot point for sea level (and hence thermocline) variations due to the increasing zonal wind variance in the western Pacific. These arguments imply a positive feedback in which CP events are self-maintaining and suggest that they may be part of the natural variability of the climate system and could occur episodically without the need for changes in external forcing.

Zusammenfassung

Im tropischen Pazifik wird die Auslenkung des Meeresspiegels auf interannualen Zeitskalen dominiert durch El Niño-Southern Oscillation (ENSO). In den letzten zwei Dekaden hat die Häufigkeit von Central Pacific ENSO (CP ENSO) Ereignissen im Gegensatz zum klassischen Eastern Pacific ENSO (EP ENSO), benannt nach den Regionen der größten Anomalie der Meeresoberflächentemperatur (SSTa), zugenommen, wodurch neue Herausforderungen an die Vorhersage von ENSO gestellt wurden. Da die Variabilität der Meeresoberflächenauslenkung im Zusammenhang mit ENSO gut durch lineare Wellendynamik beschrieben werden kann, sollen in dieser Arbeit die interannualen Schwankungen der Meeresoberflächenauslenkung über den Zeitraum von 1961 bis 2014 mit Hilfe eines linearen Multi-Moden Modells simuliert werden, um die Dynamik von ENSO, insbesondere von CP ENSO, zu untersuchen.

Für den tropischen Pazifik ist das lineare Multi-Moden Modell erstellt worden, indem die modellierten Meeresspiegelschwankungen verschiedener Vertikalmoden, welche durch monatliche Windschubspannungsanomalien aus ERA-Interim getrieben wurden (ERA-I exp. genannt), an Satellitenmessungen entlang des Äquators im Zeitraum von 1993 bis 2014 gefitted wurden. Das Ziel ist (i) die relative Bedeutung der verschiedenen Vertikalmoden für die Variabilität im Zusammenhang mit ENSO zu bewerten und (ii) die Meeresspiegelschwankungen zu simulieren. Die Ergebnisse zeigen, dass die zweite Vertikalmode dominiert, jedoch mit Beiträgen der ersten Mode im westlichen Becken, der fünften Mode im östlichen Becken und der dritten Mode auf beiden Seiten des Beckens. Das Modell ist in der Lage, sowohl die beobachteten ENSO Ereignisse als auch den Drehpunkt wiederzugeben, welcher mit dem so genannten Tilt Mode zusammenhängt. Der Drehpunkt liegt westlich vom Zentrum des Beckens, da die meiste Varianz in der Windschubspannung im westlichen Becken liegt. Ein Sensitivitätsexperiment, bei welchem der Antrieb durch räumlich homogene zonale Windschubspannung erfolgt, legt nahe, dass der Sverdrup Transport nicht von grundlegender Bedeutung für den Recharge/discharge Mechanismus bei EP ENSO Ereignissen ist, obwohl die räumliche Struktur des Windantriebs Einfluss auf die Amplitude der Warm Water Volume Mode hat.

Anomalien des Meeresspiegels, welche mit Windantrieb von NCEP/NCAR und ERA-40 rekonstruiert wurden (genannt NCP/NCAR exp. und ERA-40 exp.), stimmen im Zeitraum von

1961 bis 2002 gut mit Aufzeichnungen von Pegelstationen überein. Senitivitätsexperimente, welche nur durch die zonale Komponente der zwei Windschubspannungsprodukte angetrieben werden, legen nahe, dass der Anstieg des Meerespiegels, welcher nur im NCEP/NCAR exp. nicht jedoch im ERA-40 exp. gefunden wird, im Zusammenhang mit einem künstlichen Anstieg der ostwärtigen zonalen Windschubspannung in NCEP/NCAR im zentralen Pazifik steht. Die westwärtige Verschiebung des Drehpunktes vom Zeitraum 1961-2002 und 1993-2014 kann einem anhaltenden Anstieg der zonalen Windschubspannungsvarianz entlang des Äquators westlich von 160°W über den Zeitraum von 1961-2014 zugeschrieben werden.

Eine Regression des modellierten Meeresspiegels auf die Principal Components (PC) der EOFs der SSTa und die lead/lag Korrelation zwischen PC1 und PC2 vor und nach dem 1976/77 Klimawechsel unterstützen die Ansicht, dass EOF1 und EOF2 EP ENSO und CP ENSO Ereignisse nach dem Klimawechsel darstellen können. Allerdings konnten vor dem Klimawechsel kaum Zentralpazifik (CP) Ereignisse nachgewiesen werden. Nach dem Klimawechsel ist das Thermoklinenfeedback im CP (Nino4 Region) deutlich stärker geworden, zeitgleich mit dem häufigeren Auftreten von CP ENSO Ereignissen. Dies hängt mit der lokalen Verstärkung des Bjerknes Feedbacks zusammen, ausgelößt durch die Verschiebung des Drehpunktes für Meeresspiegelschwankungen (und damit auch Thermoklinenschwankungen) aufgrund des Anstiegs der zonalen Windvarianz im westlichen Pazifik. Diese Argumente implizieren ein positives Feedback in dem CP Ereignisse sich selbst erhalten und es liegt nahe, dass sie Teil der natürlichen Variabilität des Klimasystem sein können und episodisch auftreten können, ohne die Notwendigkeit von Veränderungen im äußeren Antrieb.

1 Introduction

The tropical Pacific encompasses about half the circumference of the Earth at the equator, and it is subject to dramatic climate variability on the interannual timescale, the El Niño-Southern Oscillation (ENSO) (*Philander*, 1989; *Neelin et al.*, 1998). Sea level integrates and reflects multiple climatic and dynamical signals. The influence of anthropogenic forcing on the regional sea level variability is not detectable over the altimetry era (since 1993 to present) (*Meyssignac et al.*, 2012). Instead, tropical Pacific sea level variability mostly results from the changes in temperature in the water column in response to natural perturbations of the climate system, i.e., ENSO, mainly through changes in wind forcing and in turn ocean circulation (*Becker et al.*, 2012; *Rhein et al.*, 2013). ENSO is the first climate phenomenon shown to depend essentially upon ocean-atmosphere coupled dynamics (*Bjerknes*, 1969) with widespread environmental impacts both locally and globally due to global teleconnections in the ocean and atmosphere (*Trenberth et al.*, 1998). Common features of ENSO are well described and understood based on nearly a half century of studies (see *Neelin et al.*, 1998; *McPhaden et al.*, 1998, and references therein). In particular, the strong thermocline in the tropics and waveguide in the equatorial regions enables the simplification of the complex ocean model to a one and a half layer, shallow water model for the tropical oceans as a first approximation. This simple model driven by monthly wind stress has potential for hindcasting interannual sea level variability and associated ENSO events (*Busalacchi and O'Brien*, 1981; *Busalacchi et al.*, 1983; *Busalacchi and Cane*, 1985) as demonstrated in this thesis (Chapter 2).

However, in recent two decades, the increasing occurrence of the Central Pacific El Niño (*McPhaden*, 2004) as shown in Figure 1.1 (right panel) with the largest sea surface temperature anomalies (SSTa) in the central Pacific in the mature phase, and the failure for the predicted 2014 El Niño event to develop (*Imada et al.*, 2016; *McGregor et al.*, 2016), post new challenges to the prediction of ENSO. Thus, better understanding the event-to-event difference of ENSO spatial patterns and evolution is important to improve the predictability of ENSO. The emergence of the Central Pacific El Niño (*McPhaden*, 2004), in contrast with the conventional Eastern Pacific El Niño (*McPhaden*, 1999) as shown in Figure 1.1 (left panel) with the largest SSTa occur in the eastern Pacific in the mature phase, is an active area of

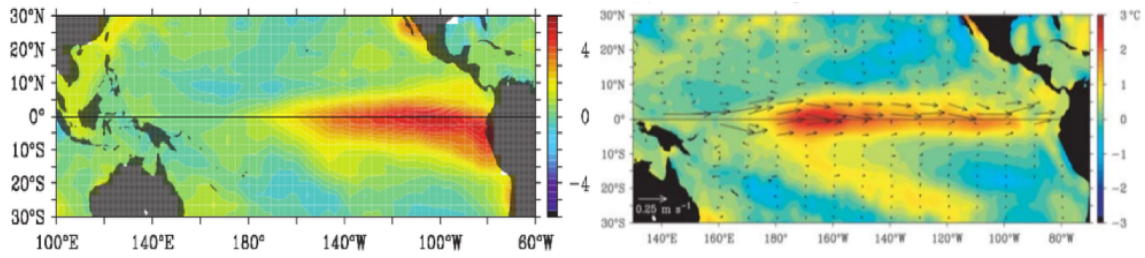

Figure 1.1: (Left) Monthly sea surface temperature anomalies (SSTa) for December 1997 relative to the monthly climatology over 1950-1979. From *McPhaden* (1999). (Right) SSTa (color shading) and anomalous surface currents (overlaid vectors) for October - December 2002. Reference periods for SST and surface currents are 1971-2000 and 1993-2001 respectively. From *McPhaden* (2004).

present-day research due to their significant different global impacts (see *Ashok and Yamagata* (2009); *Capotondi et al.* (2015) and references therein).

In this thesis, a linear, multi-mode model for the tropical Pacific is built to investigate sea level variability mainly on the interannual timescale (Chapter 2), revisit the recharge/discharge mechanism (*Jin*, 1997a,b) for Eastern Pacific ENSO (EP ENSO) with the largest SSTa occurring in the eastern equatorial Pacific in the mature phase (Chapter 2 and 3), and explore the physical mechanism for Central Pacific ENSO (CP ENSO) with the largest SSTa occurring in the central equatorial Pacific in the mature phase (Chapter 4). The following sections explain the motivations of the research in this thesis in detail.

1.1 Sea Level in Tropical Pacific

Sea level variability in the tropical Pacific is of great scientific interest as it is not only felt by the population on the ocean margins and islands directly but is also a signature of ENSO events which lead to considerable socioeconomic consequences in the tropics and elsewhere (*Becker et al.*, 2012).

1.1.1 History of Measurements

Measurements of sea level are the longest-running ocean observation system, with the very first tide gauge records installed in ports of northwestern Europe to provide information on ocean tides dating back to the mid-18th century (*Meyssignac and Cazenave*, 2012). Progressively, motivated by the increasing interest in ENSO events, the Pacific Sea Level Network, mainly using tide gauges, was established in the mid-1970s (*Wyrtki*, 1979). This developed into a central focus of the Tropical Ocean-Global Atmosphere (TOGA) Program started in 1985 aiming to provide the real-time measurements of key oceanographic variables to support

seasonal-to-interannual climate studies (*McPhaden et al.*, 1998), and contributing to the Permanent Service for Mean Sea Level (PSMSL, http://www.psmsl.org/). In spite of extending this network, the limitation of tide gauge data in spatial (sparse in situ sites) and temporal (multi-month- to multi-decade-long gaps) coverage hinders the reliable estimation of historical mean sea level.

Since the early 1990s, the arrival of remote sensing sea surface by the altimetry installed on the satellite has efficiently overcome this problem. High-precision satellite altimetry started with the launch of ERA-1 in 1991 and Topex/Poseidon in 1992 and their successors later on to measure the absolute sea level variations with respect to a reference ellipsoid that coincides with the mean shape of the Earth. The sea level data have been processed by Ssalto/Duacs and distributed by Aviso with support from Cnes (AVISO hereafter, http://www.aviso.altimetry.fr/duacs/).

Tide gauge measurements play an important role in the reconstruction of sea level in the past. For example, one method of reconstruction is described in *Becker et al.* (2012). This method combines sparse but long tide gauge records with shorter global gridded sea level time series from a ocean general circulation model or from satellite altimeter data by projecting the tide gauge data onto the spatial patterns of the Empirical Orthogonal Functions (EOFs) derived from the shorter time series. One thing to note is that there might be an issue if the shorter time series are too short to include the lower frequency trends or if the spatial patterns of the EOFs of variability change with time. *Takahashi et al.* (2011) adopted the similar method but for sea surface temperature (SST) to study the ENSO diversity which will be further discussed in Section 1.3.1.

In this thesis, however, a different method to reconstruct the sea level from 1961 to 2002 is developed. That is to build a linear, multi-mode model by fitting the model results to altimetry measured sea level from 1993 to 2014, which is described in detail in Chapter 2. Then, the tide gauge records at selected islands are used to validate reconstructed sea level (Chapter 3). Note that tide gauges measure relative sea level to the seafloor, including vertical crustal motions and thus the tide gauge records should be used with caution in the validation.

1.1.2 Changes and Causes

Roden (1963), the earliest work on the frequency spectrum of oceanographic and atmospheric variables in the tropical Pacific, has shown that coherence lengths of sea level variations are several hundred kilometers and are subject to the wind and current regimes. Since this work, tropical Pacific sea level changes are often described in the frequency space separately, e.g. the interannual, decadal, multidecadal variability or long-term trends (*Timmermann et al.*, 2010;

Merrifield, 2011; *Zhang and Church*, 2012; *Becker et al.*, 2012; *Meyssignac et al.*, 2012; *Han et al.*, 2014; *Forget and Ponte*, 2015). Alternative ways to partition sea level variability are in terms of (i) signals (phenomena of interest) and noises (the other variations), (ii) modes of variability based on EOF analysis of sea level, (iii) physical processes and (vi) forcing and response mechanism as provided by *Forget and Ponte* (2015). What follows is a brief discussion on the interannual variability and long-term trends in tropical Pacific sea level as well as their causes.

On the interannual timescale, the sea level variations are associated with ENSO (*Becker et al.*, 2012). If one performs the EOF analysis for the monthly sea level over time span 1992-2011 on the global scale (*Forget and Ponte*, 2015), temporal fluctuations of EOF1 and EOF2 are highly correlated with Nino3.4 index (SSTa averaged between 170°W–150°W, 5°S–5°N, representing EP ENSO) and the El Niño Modoki Index (EMI defined by *Ashok et al.* (2007), representing CP ENSO) respectively; the spatial patterns in the tropical Pacific display zonal seesaw in the 10°S - 10°N latitudinal band (EOF1) and a monopole centered on the central equatorial region (EOF2). Sea level trends are not geographically uniform, are predominant in the western Pacific, and have opposite signs pre-altimetry era compared to the altimetry era (*Timmermann et al.*, 2010). During the altimetry era, the sea level rise rate in the western tropical Pacific (over 10 $mmyr^{-1}$) is about 3 times of global mean value (*Timmermann et al.*, 2010; *Qiu and Chen*, 2012).

Roden (1963) noted a strong and direct relation between changes of sea level and of SST at low frequencies, indicating that the regional sea level variability mostly results from temperature changes. This has been confirmed by numerous studies as reviewed by *Cazenave and Remy* (2011); *Meyssignac and Cazenave* (2012); *Rhein et al.* (2013) and a more recent study by *Forget and Ponte* (2015). In the tropical Pacific, the interannual variations and trend patterns of sea level are mostly associated with the changes of ocean temperature through changes in the ocean circulation mostly driven by wind forcing (*Busalacchi and Cane*, 1985; *Timmermann et al.*, 2010). They are not stationary but fluctuate both in space and time in response to natural climate modes of the ocean-atmosphere coupled system, e.g. ENSO, PDO (Pacific Decadal Oscillation, see *Liu* (2012) and references therein).

1.2 Past Perspective: Eastern Pacific ENSO

El Niño, an oceanic interannual climate variability including the warming/cooling of eastern/western tropical Pacific Ocean, and the Southern Oscillation, an interannual seesaw in tropical sea level pressure between the eastern and western hemispheres (*Walker*, 1923), are

generated by coupled ocean-atmosphere interactions, first proposed by *Bjerknes* (1969). As a result, they are often referred to as El Niño - Southern Oscillation (ENSO) including both warm and cool phases of this interannual climate mode in the ocean-atmosphere coupled system. As mentioned above, due to the different locations of maximum SSTa and associated atmospheric heating, ENSO events are grouped into EP ENSO (Figure 1.1 left panel) and CP ENSO (Figure 1.1 right panel) (*Yeh et al.*, 2009). This section provides the overview for EP ENSO, whereas the next section (Section 1.3) covers CP ENSO.

1.2.1 Description of EP ENSO

In 1970s and early 1980s, despite impressive scientific advances achieved in understanding El Niño (e.g. *Wyrtki*, 1975), the extreme 1982/83 El Niño was not recognized until it was well developed, reflecting the urgent need for improved monitoring, understanding and prediction of El Niño. As a result, the decade-long (1985-1994) Tropical Ocean - Global Atmosphere (TOGA) program was implemented to provide real-time measurements of the following oceanographic variables: sea level, SST, subsurface temperature, ocean currents and surface winds. The significantly expanded observational database led to fundamental progress in our understanding of the physical processes responsible for ENSO (Section 1.2.2) and to the improvement of ENSO prediction from coupled ocean-atmosphere models (*Neelin et al.*, 1998; *McPhaden et al.*, 1998, and references therein).

The characteristics of EP ENSO are documented in many observational studies (e.g. *Delcroix*, 1998; *McPhaden et al.*, 1998). *Delcroix* (1998) reported that, during warm events, SST is higher than average in the east (Figure 1.1 left panel), sea level increases/decreases in the east/west with the pivot point in the west, and westerly wind anomalies occur in the west, confirming the Bjerknes feedback hypothesized by *Bjerknes* (1969) and introduced in Section 1.2.3. The signals are most pronounced in the equatorial band. These authors used the Southern Oscillation Index (SOI) (*Wright*, 1977) to identify EP ENSO. Alternative indices for ENSO but based on SSTa are documented in Table 1 of *Ashok et al.* (2007), among which the Nino3 index (*Trenberth*, 1997), spatially averaged SSTa over the Nino3 region (150°W - 90°W, 5°S - 5°N), is more commonly used for EP ENSO than the aforementioned Nino3.4 index (*Yeh et al.*, 2009).

A very important oceanic variable among those variables mentioned above in the TOGA program for understanding ENSO is the subsurface temperature, which gives the depth of thermocline measured by 20°C isotherm and in turn the Warm Water Volume (WWV) that goes with EP ENSO and implies the ocean 'memory' crucial to the periodicity of ENSO (*Wyrtki*, 1985; *Jin*, 1997a; *Meinen and McPhaden*, 2000). Besides, it is well known that the

thermocline depth in the tropics is proportional to sea level (*Rebert et al.*, 1985). Therefore the sea level is usually used as proxy data for the thermocline depth and the zonally integrated sea level along the equator as the proxy for the WWV in the equatorial Pacific (*Wyrtki*, 1985; *Clarke*, 2010). This is why to focus on the sea level variations in the tropical Pacific in this thesis (Chapter 2) to revisit the recharge/discharge mechanism for EP ENSO (*Jin*, 1997a,b) introduced in Section 1.2.3. The WWV in the equatorial band discharges (recharges) during the warm (cold) phase of EP ENSO (*Jin*, 1997a), demonstrated by the observational results that WWV leads Nino3 index and wind stress by about 7 months (*Meinen and McPhaden*, 2000).

1.2.2 Key Physical Processes in Tropical Pacific

In the tropical Pacific, the important physical processes in the large-scale ocean-atmosphere interactions responsible for ENSO (*Collins et al.*, 2010, and references therein) are listed below:

1. **Thermal damping (negative feedback)**. The atmospheric damping of SSTa generally consists of sensible and latent heat fluxes, and surface short wave radiation and long wave radiation fluxes.
2. **Mean upwelling (negative feedback)**. The mean upwelling of subsurface cold water in the eastern equatorial Pacific damps the positive thermal anomaly there, and increases the climatological zonal temperature gradient along the equator.
3. **Thermocline feedback (positive feedback)**. During El Niño, a flattened equatorial thermocline (shallower in the east and deeper in the west) leads to a positive SSTa in the eastern Pacific, through vertical advection of warmer subsurface water by upwelling in the east.
4. **Zonal advective feedback (positive feedback)**. The anomalous eastward advection of the mean SST gradient contributes to positive SSTa in the eastern Pacific.
5. **Ekman feedback (positive feedback)**. The anomalous westerly wind stress during El Niño suppresses the pumping of subsurface cold water upwards.
6. **Atmospheric intraseasonal variability (positive feedback)**. The intraseasonal atmospheric disturbances known as westerly wind events induce downwelling Kelvin waves propagating eastward and deepening the thermocline in the east.

The Bjerknes stability index (*Jin et al.*, 2006) including the first five processes in the framework of the recharge/discharge mechanism by *Jin* (1997a) (Section 1.2.3) is useful to qualitatively estimate ENSO behaviour (*Kim and Jin*, 2011; *Lübbecke and McPhaden*, 2014; *Im et al.*, 2015; *Wengel et al.*, 2017). Three main processes are thermocline feedback, zonal

advective feedback and thermal damping since the theoretical works of *Hirst* (1986) and *Jin and Neelin* (1993). In particular, the relative importance the thermocline feedback and zonal advective feedback in the equatorial Pacific to a large extent determines the main characteristics of ENSO (*An and Wang*, 2000; *Kang et al.*, 2004; *Belmadani et al.*, 2010; *Dewitte et al.*, 2013), such as the emergence of CP ENSO in recent two decades as compared to EP ENSO (*Capotondi*, 2013; *Lübbecke and McPhaden*, 2014; *Chen and Majda*, 2017), a topic introduced in Section 1.3.2.

1.2.3 Physical Explanations

The growth of EP El Niño (EP La Niña) is supported by the Bjerknes feedback (*Bjerknes*, 1969) that includes three components (*Lübbecke and McPhaden*, 2017; *Dippe et al.*, 2017): (i) the anomalous westerly (easterly) wind stress in the west exciting downwelling (upwelling) equatorial Kelvin waves that propagate eastward and deepen (elevate) the thermocline in the east, (ii) the fluctuations of thermocline in the east induce local SSTa, i.e. the thermocline feedback documented in the previous section, and (iii) the positive (negative) SSTa in the eastern equatorial Pacific leading to anomalous westerly (easterly) wind to the west. As noted in Section 1.2.1, the thermocline depth anomalies here are inferred from the variability of sea level data used in this thesis.

However, the Bjerknes feedback does not help in understanding the osillatory nature of EP ENSO. What drives the transitions between the warm events and cold events? It is ultimately associated with the ocean 'memory' provided by slow ocean adjustment in response to wind forcing (*Neelin et al.*, 1998). Considering the ocean dynamics, especially wind-forced or boundary reflected Rossby waves and Kelvin waves, as crucial aspects, four mechanisms have been proposed: Western Pacific Oscillator (*Weisberg and Wang*, 1997), Advective-Reflective Oscillator (*Picaut et al.*, 1997) and the other two as listed below:

1. **Delayed Oscillator**. Introduced by *Suarez and Schopf* (1988), the delayed oscillatory attributes the transition of phase to the reflections of Rossby waves, generated in the eastern coupling region, off the western boundary.
2. **Recharge/Discharge Oscillator (RDO)**. *Wyrtki* (1985) first attached the importance of the buildup (loss) of the WWV in the western Pacific prior to (after) the El Niño to the ENSO cycle. Based on this idea of recharge/discharge process and the coupled model of *Zebiak and Cane* (1987), *Jin* (1997a) developed the well-known RDO attributing a transition phase to the recharge/discharge of the upper ocean heat content or WWV in the entire equatorial Pacific, demonstrated by observations (e.g. *Meinen*

and McPhaden (2000, 2001); *Bosc and Delcroix* (2008)).

An example is the strong 1997/98 El Niño (*McPhaden et al.*, 1998). At least a year before the onset of this event, there was a build-up of the WWV (depression of thermocline) in the western equatorial Pacific due to stronger than normal trade winds associated with weak 1995/96 La Niña. The depression of the thermocline propagated eastward leading to a build-up of basinwide WWV and positive SSTa in the east. Then the Bjerknes feedback begins. As such, this event is initiated by westerly wind events over the western Pacific and matured in late 1997 and early 1998, suggesting that the WWV built up over the equatorial basin is a precursor of El Niño event. On the other hand, during the Bjerknes feedback phase, the thermocline deepened in the east and shoal in the west. The discharge of the western Pacific WWV slowly developed into the depletion of the basinwide WWV till the onset of the next La Niña. Thus the warm water in the equatorial band is built up at the onset of El Niño and lost to the higher latitudes at the end of El Niño.

Note that the WWV across the equatorial basin (focus of the RDO) provides higher predictability for EP ENSO than the WWV in the western Pacific (focus of the delayed oscillatory theory) (*Li and Clarke*, 1994; *Meinen and McPhaden*, 2000). The delayed oscillator failed to predicted the aforementioned extreme 1997/98 EP El Niño for which the westerly wind events over the western Pacific are important (*McPhaden et al.*, 1998; *McPhaden*, 1999).

With respect to the RDO theory, however, there remains debate on the source of the disequllibrium associated with the WWV. *Jin* (1997a) attibuted the discharge of zonal mean WWV to the imbalance between the meridional Sverdrup transport and the western boundary current transport. *Bosc and Delcroix* (2008) claimed that the equatorial WWV mostly come from the net convergence and divergence of Ekman and geostrophic meridional transport. On the other hand, *Meinen and McPhaden* (2001) found that zonal transport in the equatorial region is not negligible for the recharge/discharge of WWV. Based on the analytical study by *Clarke* (2010), the strong dependence of long Rossby wave speed on latitude and the reflection of wave energy at ocean boundaries is crucial to the existence of the disequllibrium WWV. This disagreement leads us to revisit the role of Sverdrup transport in the RDO mechanism in Chapter 2.

1.3 Present Perspective: Emergence of Central Pacific ENSO

As mentioned above (Figure 1.1), the SSTa patterns and evolution of events are different during CP ENSO and EP ENSO. The following subsections introduce the scientific background of

CP ENSO.

1.3.1 Description of CP ENSO

Since the late 1970s, ENSO events with SSTa's in the central Pacific sandwiched by opposite SSTa in the eastern and western equatorial Pacific have been observed (*Ashok et al.*, 2007). To identify these events, two indices were constructed: (i) the Trans-Niño Index (TNI, *Trenberth and Stepaniak* (2001)) that is normalized SSTa over Nino1+2 region (0° - 10°S, 90°W - 80°W) minus those in Nino4 region (5°N - 5°S, 160°E - 150°W), and (ii) the El Niño Modoki Index (EMI, *Ashok et al.* (2007)) that is SST averaged over the central Pacific (165°E - 140°W, 10°S - 10°N) minus SST averaged over the western Pacific (125°E - 145°E, 10°S - 20°N) and the eastern Pacific (110°W - 70°W, 15°S - 5°N). The EMI, in comparison with the TNI, is used in this thesis by considering the effects of the western tropical Pacific where the CP ENSO events are triggered (*Ashok et al.*, 2007; *McPhaden*, 2004).

Take the 2002/03 CP El Niño (*McPhaden*, 2004) as an example. During the second half of 2002, westerly wind anomalies excited equatorial waves decreasing the zonal SST gradient, and drove intense eastward currents advecting the western Pacific warm pool to the east of the date line. During October 2002 - January 2003, this warm event reached its peak phase with largest (shorted-lived and weak) SSTa's concentrated in the central (eastern) Pacific (Figure 1.1 right panel). Unusual easterly wind anomalies confined to the east of 100°W - 120°W during this event occurred along the equator, indicating different patterns of atmospheric convection from those of EP El Niño (see Figure 2 in *Ashok and Yamagata*, 2009).

Ashok et al. (2007) noted the resemblance between these SSTa patterns and the EOF2 of SSTa in the tropical Pacific and the high correlation between EMI and the time series for the principal component of EOF2 (0.91) after the 1976/77 climate shift (*Trenberth et al.*, 1998). Therefore they claimed that EOF2 (EOF1) of SSTa represents the CP ENSO (EP ENSO) mode. However, some studies address the role of the nonlinearity of ENSO in the occurrence of CP ENSO (*Takahashi et al.*, 2011; *Dommenget et al.*, 2013). This disagreement between *Ashok et al.* (2007) and *Takahashi et al.* (2011) comes from the controversy on the reason for the regime shift in the lead/lag correlations between the TNI and Nino3.4 index with the change in sign of the lead/lag relationship found by *Trenberth and Stepaniak* (2001) associated with the 1976/77 climate shift (*Trenberth et al.*, 1998). Was the regime shift caused by the increasing occurrence of CP ENSO or is the regime shift a statistical artifact caused by the extreme 1982/83 and 1997/98 EP El Niño events? Thus in this thesis, the view of *Ashok et al.* (2007) is tested in Chapter 4 by presenting the signature of CP ENSO in a linear ocean model.

1.3.2 Physical Explanations

To understand the emergence of CP ENSO, the quantitative evaluation of physical processes (see Section 1.2.2) is necessary (*Capotondi et al.*, 2015, and references therein). In particular, the selection of EP ENSO and CP ENSO are to a large extent determined by the relative importance of the thermocline feedback and zonal advective feedback (Section 1.2.2). Figure 1.2 illustrates the relationship of these two processes along the equator, where several features can be obtained: (i) the thermocline depth in the eastern Pacific is much shallower than that in the western and central Pacific coincident with high regression coefficients of SSTa onto thermocline depth anomalies indicating stronger thermocline feedback in the eastern Pacific (bottom panel), (ii) the zero skewness of SST and the thermocline pivot point both locate at 150°W, i.e. eastern edge of Nino4 region, (iii) in the Nino4 region, the regression coefficients of SSTa onto the thermocline depth anomalies are negative, indicating the strong zonal advective feedback, and (iv) the zero skewness of SST (150°W) locates to the west of the zero skewness of thermocline depth (120°W) due to increased warming by zonal advective feedback in between.

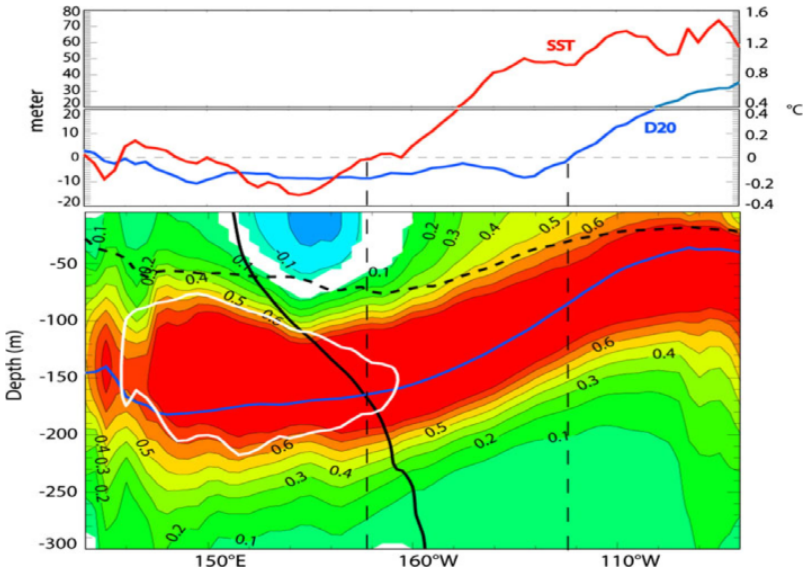

Figure 1.2: (Bottom) Vertical section of the regression between temperature and thermocline depth anomalies over 1958–2008. The black thick line indicates the zero contour of the first EOF mode of temperature anomalies. The blue thick line indicates the mean thermocline depth and the black thick dashed line indicates the mixed layer depth. The intersection between the black line and the blue line therefore stands for the position of the thermocline pivot. The non-colored area indicates where the regression values is below the 95% confidence level. The white contour indicates the –0.4°C contour of the dominant EOF of the 7-year low-pass filtered temperature anomalies and indicates where stratification changes at decadal timescale are the largest. (Top) The skewness of thermocline depth anomalies (blue line—left scale) and temperature anomalies (red line—right scale). The vertical dashed lines indicate the position of the zero crossing for SST and themocline depth. From *Dewitte et al.* (2013).

The maximum SSTa associated with CP ENSO occurs in the central Pacific where zonal advective feedback is not negligible (*Kang et al.*, 2004; *Belmadani et al.*, 2010; *Hu et al.*, 2013; *Chen and Majda*, 2017; *Capotondi et al.*, 2015, and references therein). However, the role of thermocline feedback in CP ENSO remains under debate. *Yeh et al.* (2009) suggest that a flatten thermocline in the equatorial Pacific due to global warming and resultant increasing thermocline feedback in the central Pacific contributes to the increasing occurrence of CP ENSO events. The increased thermocline feedback after the 1976/77 is confirmed by *Dewitte et al.* (2013). On the other hand, *McPhaden et al.* (2011) find the dominant flavor of ENSO changes from EP ENSO during 1980-1999 to CP ENSO during 2000-2010, concurrent with a steeper thermocline slope, and conclude that this change is related to the natural decadal variability. *Lübbecke and McPhaden* (2014) argue that the cooler background state during 2000-2010 in the central-eastern tropical Pacific led to a westward shift in the ascending branch of the Walker circulation and smaller zonal wind fetch, which is favorable for CP ENSO and weakens the thermocline feedback in the central-eastern Pacific. Therefore, the dynamics governing ENSO diversity and the role of thermocline feedback remains unclear, which will be explored in Chapter 4.

1.4 Modelling ENSO-related Sea Level with Shallow Water Models

Sea level variations at ENSO-frequency in the tropical Pacific is almost exclusively baroclinic, mainly characterized by the wind-forced baroclinic waves (*Forget and Ponte*, 2015). The observations also highlight the importance of the oceanic equatorial Kelvin waves and Rossby waves for ENSO dynamics (e.g. *White et al.*, 1990; *Kessler*, 1990; *Chelton and Schlax*, 1996). Based on the theory of linear wave dynamics (*Gill and Clarke*, 1974; *McCreary*, 1981; *Gill*, 1982), the wind-driven, large-scale, low-frequency oceanic motion can be separated into an infinite number of baroclinic vertical normal modes that are eigensolutions of a stratified fluid linearized about a state of rest. Each vertical normal mode corresponds to a group of shallow water equations referred to as a shallow water model (SWM). *Moon et al.* (2004) pointed out that interannual variations in the relative importance of different vertical wave modes is important for the predictability of ENSO. Linear SWM's for the gravest first two baroclinic modes driven by observed wind stress anomalies are able to produce sea level anomalies comparable to observations (*Busalacchi and Cane*, 1985), outperforming that using only a single mode (*Busalacchi and O'Brien*, 1981). The simple SWM's driven by idealized winds improve our understanding of the fundamental dynamics of ENSO (*Cane and Sarachik*, 1981), such as

the recharge/dischage of the WWV (*Clarke*, 2010; *McGregor et al.*, 2016). For the prediction of ENSO, the oceanic SWM was incorporated into the intermediate coupled model of *Zebiak and Cane* (1987) which was the first forecast model for ENSO and led to the built-up of the RDO theory (*Jin*, 1997a) (Section 1.2.3). Hence, for the purposes of better understanding the relative importance of vertical baroclinic modes in the interannual variability and those illustrated in previous sections, the AVISO sea level data with comprehensively spatial and temporal coverage as compared to tide gauge records used in previous studies is more favorable to build a linear, multi-mode model (Chapter 2).

1.5 Scientific Questions Addressed in This Thesis

In this thesis, a linear multi-mode model is built with the help of satellite measured sea level, driven by ERA-Interim monthly mean wind stress provided by the European Centre for Medium-Range Weather Forecasts (ECMWF) (*Berrisford et al.*, 2009) to simulate the interannual sea level variations during the satellite era (1993-2014) in Chapter 2 to answer the following questions:

- Which vertical baroclinic modes are important for ENSO-related sea level variations in the tropical Pacific? Does the model capture the characteristics of ENSO (e.g. the pivot point of sea level)? Is the Sverdrup transport fundamental to the RDO mechanism for EP ENSO?

This model is then used to reconstruct the sea level variations in the pre-satellite era (1961-2002) driven by monthly wind anomalies from two popular reanalysis datasets, i.e. the 40-yr European Centre for Medium-Range Weather Forecasts (ECMWF) Re-analysis (ERA-40) (*Kalnay et al.*, 1996) and the National Center for Environmental Prediction/National Center for Atmospheric Research (NCEP/NCAR) Reanalysis (*Uppala et al.*, 2005) to answer the following question in Chapter 3:

- Which wind forcing dataset is more reliable? What are the changes in the characteristics of ENSO-related sea level variations and their causes, particularly regarding the pivot point of sea level?

Based on the simulations from Chapter 2 and 3, the following questions are addressed in Chapter 4:

- Do the EOF1 and EOF2 of SSTa in the tropical Pacific represent EP ENSO and CP ENSO? What is the role of the thermocline feedback in, and what is the underlying mechanism for, the emergence of CP ENSO?

2 Interannual Variability of Tropical Pacific Sea Level from 1993 to 2014

In this chapter, a linear multi-mode model is built by fitting the model results for multiple vertical baroclinic modes to the satellite measured sea level over the time span 1993-2014. As such the important vertical modes and their influences are obtained. In addition, the role of Sverdrup transport in the recharge/discharge mechanism is explored with the help of the experiment driven by spatially uniform zonal wind stress.

Citation: **Zhu, X., R. J. Greatbatch, and M. Claus (2017), Interannual variability of tropical pacific sea level from 1993 to 2014, Journal of Geophysical Research: Oceans, 122 (1), 602–616.**

The candidate's contribution to this publication are as below:

1. *Setting up and running of the model*
2. *Analysis of the model results*
3. *Preparing and analysis of the observational datasets*
4. *Production of all figures*
5. *Contributing to the ideas in the manuscript*
6. *Drafting the first version of the manuscript*

AGU PUBLICATIONS

JGR

Journal of Geophysical Research: Oceans

RESEARCH ARTICLE

10.1002/2016JC012347

Interannual variability of tropical Pacific sea level from 1993 to 2014

Xiaoting Zhu [1], **Richard J. Greatbatch** [1,2], **and Martin Claus** [1]

[1]Ocean Circulation and Climate Dynamics, GEOMAR Helmholtz Centre for Ocean Research Kiel, Kiel, Germany, [2]Faculty of Mathematics and Natural Sciences, University of Kiel, Kiel, Germany

Key Points:
- A linear multimode model driven by reanalysis wind stress can reproduce satellite-derived tropical sea level variability
- The weight of each mode is assigned by fitting model sea level to the altimeter along the equator. Modes higher than six cannot be weighted
- The model shows that the Sverdrup transport is not fundamental to the recharge/discharge mechanism

Correspondence to:
X. Zhu,
xzhu@geomar.de

Citation:
Zhu, X., R. J. Greatbatch, and M. Claus (2017), Interannual variability of tropical Pacific sea level from 1993 to 2014, *J. Geophys. Res. Oceans*, *122*, 602–616, doi:10.1002/2016JC012347.

Received 16 SEP 2016
Accepted 13 DEC 2016
Accepted article online 22 DEC 2016
Published online 27 JAN 2017

Abstract A multimode, linear reduced-gravity model, driven by ERA-Interim monthly mean wind stress anomalies, is used to investigate interannual variability in tropical Pacific sea level as seen in satellite altimeter data. The model output is fitted to the altimeter data along the equator, in order to derive the vertical profile for the model forcing, showing that a signature from modes higher than mode 6 cannot be extracted from the altimeter data. It is shown that the model has considerable skill at capturing interannual sea level variability both on and off the equator. The correlation between modeled and satellite-derived sea level data exceeds 0.8 over a wide range of longitudes along the equator and readily captures the observed ENSO events. Overall, the combination of the first, second, third, and fifth modes can provide a robust estimate of the interannual sea level variability, the second mode being dominant. A remarkable feature of both the model and the altimeter data is the presence of a pivot point in the western Pacific on the equator. We show that the westward displacement of the pivot point from the center of the basin is strongly influenced by the fact that most of the wind stress variance is found in the western part of the basin. We also show that the Sverdrup transport is not fundamental to the dynamics of the recharge/discharge mechanism in our model, although the spatial structure of the wind forcing does play a role in setting the amplitude of the "warm water volume."

1. Introduction

More than 40 years ago, interannual sea level variability in the tropical Pacific was being studied using linear, reduced-gravity models driven by estimates of the observed surface wind stress [*Busalacchi and O'Brien*, 1981; *Busalacchi et al*., 1983]. At that time, the only available sea level data were from the sparse tide gauge record. However, with the advent of satellite data, there has been a revolution in the available data coverage for sea level. Here, we revisit the ability of linear models to capture interannual variability in tropical Pacific sea level, this time using a multimode modeling system and taking advantage of the temporally and spatially comprehensive altimetric sea level data produced by Ssalto/Duacs and distributed by Aviso with support from Cnes (http://www.aviso.altimetry.fr/duacs/).

In the tropical Pacific, interannual variability is dominated by the El Niño-Southern Oscillation (ENSO) phenomenum, with widespread environmental impacts locally, but also around the world due to the global teleconnections in the ocean and the atmosphere [*Philander*, 1989; *Trenberth et al*., 1998]. Observational studies [e.g., *Delcroix*, 1998; *Forget and Ponte*, 2015] have shown that sea level variations associated with ENSO feature an east-west contrast along the equator and zonally uniform anomalies near the equator. These features are also captured by analytical solutions for the linear response of the tropical Pacific Ocean to low-frequency wind forcing [*Clarke*, 2010], where they correspond to what Clarke calls the "tilt" mode and "equatorial warm water volume (WWV)", respectively (see *Meinen and McPhaden* [2000] and *Meinen and McPhaden* [2001] for an early discussion of these modes). According to *Clarke* [2010], the tilt mode is a quasi-steady response to wind forcing that varies in phase with the wind stress forcing, that is, the balance of the zonal wind stress by the zonal pressure gradient; however, the WWV mode lags the wind stress due to the strong dependence of the westward propagation speed for long Rossby waves on latitude. The phase lag is a key feature of the recharge/discharge mechanism for ENSO [*Jin*, 1997] as reviewed by *Neelin et al*. [1998].

The early studies in the 1970s and 1980s suggested an important role for Kelvin and Rossby waves in the dynamics of the tropical oceans and, indeed, in the dynamics of ENSO. Recent work has confirmed that the interannual variability of sea level at low latitudes is almost exclusively baroclinic in origin [*Forget and Ponte*,

2015]. Large-scale, low-frequency (interannual) oceanic motion can be separated into an infinite number of baroclinic vertical normal modes [*Gill and Clarke*, 1974; *Gill*, 1982], of which the first few modes usually dominate. *Moon et al.* [2004] claimed that interannual variations in the relative importance of different vertical wave modes is important for the predictability of ENSO and *Dewitte et al.* [1999] analyzed the contributions of the first four baroclinic modes to sea level variability for the period 1985–1994 using an ocean general circulation model. The authors found that the first mode is most dominant in the western Pacific and the second mode in the eastern Pacific. Other authors have also noted the dominance of the first and second modes [*Cane*, 1984; *Busalacchi and Cane*, 1985; *Yu and McPhaden*, 1999; *McPhaden and Yu*, 1999].

Nevertheless, the relative importance of the different vertical modes is still not adequately explored. To provide more information about the relative importance of the different baroclinic modes for explaining the interannual variability of sea level in the tropical Pacific Ocean, we conduct simulations using a multimode modeling system. We assign the weighting to each mode with the help of altimeter data without assuming, a priori, the vertical profile in the ocean for the wind-induced forcing, different from previous studies [*Gill and Clarke*, 1974; *Cane*, 1984; *Dewitte et al.*, 1999]. In particular, we fit the model results to the altimetric measurements along the equator in order to diagnose the projection coefficients for each mode for the vertical profile of the model forcing.

Clarke [2010] argues that the origin of the disequilibrium WWV mode is the strong dependence of the propagation speed for long Rossby waves on latitude. On the other hand, in the original recharge/discharge theory put forward by *Jin* [1997], an important role was assigned to the Sverdrup transport for transferring mass to and from the equator. We address the role of the Sverdrup transport in our model using spatially uniform wind stress forcing given by the time series of the zonally averaged zonal wind stress along the equator, for which the Sverdrup transport is zero.

The paper is organized as follows. The description of the model and the methods employed are outlined in the section 2. Section 3 shows the results and discusses the recharge/discharge mechanism using the model. Finally, section 4 summarizes the main conclusions.

2. Methods

2.1. Basic Equations

Our starting point is the Boussinesq, hydrostatic equations for a continuously stratified ocean linearized about a state of rest. In spherical coordinates, these are given by

$$\frac{\partial u}{\partial t}-fv=-\frac{1}{\rho_o a\cos\theta}\frac{\partial p'}{\partial\lambda}+\frac{\tau_s^x}{\rho_o H_E}G(z)+F^u \tag{1}$$

$$\frac{\partial v}{\partial t}+fu=-\frac{1}{\rho_o a}\frac{\partial p'}{\partial\theta}+\frac{\tau_s^y}{\rho_o H_E}G(z)+F^v \tag{2}$$

$$0=-\frac{\partial p'}{\partial z}-g\rho' \tag{3}$$

$$\frac{1}{a\cos\theta}\left[\frac{\partial u}{\partial\lambda}+\frac{\partial(v\ \cos\theta)}{\partial\theta}\right]+\frac{\partial w}{\partial z}=0 \tag{4}$$

$$\frac{\partial\rho'}{\partial t}+w\frac{\partial\bar{\rho}}{\partial z}=0 \tag{5}$$

where θ is latitude, λ is longitude, a is the radius of the Earth, $f=2\Omega\sin\theta$ is the Coriolis parameter, g is the gravitational acceleration, ρ_o a representative density for sea water, u, v, w are the velocity components in the eastward, northward, and vertically upward directions, respectively, ρ' is the density perturbation, p' is the pressure perturbation, $(\tau_s^x,\ \tau_s^y)$ is the surface wind stress treated as a body force with a vertical structure $G(z)$, H_E is a depth scale for the surface Ekman layer (here independent of both space and time), and F^u, F^v is the lateral mixing of momentum with horizontal eddy viscosity coefficient, A_h, given by

$$F^u(u,v)=\frac{A_h}{a^2}\left[\frac{1}{\cos^2\theta}\frac{\partial^2 u}{\partial\lambda^2}+\frac{1}{\cos\theta}\frac{\partial}{\partial\theta}\left(\cos\theta\frac{\partial u}{\partial\theta}\right)+u\left(1-\tan^2\theta\right)-\frac{2\sin\theta}{\cos^2\theta}\frac{\partial v}{\partial\lambda}\right] \tag{6}$$

$$F^v(u,v)=\frac{A_h}{a^2}\left[\frac{1}{\cos^2\theta}\frac{\partial^2 v}{\partial\lambda^2}+\frac{1}{\cos\theta}\frac{\partial}{\partial\theta}\left(\cos\theta\frac{\partial v}{\partial\theta}\right)+v\left(1-\tan^2\theta\right)-\frac{2\sin\theta}{\cos^2\theta}\frac{\partial u}{\partial\lambda}\right]. \tag{7}$$

The boundary conditions are, at the surface $z = 0$,

$$p'=\rho_o g\eta \quad and \quad w=\frac{\partial\eta}{\partial t} \tag{8}$$

where η denotes the sea level anomaly, and at the bottom $z=-H$, $w = 0$, where H is the total depth of the ocean (assumed here to be flat).

As is well known, the solution to these equations can be expressed as the superposition of a infinite discrete set of vertical normal modes [*Gill and Clarke*, 1974; *Gill*, 1982], so that the pressure perturbation p', for example, can be expressed as

$$\frac{p'}{\rho_o g}=\sum_{n=1}^{\infty}\hat{p}_n(z)\eta_n(\lambda,\theta,t) \tag{9}$$

where the subscript n refers to the nth normal mode, $\hat{p}_n(z)$ denotes the corresponding normalized vertical structure function for pressure satisfying $\int_{-H}^{0}\hat{p}_n^2(z)dz=1$, and the horizontal structure associated with each vertical mode is obtained by solving the shallow water equations

$$\frac{\partial u_n}{\partial t}-fv_n=-\frac{g}{a\cos\theta}\frac{\partial\eta_n}{\partial\lambda}+\frac{\tau_s^x}{\rho H_E}G_n+F_n^u \tag{10}$$

$$\frac{\partial v_n}{\partial t}+fu_n=-\frac{g}{a}\frac{\partial\eta_n}{\partial\theta}+\frac{\tau_s^y}{\rho H_E}G_n+F_n^v \tag{11}$$

$$\frac{\partial\eta_n}{\partial t}+\frac{H_n}{a\cos\theta}\left[\frac{\partial u_n}{\partial\lambda}+\frac{\partial(\cos\theta v_n)}{\partial\theta}\right]=0. \tag{12}$$

Here repeated variables are consistent with those in equations (1–5), except for the subscript n referring to the nth normal mode, H_n is the equivalent depth determined by the wave speed $c_n=\sqrt{gH_n}$, and $G_n=\int_{-H}^{0}G(z)\hat{p}_n(z)dz$ is the wind forcing profile projection factor. The sea surface height anomaly, which is to be compared to that from the satellite altimeter, is then given by

$$\eta=\sum_{n=1}^{\infty}\hat{p}_n(0)\eta_n(\lambda,\theta,t). \tag{13}$$

Here, we do not specify the vertical profile of the wind forcing, $G(z)$, a priori and first solve these equations with $G_n=1$ to obtain a corresponding field for η_n which we denoted as η_n^*, excluding the barotropic mode ($n = 0$). We then make a least squares fit of the model-computed sea level anomalies to the sea level anomalies from the altimeter data. The fit is carried out along the equator across the whole of the equatorial Pacific, to obtain fitting coefficients γ_n for each mode. The model-computed sea level is then given by

$$\eta=\sum_{n=1}^{N}\gamma_n\hat{p}_n(0)\eta_n^*(\lambda,\theta,t) \tag{14}$$

where N is the number of modes used for the fit. The implied projection coefficients, G_n are given by

$$G_n=\gamma_n \tag{15}$$

and the vertical profile for the wind forcing can then be obtained from

$$G(z)=\sum_{n=1}^{N}\hat{p}_n(z)\gamma_n. \tag{16}$$

2.2. Model Setup

The model domain extends from 112°E to 70°W zonally and from 12°S to 18°N meridionally, similar to that of *Busalacchi and O'Brien* [1981], with the 300 m isobath taken as the coastline, and the horizontal resolution is 0.5° in latitude and longitude. The eastern/western boundaries are treated as solid walls. Sponge layers,

damping the velocity field only, with e-folding scale of 5° in latitude, are applied to the northern and southern boundaries to eliminate wave propagation along those boundaries. The scale depth H_E is chosen to be 300 m and the eddy viscosity coefficient A_h is 5000 $m^2\ s^{-1}$ everywhere (For this choice of lateral eddy viscosity, the damping time scale for a mode with gravity wave speed $c = 1$ m s^{-1} is comparable to that implied by the model of *McCreary* [1981] using vertical mixing. Here we have used the equatorial radius of deformation for the length scale to derive the damping time scale for the lateral mixing. The similarity between the two damping time scales shows that the damping we use here is similar to that implied by the McCreary model). Monthly mean wind stress anomalies from January 1979 to September 2014 are used to force the model. Anomalies are computed relative to the climatological monthly mean for each month for the period 1993–2012 and are derived from ERA-interim monthly mean wind stress provided by the European Centre for Medium-Range Weather Forecasts (ECMWF) [*Berrisford et al*., 2009]. The satellite measured sea level anomalies from January 1993 to September 2014 are those produced by Ssalto/Duacs and distributed by Aviso with support from Cnes (http://www.aviso.altimetry.fr/duacs/).

To derive the vertical normal modes, the vertical profile of the buoyancy frequency is first calculated within the region occupied by the model domain using the temperature and salinity data from the World Ocean Atlas 2013 data set [*Locarnini et al*., 2013]. The resulting profiles are then averaged to produce an averaged buoyancy frequency profile within the model domain. The averaged buoyancy frequency profile is then used to compute the vertical modes. The resulting wave speeds of the first five baroclinic modes are 2.88, 1.72, 1.10, 0.82, and 0.67 m s^{-1}, respectively, and the corresponding vertical structure functions, $\hat{p}_n(z)$, are shown in Figure 1a. The horizontal resolution of 0.5° in latitude and longitude is sufficient to resolve the equatorial baroclinic Rossby radius of deformation $\sqrt{\frac{c}{\beta}}$ for the selected normal modes, where β is the latitudinal gradient of the Coriolis parameter given by $\beta = \frac{2\Omega cos(\theta)}{a}$.

Two additional model experiments are carried out using exactly the same setup as above. In the first (referred to as experiment ZMW), the meridional wind stress is set to zero and the zonal wind stress is spatially uniform over the model domain. In this experiment, the zonal wind stress is given by the time series of the zonal average along the equator of the zonal wind stress anomalies from the standard experiment; that is from ERA-Interim. In the second, the meridional wind stress is again zero but the zonal wind stress is given by the time series of the zonal mean zonal wind stress at each latitude (referred to as experiment LatZM). The vertical profile for the model forcing in both these experiments is the same as in the standard run. In experiment ZMW, because the wind stress is spatially uniform, the Sverdrup transport is zero.

3. Results

As described in section 2, the vertical structure of the wind forcing profile, given by $G(z)$ in equations (1) and (2), is deduced from the model solution by fitting monthly mean anomalies of the model sea level to the AVISO data along the equator. The coefficients G_n (see equations (15) and (16)) obtained from the fitting, and using increasing numbers of vertical modes, are shown in Table 1. It is clear that the weighting assigned to modes 1 and 2 is quite stable once three or more modes are used. However, increasing the number of modes from 4 to 5 reduces the weighting given to mode 4 and puts more weight into modes 3 and 5. Adding a sixth mode does not change this picture but using seven modes or more leads to the appearance of large weightings that largely cancel out. This behavior is an indication that beyond mode 6, it is no longer possible to separate the signature of the modes in the AVISO data. Equation (16) can be used to construct the wind forcing profile, as shown in Figure 1b when using five modes and when using four and six modes in Figure 1c. In all cases, the profile is strongly surface intensified, as one would expect, but with a clear improvement in going from four to five or six modes. Note, in particular, the reduced amplitude below 200 m depth when using five or six modes and also that there is little change in going from five to six modes. Clearly, further reducing the amplitude below 200 m depth would require an accurate estimate of γ_n for modes higher than 6, something that is not possible through fitting our model solutions to the altimeter data. Since adding the sixth mode makes very little contribution to our results (the coefficient γ_6 is close to zero) we work with five modes in what follows.

Before leaving Table 1, it is worth commenting on the weighting when using five modes. Note, in particular, the dominance of mode 2 but also that some role is given to mode 3, followed by modes 1 and 5, with the

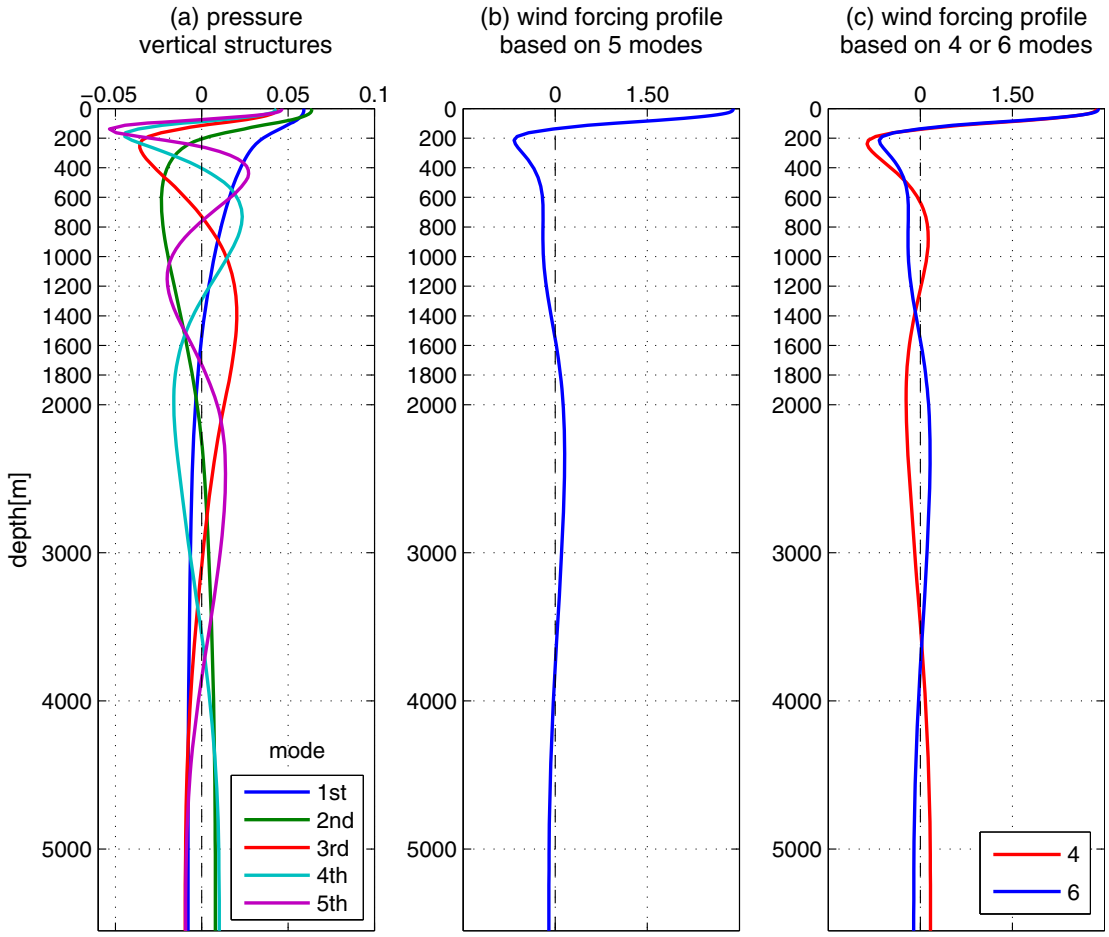

Figure 1. (a) The vertical structure functions, $\hat{p}_n$, for modes 1–5. (b) The wind stress profile, $G(z)$, obtained using five modes. (c) Same as Figure 1b but using four (red line) and six modes (blue line).

smallest weighting being given to mode 4. These weightings assign the amplitude that is given to the forcing for each mode in equations (10) and (11), with $G_n = \gamma_n$ (equation (15)). It is, therefore, no surprise that the second mode dominates our results, although with some role for modes 1, 3, and 5, as we shall see. There are two reasons for favoring mode 5 over mode 4. The first is the consistency between the weightings attached to each mode when going from five to six modes to make the fit (see Table 1). The second is the improved vertical structure of the wind forcing profile shown in Figure 1 when using five or six modes as

Table 1. Projection Coefficients G_n (Unit: $m^{1/2}$) Obtained by the Fitting When Using Different Numbers of Modes

	G_1	G_2	G_3	G_4	G_5	G_6	G_7	G_8	G_9
Two modes	7.07	29.73							
Three modes	7.85	16.01	28.00						
Four modes	7.96	18.66	10.25	17.73					
Five modes	7.76	18.48	14.91	4.25	9.36				
Six modes	7.76	18.48	14.92	4.15	9.54	−0.13			
Seven modes	7.58	18.30	16.45	−1.66	33.98	−49.09	31.41		
Eight modes	7.54	18.40	16.12	−1.59	36.42	−64.39	62.43	−17.15	
Nine modes	7.71	19.26	13.07	3.79	18.12	4.11	−164.94	317.01	−178.16

Table 2. Projection Coefficients G_n (Unit: $m^{1/2}$) When Specifying the Vertical Profile $G(z)$ Given by $G(z)=H_E/D$ Over a Surface Ekman Layer of Depth D and $G(z)=0$ Below

D	G_1	G_2	G_3	G_4	G_5	G_6
50 m	18.63	19.88	13.24	12.71	13.23	11.81
100 m	18.41	18.39	10.48	7.92	5.90	2.98
150 m	16.54	14.92	6.41	2.51	−0.55	−2.64
200 m	15.34	11.87	2.76	−1.47	−3.66	−3.23
250 m	14.24	9.21	0.08	−3.44	−3.82	−1.31

distinct from four modes, a point already noted above. Nevertheless, whether or not the fitting is really able to distinguish between the fourth and fifth modes is a moot point, given that the difference in the gravity wave speeds for the two modes is only 0.15 m s^{-1}. Another concern is the impact of the mean flow on the modes, an issue discussed by *McPhaden et al*. [1986] who note that the higher the mode, the more likely is an impact from the background flow. On the other hand, as shown by *Brandt et al*. [2016], mode 4 plays a role in the annual cycle of the equatorial Atlantic and is well represented by dynamics linearized about a state of rest. Regarding the dominance of mode 2 in the tropical ocean, this was already pointed out by *Philander and Pacanowski* [1980] and is discussed in detail there. We believe the difference between our results and previous studies, in particular *Cane* [1984], *Busalacchi and Cane* [1985], *Yu and McPhaden* [1999], and *McPhaden and Yu* [1999], is that we do not assume a vertical structure for the model forcing a priori, rather determining it by fitting the model to the AVISO data. We note that the common practice in previous studies, for example, *Cane* [1984], has been to assume that the vertical structure function $G(z)$ in equations (1) and (2) is equal to H_E/D over a surface Ekman layer of depth D and is zero below. Table 2 shows the projection coefficients G_n in this case for different choices of the depth D. These projection coefficients can be compared directly to those shown in Table 1. It is immediately apparent that the first mode now has a similar weight to that given to the second mode and also that less weight is given to the higher modes (apart from the case with the shallowest D, i.e., $D = 50$m), consistent with the relative weightings of the modes found in previous studies. The different weightings given to the modes in our case therefore follows directly from the freedom we give our model to determine the vertical structure function $G(z)$ by fitting to the altimeter data. It is also interesting to note that if the depth D were to vary in time (as one would expect in a more realistic model), then one would expect the transition at the base of the Ekman layer to be smoothed out and look something like our derived vertical profile shown in Figure 1.

The Hovmoeller diagrams of monthly mean sea level anomalies along the equator (Figure 2c) and higher latitudes (Figure 3b) exhibit remarkably similar patterns as those seen in the altimetric observations (Figures 2b and 3a), illustrating the practical value of regarding the wind forcing as the null hypothesis for the origin of interannual sea level variability over the tropical Pacific. In particular, the model successfully captures the ENSO events of various strengths and flavors, including both conventional El Niño (97/98, 06/07, 09/10) and Modoki El Niño (94/95, 02/03, 04/05, i.e., positive anomalous sea levels do not extend to the eastern boundaries) [*Ashok et al*., 2007] events as well as the 95/96, 98/99, 07/08, 10/11 La Niña events. Along the equator (Figures 2b and 2c), El Niño events are featured by positive anomalous sea level in the east and negative in the west, and vice versa during La Niña events. The features, especially during the strong 97/98 El Niño and 98/99 La Niña, extend to other latitudes (Figures 3a and 3b), by means of Kelvin wave propagation along the eastern boundary and subsequent Rossby wave propagation into the basin interior. This is in accordance with inferences from the observed surface dynamic height anomaly made, for example, by *Delcroix* [1998].

In contrast to the typically eastward propagation along the equator (Figure 2), events away from the equator generally propagate westward (Figure 3). The propagation speeds along 10°S, 5°S, 5°N, and 10°N in the model (Figure 3b) are comparable to those in the observations (Figure 3a), although at 15°N, the modeled propagation speeds seem higher, even though many of the same events are seen in both the observations and the model. A notable feature of both the model and the observations is an underlying symmetry about the equator, which though not perfect, reflects the importance of the equatorial regions for generating off-equatorial anomalies, be that by direct wind forcing or by wave propagation processes, as described above.

Another notable feature along the equator (Figure 2) is the presence of a pivot point in the western equatorial Pacific where anomalies tend to change sign and the variability is notably reduced. The pivot point tends to be further west in the observations than in the model, no doubt reflecting processes missing from our linear model set-up (e.g., zonal advection processes along the equator that are known to be important in the western, central Pacific [e.g., *Dewitte et al*., 2013]). Comparing Figures 2c and 2e, it is clear that the spatial structure of the wind forcing matters for the location of the pivot point. In the Figure 2e, the wind

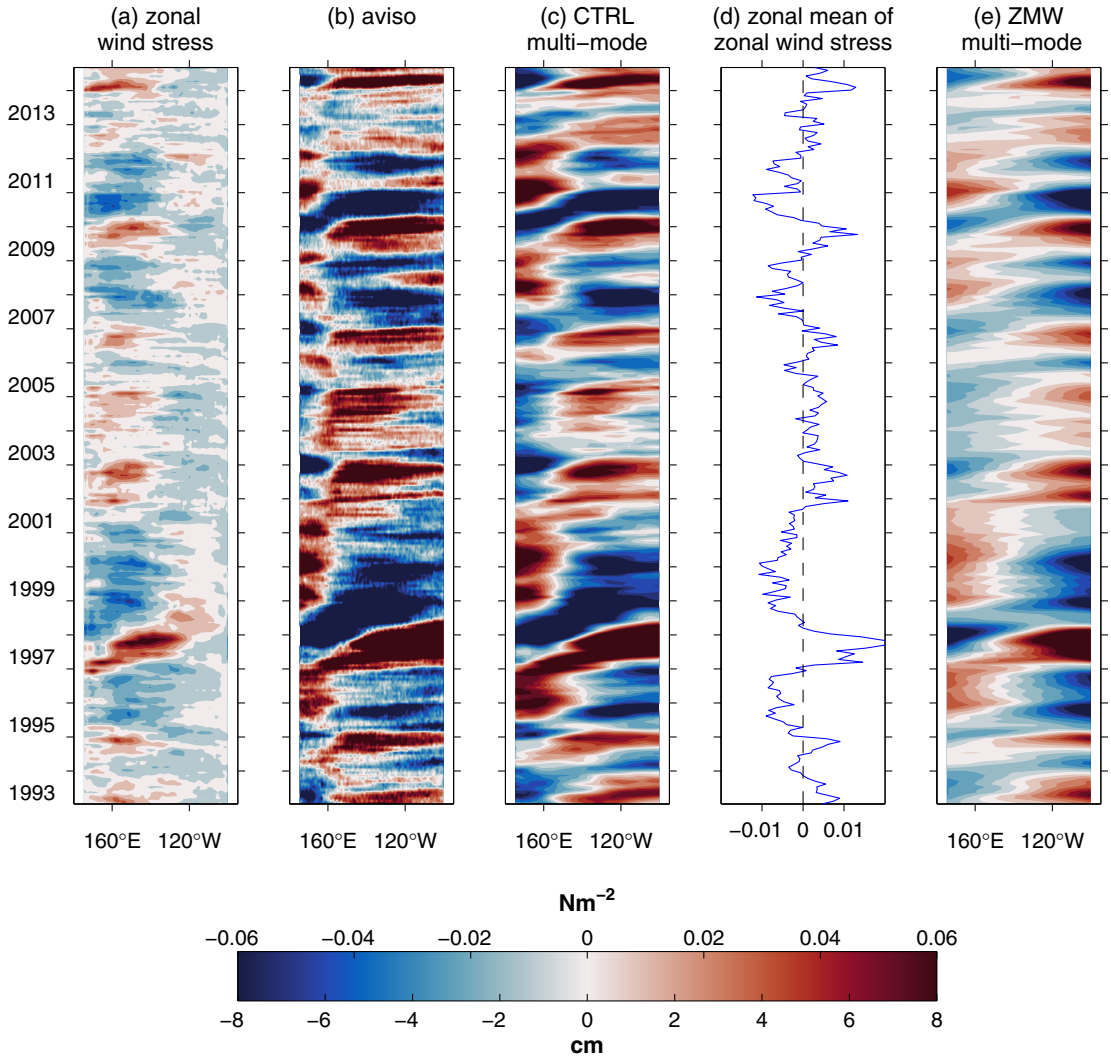

Figure 2. Hovmoeller diagrams along the equator for (a) the zonal wind stress from ERA-Interim used to drive the standard model and (d) the zonal mean zonal wind stress. Also shown are monthly mean sea level anomalies along the equator for (b) AVISO, (c) the multimode model (standard version), (e) the model when driven by the time series of zonal mean zonal wind stress along the equator (shown in Figure 2d), and zero meridional wind stress (experiment ZMW). Units are Nm^{-2} for wind stress and centimeters for sea level.

forcing is purely zonal and spatially uniform and is given by the time series of the zonal mean of the anomalous zonal wind stress along the equator shown in Figure 2d. While it is notable that this experiment captures the same events as the standard experiment (Figure 2b), the pivot point in this experiment is less distinct and is shifted eastward. Looking at Figure 2a, we can see that in reality, most of the variability in the zonal wind stress along the equator is found in the western part of the basin. If the wind stress anomalies are always close to being in equilibrium with the anomalous zonal gradient of sea level along the equator, as implied by the "tilt" mode of *Clarke* [2010], then we would expect the pivot point to the shifted westward in Figure 2c compared to Figure 2e so that it coincides with the region where the variability in the zonal wind stress is highest. That the pivot point tends to be shifted westward from the center of the basin even in Figure 2e is an indication that the recharge/discharge mechanism is operating in our model, an issue discussed further later.

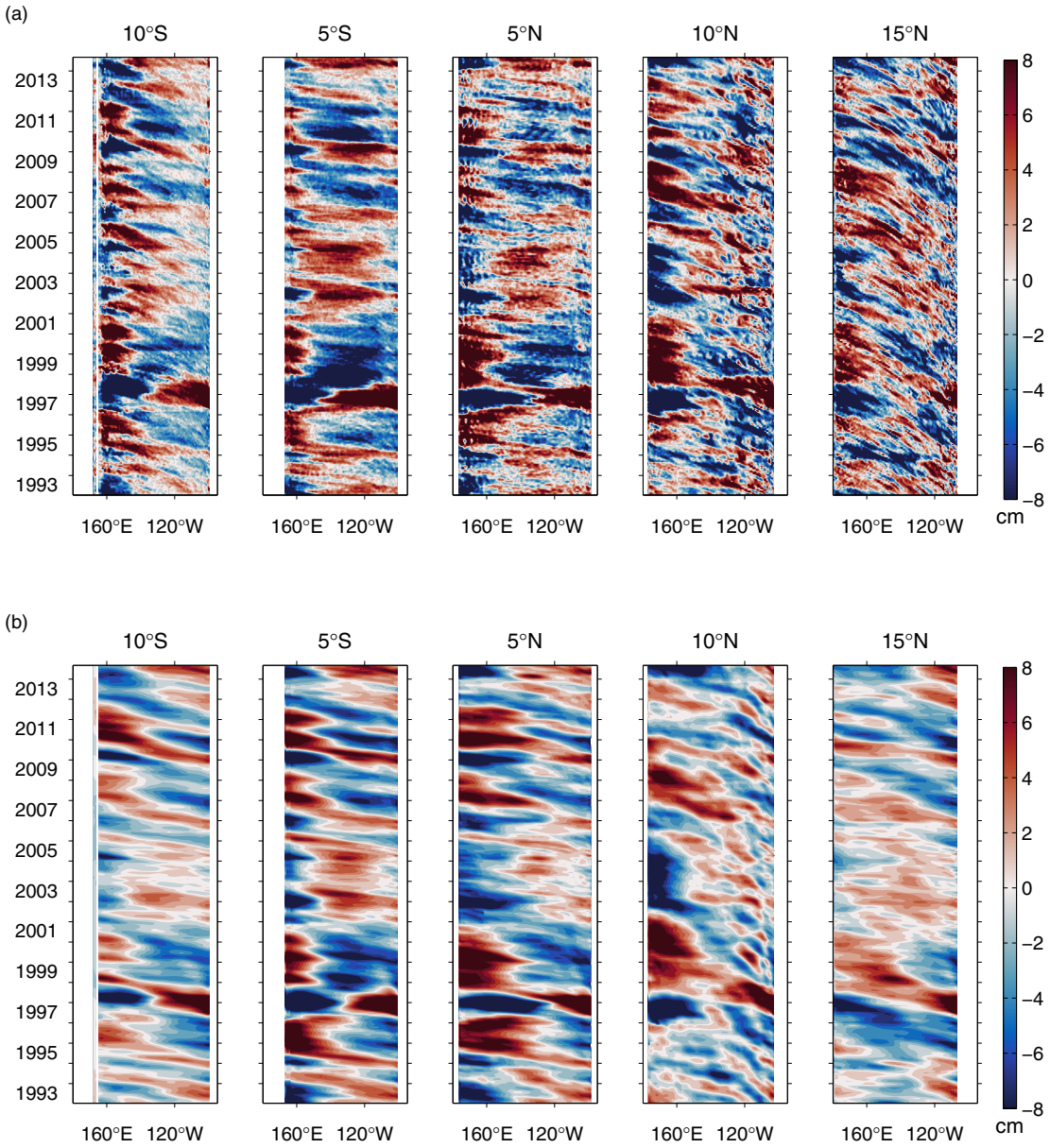

Figure 3. Hovmoeller diagrams of sea level anomalies along 10°S, 5°S, 5°N, 10°N, and 15°N from (a) AVISO and (b) the standard version of the multimode model. Units are centimeters.

Figure 4 shows the contribution to model sea level from each of the five modes. The dominance of the second mode is immediately apparent. Modes 3 and 5, nevertheless, have a role to play; this can be seen most clearly during the major El Niño events of 1997/1998 and 2009/2010, the largest amplitude events in the wind forcing time series. The same conclusion applies if we redraw Figure 4, but this time for the model run shown in Figure 2e that uses spatially uniform wind stress (not shown), implying that the spatial structure of the wind stress is not important for determining the role played by the different modes along the equator. The importance of the second mode is also seen in Figure 5 where the standard deviation of the sea

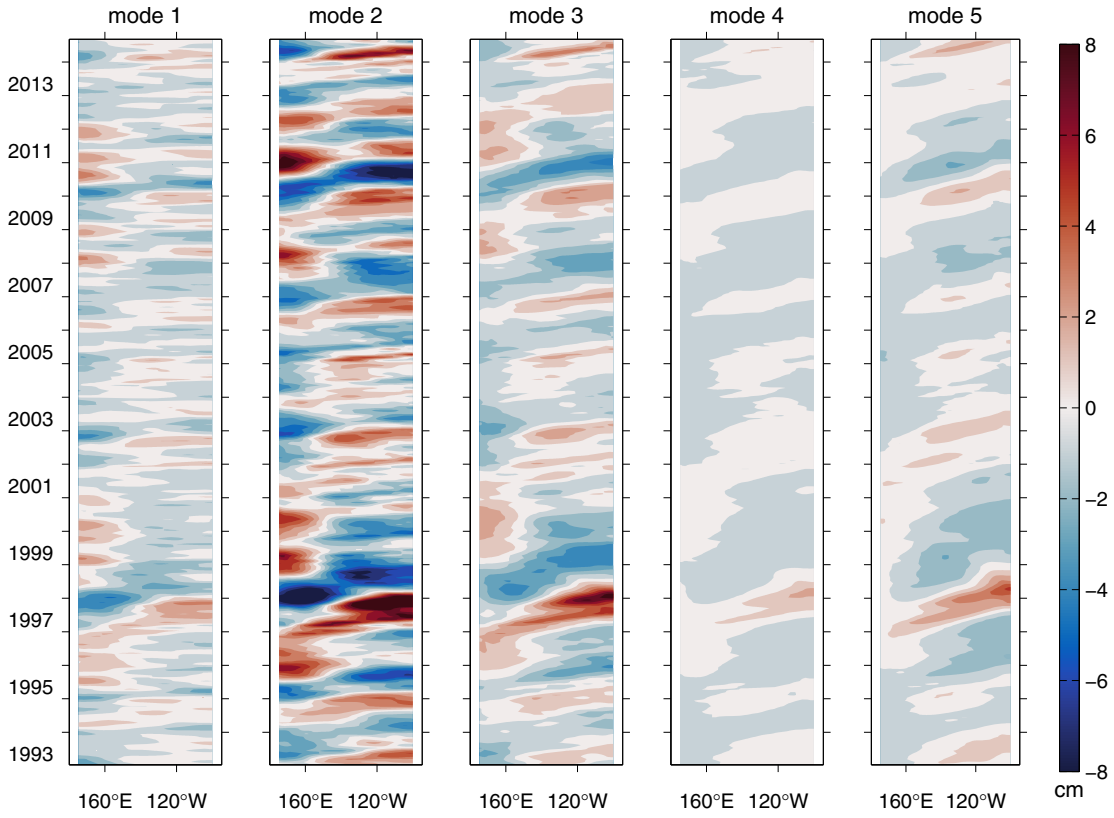

Figure 4. Hovmoeller diagrams along the equator for the contribution to sea level from modes 1–5 in the standard model run. Units are centimeters.

level variability associated with each model is plotted (note the different scale used for the plots for individual modes). Some role for mode 1 is apparent in the western Pacific, for mode 3 in both the western and eastern Pacific and for mode 5 in the eastern Pacific. The dominance of mode 2, even in the western Pacific, is in contrast to the findings of *Dewitte et al*. [1999] that mode 1 was, if anything, slightly more important that mode 2 in the west in their model study covering the period 1985–1994 (see also *Doi et al*. [2010] who make a similar claim). Comparing the full, multimode model with the AVISO data, it is clear that the amplitude of the variability captured by the model is similar to that seen in the observations in the equatorial region and to some extent off the equator near the western and eastern boundaries, especially in the west. However, it is also clear that the model lacks variability in off-equatorial latitudes, one possible reason being the lack of tropical instability waves in the model. Nevertheless, as we noted when discussing Figure 3, many of the events present in the AVISO data are also present in the model.

Figure 6 shows the correlation between the model results and altimetric measurements. It should be noted that a high correlation does not necessarily imply good model performance since correlation contains no information about amplitude, something that should be borne in mind when interpreting the figure. In particular, mode 4 explains little amplitude (Figure 5) but still shows skill with correlation comparable to mode 3. The multimode model (Figure 6a) nevertheless shows high correlations exceeding 0.7 (red coloring) over wide regions, especially near the western and eastern boundaries as well as along the equator where correlations widely exceed 0.8. A notable exception is the reduced correlation near the date line along the equator that arises from the misplacement of the pivot point in the model, noted when discussing Figure 2. There is clearly a related band of reduced correlation that extends eastward from the date line as one moves off the

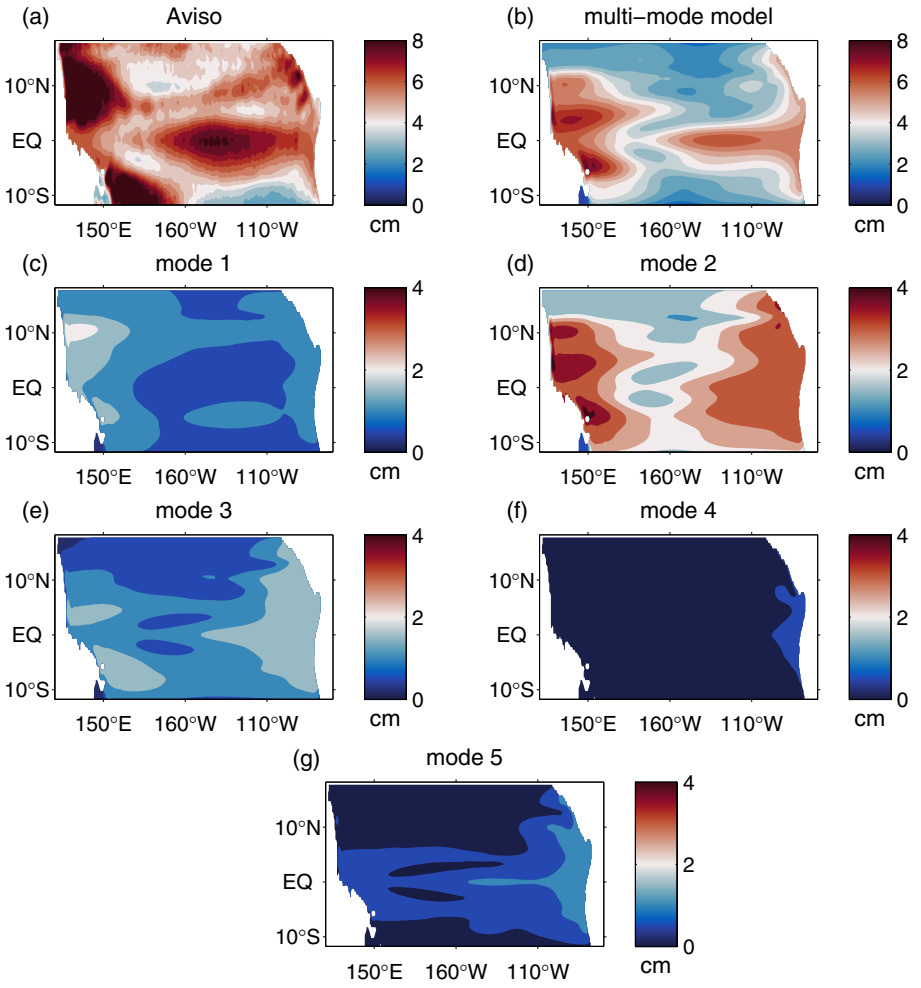

Figure 5. The standard deviations of monthly mean sea level anomalies from (a) AVISO, (b) the multimode model, and (c–g) the contribution from modes 1–5, respectively. Units are centimeters.

equator that is suggestive of a discrepancy between the Rossby wave propagation speeds in the model and the observations, although how this is linked to the reduced correlation on the equator is not clear. This is also the region where the amplitude in the model is low compared to that in AVISO (Figure 5) suggesting the role of processes missing from the model. The longitudinal structure of the correlation along the equator resembles the results from the ocean general circulation model in *Dewitte et al.* [1999] (see their Figure 6), despite the fact the phase speed for each mode is zonally uniform in our model and we are comparing our model sea level anomalies to observations, not to sea level from a model as they are doing. Indeed, it is an interesting point that our model, which uses zonally uniform gravity wave speeds for each mode, shows considerable success at the equator despite the along-equator variations in the gravity wave speeds derived from a normal mode analysis noted by *Picaut and Sombardier* [1993] and also by *Dewitte et al.* [1999]. Interestingly, *Dewitte et al.* [1999] note a drop in the wave speed associated with the baroclinic modes in their model just to the west of the date line (see their Figure 7b). Such a drop in wave speed may be a factor in the misplacement of the pivot point in our model and suggests a role for physical processes other than linear wave dynamics. As noted earlier, a possible candidate is zonal advection which is known to play a role in the western-central Pacific [*Dewitte et al.*, 2013]. Advective processes may also play a role off the equator.

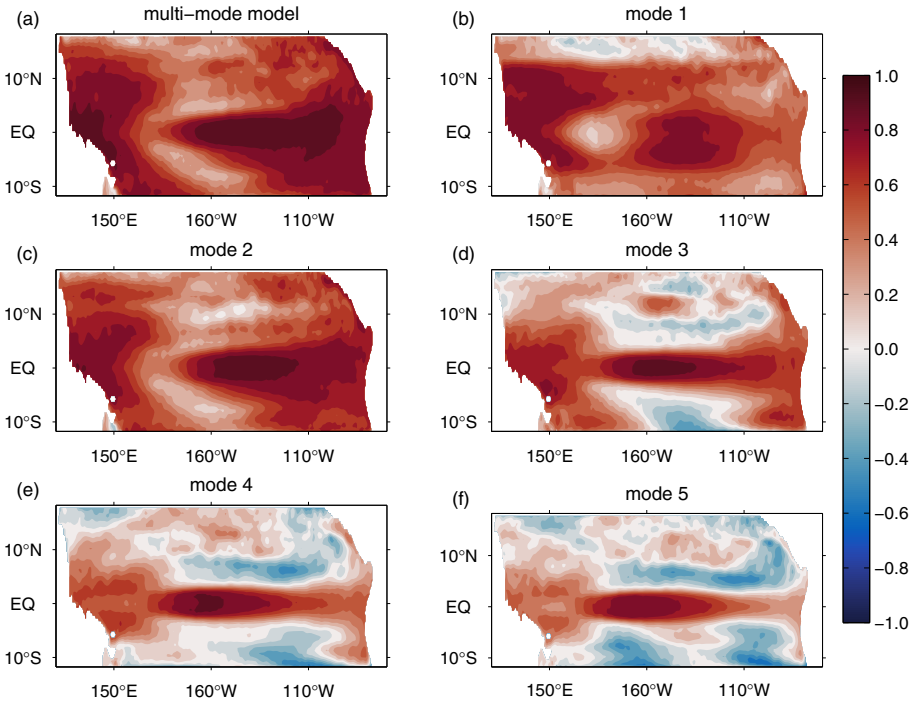

Figure 6. The correlation coefficients between monthly mean sea level anomalies from AVISO and those from (a) the multimode model and (b–f) the contribution from modes 1–5, respectively.

The correlation maps for each individual mode are shown in Figures 6b–6f. It is clear that, overall, the multimodel (Figure 6a) shows better performance compared to any single mode, although mode 1 shows generally higher correlations between 5°N and 10°N. Once again, the second mode comes closest to the performance of the multimode model. Overall, the first two modes show the best performance among the modes in the off-equatorial Pacific (poleward of 5°N/S), whereas the higher modes show high correlation in the equatorial region (5°S–5°N) where modes 3 and 5, in particular, have a role to play, as we noted when discussing Figures 4 and 5. The phase in the eastern equatorial Pacific is almost exclusively affected by mode 2, with modes 1, 4, and 5 playing relatively little role there, while in the west mode 1 becomes more prominent. In the central equatorial Pacific, the correlation maxima slightly shift westward when going from lower to higher modes presumably related to the slower wave propagation speeds and the greater importance of local wind forcing.

Finally, we can examine the recharge/discharge mechanism [*Jin*, 1997] using our model (see *Neelin et al.* [1998] for a review including discussion of the recharge/discharge mechanism). As noted earlier, *Clarke* [2010] characterizes interannual equatorial variability, such as associated with ENSO, with what he calls the "tilt'" mode, in which the thermocline is tilted along the equator in quasi-equilibrium with the zonal wind forcing, and the warm water volume (WWV) associated with a net upward or downward displacement of the thermocline along the equator. *Clarke* [2010] argues that the existence of the WWV depends critically on the variation of the propagation speed for long Rossby waves with latitude and is not related to meridional divergence of the flow due to the wind forcing, as suggested, for example, in the original paper by *Jin* [1997] where an important role is assigned to the Sverdrup transport. We can investigate these modes in our model by looking at the correlation (see Figure 7) between $\bar{\eta}$, the zonal mean sea level along the equator, and the zonal mean of the zonal wind stress along the equator (referred to as $\overline{\tau_x}$ hereafter) shown in Figure 2d. Here, $\bar{\eta}$ is the signature of the WWV volume, being positive/negative when there is a greater volume of warm/cold water along the equator than in the mean.

First, Figure 7a shows the autocorrelation of $\overline{\tau_x}$ indicating a weak tendency for oscillatory behavior with period of about 54 months (~4.5 years) (the dashed blue lines, here, and also in Figures 7b and 7c indicate

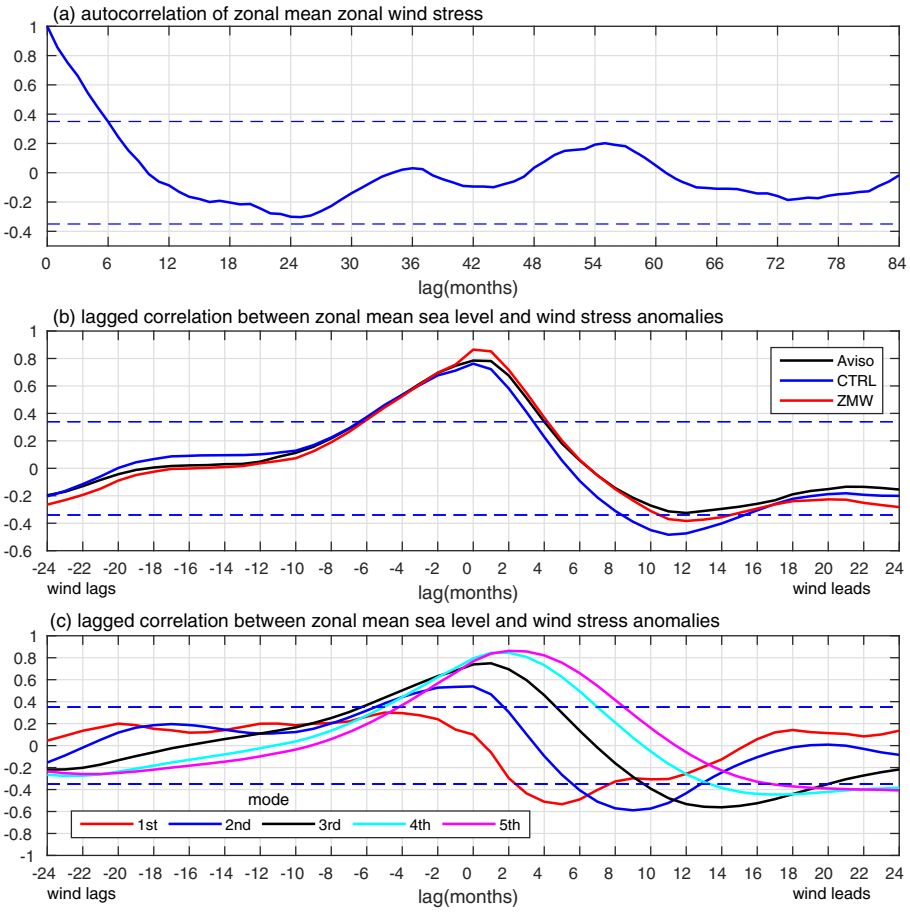

Figure 7. (a) The autocorrelation of zonal mean zonal wind stress along the equator. (b) Lagged correlations between zonal mean monthly sea level anomalies and zonal mean zonal wind stress anomalies along the equator for AVISO, the multimode model in the standard version (labeled CTRL) and model run driven by the time series of zonal mean zonal wind stress along the equator (labelled ZMW). (c) As Figure 7b but for each of modes 1–5 from the standard model run. The horizontal lines indicate the thresholds for correlations to be different from zero at the 95% level and are computed using the method of *Ebisuzaki* [1997].

the 95% significance level). As can be seen from Figure 7b, the correlation between $\overline{\tau_x}$ and $\bar{\eta}$ from the standard multimode model agrees well with that from AVISO. The maximum negative correlation occurs at about 12 months after the peak in the zonal mean zonal wind stress, implying that the WWV lags $\overline{\tau_x}$ by about 1 year or about a quarter cycle of the wind forcing after the wind stress maximum, in agreement with *Clarke* [2010]. In other words, roughly 1 year after a maximum in the eastward wind stress anomaly along the equator, the volume of warm water along the equator reaches a minimum, similar to what is shown in the schematic of *Jin* [1997], his Figure 1. For individual modes (Figure 7c), the WWV of modes 1–5 lag $\overline{\tau_x}$ by about 5, 9, 14, 18 months, and around 20 months (noting that there is no distinct minimum for mode 5), respectively. The increasing lag with mode number is an indication of the reduced wave speeds associated with the higher modes and, in particular, the reduced off-equatorial Rossby wave speeds leading to a slower off-equatorial adjustment, consistent with *Clarke* [2010]. Different from Figure 1 in *Jin* [1997] is the positive correlation at lag 0 that arises when using sea level from both the multimode model and the AVISO data. It is this positive correlation that has a tendency to shift the pivot point, noted when discussing Figure 2, to the west. Assuming that the thermocline slope along the equator is always in equilibrium with the zonal wind stress [see *Clarke*, 2010], then when the anomalous zonal mean zonal wind stress is eastward (westward), the thermocline will be relatively deep in the east (west) and shallow in the west (east). However, the

zero crossing, that is, the pivot point, will be shifted westward from the center of the basin because the anomalous zonal mean thermocline depth is simultaneously displaced downward (upward). Nevertheless, as we noted earlier, this effect seems to be less important than the presence of maximum wind stress variability along the equator in the west. Looking at the individual modes, this positive correlation increases with mode number and for mode 1, is quite weak with the peak positive correlation actually occurring about 4 months before the maximum in zonal mean zonal wind stress. Again, this behavior is an indication of the reduction in the speed of the adjustment process as the mode number increases.

The sensitivity of the recharge/discharge mechanism to the spatial structure of the wind forcing is illustrated by the results of experiment ZMW that uses a spatially uniform zonal wind stress given by the time series of $\overline{\tau_x}$, shown in the Figure 2d, and zero meridional wind stress (see Figure 2e). Figure 7b shows that the correlation between $\overline{\tau_x}$ and $\bar{\eta}$ from this experiment is very little changed from that in the standard experiment showing that the basic dynamics of the recharge/discharge mechanism is not affected in our model by the spatial structure of the wind forcing. Since the Sverdrup transport is zero in this experiment (since the curl of the wind stress is zero), it follows immediately that the recharge/discharge mechanism in our model does not fundamentally depend on the Sverdrup transport, as in the original theory of *Jin* [1997]. Rather our results are consistent with the conclusion of *Clarke* [2010] concerning the variation of the long Rossby wave speed with latitude, especially given the lag dependence on mode number noted when discussing Figure 7c.

The spatial structure of the wind stress, nevertheless, does matter for the amplitude of the WWV along the equator. This is illustrated in Figure 8 showing the time series of the modeled zonal mean sea level along the equator (corresponding to the WWV) compared to AVISO data. We first note that the amplitude captured by the standard model (labeled CTRL) is generally less than that seen in AVISO, although still a significant fraction of the latter, and that the two time series are highly correlated. Next we note that the amplitude in the model run with spatially uniform forcing (labeled ZMW) is less than that in CTRL indicating a role for the spatial structure of the wind forcing in determining the amplitude of the WWV. In a further experiment (labelled LatZM), only the zonal wind stress is used and this is given by the time series of the zonal mean of the zonal wind stress at each latitude and so has no variations with longitude. Generally, this increases the amplitude of the WWV along the equator compared to ZMW but still does not explain all the amplitude captured by CTRL, implying a role for zonal variations in the zonal wind stress along the equator for determining the amplitude of the WWV (note that the WWV in CTRL does not depend on the meridional wind stress as can easily be shown by running an experiment driven by the zonal wind stress only).

To understand this further, we note that zonally integrating equation (12) gives us the equation for $\bar{\eta}_n$, the contribution to $\bar{\eta}$ from mode n,

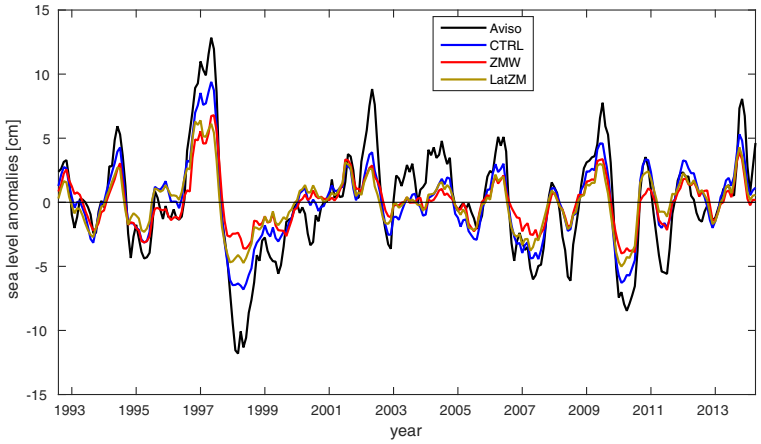

Figure 8. The time series of the zonal mean sea level anomaly along the equator from AVISO, the standard experiment (CTRL), the experiment with spatially uniform wind stress (ZMW), and the experiment run using zonal wind stress that is zonally uniform at each latitude (LatZM).

$$(\lambda_E-\lambda_W)\frac{\partial\bar{\eta}_n}{\partial t}+\frac{H_n}{a\cos\theta}\frac{\partial}{\partial\theta}\left(\int_{\lambda_W}^{\lambda_E}\cos\theta\ v_n d\lambda\right)=0. \quad (17)$$

where λ_E and λ_W are the longitudes at the eastern and western boundaries of the model domain, respectively. *Clarke* [2010] noted that in his analytic solutions, there is a tendency for the zonal and meridional divergence to cancel (as in the Sverdrup balance). However, as is clear from equation (17), for $\bar{\eta}_n$ to change, there must be a net meridional divergence at the equator, as indicated by the derivative with respect to latitude. We have seen that to understand the basic dynamics it is enough to consider the case with spatially uniform wind forcing (for which the Sverdrup transport is zero). Consider the spin-up from a state of rest with $\eta_n=0$ following the sudden switch-on of a spatially uniform zonal wind forcing. For eastward wind forcing, the associated Ekman transport leads to convergence on the equator and an increase in η_n, consistent with the picture at zero lag in Figures 7b and 7c. More than an equatorial Rossby radius from the equator, there is a corresponding Ekman divergence, leading to a reduction in η_n. The reduction in η_n propagates to the equator as Kelvin waves along the western boundary and then along the equator as equatorial Kelvin waves, leading to the negative correlation in Figures 7b and 7c at positive lags. It should be noted that the effect of wave propagation is to counter the Ekman convergence/divergence so that in steady state, $u=v=0$ and the zonal wind stress is exactly balanced everywhere by the zonal pressure gradient given by an east-west slope in η_n [e.g., *McCreary*, 1981] (It is worth noting that in the general case, the final steady state is given by the Sverdrup balance everywhere in the domain. Since the Sverdrup balance applies to the steady state, at least in the context of the linear dynamics being considered here, it follows immediately that the recharge/discharge mechanism cannot be associated with Sverdrup balance since the recharge/discharge mechanism is fundamentally unsteady.). The correlations we see in Figures 7b and 7c therefore arise from the incomplete nature of the adjustment to the changing wind forcing across the model domain, including the off-equatorial regions, with longer lags the higher the mode, consistent with the longer adjustment time the higher the mode. This interpretation is basically as described in the review paper by *Neelin et al.* [1998] but here nicely illustrated using our multimode model and shown to be consistent with satellite altimeter data, that is, AVISO.

4. Summary

We have used a multimode shallow water model to examine sea level variability as seen in satellite altimetry (AVISO) over the period 1993–2014 (see http://www.aviso.altimetry.fr/duacs/). The weighting given to each mode was assigned by fitting the model results to the observed sea level variability along the equator. The weighting in turn defines the vertical profile for the wind stress forcing which, as can be seen in Figures 1b and 1c is strongly surface intensified, as one would expect. Using seven or more modes, it was not possible to assign a realistic weight to each mode, presumably because the signal associated with mode 7 or higher cannot be extracted from the AVISO data. Since the sixth mode is associated with basically zero amplitude, we used the first five modes for our study.

The results show a remarkable agreement between the model sea level and the AVISO data, particularly along the equator but also at higher latitudes where the main events in the monthly mean AVISO data are captured. The model successfully captures the ENSO events of various strengths and flavors, including the conventional El Niño events of 1997/1998, 2006/2007 and 2009/2010) and the Modoki El Niño events of 1994/1995, 2002/2003, and 2004/2005 [*Ashok et al.*, 2007] as well as the 1995/1996, 1998/1999, 2007/2008 and 2010/2011 La Niña events. The dominance of the second baroclinic mode is apparent, although with some role for modes 1, 3, and 5, particularly in the western equatorial Pacific for mode 1, the eastern equatorial Pacific for mode 5, and both regions for mode 3. The higher modes are particularly prominent during the major El Niño events of 1997/1998, 2006/2007, and 2009/2010 (see Figure 4) when the wind forcing is particularly large in amplitude. We argue that one reason for differences in the weighting assigned to the different modes here from previous studies is the freedom we give the model to choose the vertical profile for the wind forcing in the model based on the fitting to the altimeter data.

An interesting feature of our results is the presence of a pivot point in the western Pacific on the equator, either side of which sea level variations tend to be 180° out of phase. The placement of the pivot point seems to depend mostly on the fact that most of the variations in zonal wind stress are found in the western part of the basin, although there is also a signature from the recharge/discharge mechanism in which

eastward/westward zonal mean zonal wind stress anomalies are associated with a downward/upward displacement of the zonal mean thermocline along the equator at zero lag. We also showed that the recharge/discharge mechanism in the model does not depend for its basic dynamics on the spatial structure of the wind forcing and, in particular, on the Sverdrup transport as in the original theory of *Jin* [1997], and is more in agreement with the approach of *Clarke* [2010]. The spatial structure of the wind forcing nevertheless has a role to play in determining the amplitude of the "warm water volume" along the equator.

Acknowledgments
Xiaoting Zhu is grateful for funding from the China Scholarship Council (201306330071).This study has also been supported by the Deutsche Forschungsgemeinschaft as part of the Sonderforschungsbereich 754 "Climate-Biogeochemistry interactions in the Tropical Ocean", through the German Ministry for Education and Research (BMBF) through MiKlip2, subproject 01LP1517D (ATMOS-MODINI) and SACUS (03G0837A), and by the European Union 7th Framework Programme (FP7 2007-2013) under grant agreement 603521 PREFACE project. We are also grateful to two anonymous reviewers for their helpful comments. The data used in this study can be obtained from Xiaoting Zhu (xzhu@geomar.de) on request.

References

Ashok, K., S. K. Behera, S. A. Rao, H. Weng, and T. Yamagata (2007), El Nino Modoki and its possible teleconnection, *J. Geophys. Res.*, *112*, C11007, doi:10.1029/2006JC003798.
Berrisford, P., D. Dee, K. Fielding, M. Fuentes, P. Kallberg, S. Kobayashi, and S. Uppala (2009), The ERA-Interim Archive, *ERA Rep. Ser.*, *1*(1), 1–16.
Brandt, P., M. Claus, R. J. Greatbatch, R. Kopte, J. M. Toole, W. E. Johns, and C. W. Böning (2016), Annual and semi-annual cycle of equatorial Atlantic circulation associated with basin mode resonance, *J. Phys. Oceanogr.*, *46*(10), 3011–3029.
Busalacchi, A. J., and M. A. Cane (1985), Hindcasts of sea level variations during the 1982-83 El Nino, *J. Phys. Oceanogr.*, *15*(2), 213–221.
Busalacchi, A. J., and J. J. O'Brien (1981), Interannual variability of the equatorial Pacific in the 1960's, *J. Geophys. Res.*, *86*(C11), 10,901–10,907, doi:10.1029/JC086iC11p10901.
Busalacchi, A. J., K. Takeuchi, and J. J. O'Brien (1983), Interannual variability of the equatorial Pacific Revisited, *J. Geophys. Res.*, *88*(C12), 7551–7562, doi:10.1029/JC088iC12p07551.
Cane, M. A. (1984), Modeling sea level during El Nino, *J. Phys. Oceanogr.*, *14*(12), 1864–1874.
Clarke, A. J. (2010), Analytical theory for the quasi-steady and low-frequency equatorial ocean response to wind forcing: The tilt and warm water volume modes, *J. Phys. Oceanogr.*, *40*(1), 121–137, doi:10.1175/2009JPO4263.1.
Delcroix, T. (1998), Observed surface oceanic and atmospheric variability in the tropical Pacific at seasonal and ENSO timescales: A tentative overview, *J. Geophys. Res.*, *103*(C9), 18,611–18,633, doi:10.1029/98JC00814.
Dewitte, B., G. Reverdin, and C. Maes (1999), Vertical structure of an OGCM simulation of the equatorial Pacific ocean in 1985-94, *J. Phys. Oceanogr.*, *29*(7), 1542–1570.
Dewitte, B., S.-W. Yeh, and S. Thual (2013), Reinterpreting the thermocline feedback in the western-central equatorial pacific and its relationship with the Enso modulation, *Clim. Dyn.*, *41*(3-4), 819–830, doi:10.1007/s00382-012-1504-z.
Doi, T., T. Tozuka, and T. Yamagata (2010), Equivalent forcing depth in tropical oceans, *Dyn. Atmos. Oceans*, *50*(3), 415–423, doi:10.1016/j.dynatmoce.2010.03.001.
Ebisuzaki, W. (1997), A method to estimate the statistical significance of a correlation when the data are serially correlated, *J. Clim.*, *10*(9), 2147–2153.
Forget, G., and R. M. Ponte (2015), The partition of regional sea level variability, *Prog. Oceanogr.*, *137*, 173–195, doi:10.1016/j.pocean.2015.06.002.
Gill, A. E. (1982), *Atmosphere-Ocean Dynamics*, 662 pp., Academic, San Diego, Calif.
Gill, A. E., and A. J. Clarke (1974), Wind-induced upwelling, coastal currents and sea-level changes, *Deep Sea Res. Oceanogr. Abstr.*, *21*, 325–345.
Jin, F.-F. (1997), An equatorial ocean recharge paradigm for ENSO. Part I: Conceptual model, *J. Atmos. Sci.*, *54*(7), 811–829.
Locarnini, R. A., et al. (2013), *World Ocean Atlas 2013. Vol. 1: Temperature*, edited by S. Levitus and A. Mishonov *NOAA Atlas NESDIS*, 73, 40 pp.
McCreary, J. (1981), A linear stratified ocean model of the equatorial undercurrent, *Philos. Trans. R. Soc. London A*, *298*(1444), 603–635.
McPhaden, M. J., and X. Yu (1999), Equatorial waves and the 1997–98 El Nino, *Geophys. Res. Lett.*, *26*(19), 2961–2964.
McPhaden, M. J., J. A. Proehl, and L. M. Rothstein (1986), The interaction of equatorial kelvin waves with realistically sheared zonal currents, *J. Phys. Oceanogr.*, *16*(9), 1499–1515.
Meinen, C. S., and M. J. McPhaden (2000), Observations of warm water volume changes in the equatorial pacific and their relationship to El Niño and La Niña, *J. Clim.*, *13*(20), 3551–3559.
Meinen, C. S., and M. J. McPhaden (2001), Interannual variability in warm water volume transports in the equatorial pacific during 1993-99*, *J. Phys. Oceanogr.*, *31*(5), 1324–1345.
Moon, B.-K., S.-W. Yeh, B. Dewitte, J.-G. Jhun, I.-S. Kang, and B. P. Kirtman (2004), Vertical structure variability in the equatorial pacific before and after the pacific climate shift of the 1970s, *Geophys. Res. Lett.*, *31*, L03203, doi:10.1029/2003GL018829.
Neelin, J. D., D. S. Battisti, A. C. Hirst, F.-F. Jin, Y. Wakata, T. Yamagata, and S. E. Zebiak (1998), ENSO theory, *J. Geophys. Res.*, *103*(C7), 14,261–14,290, doi:10.1029/97JC03424.
Philander, S. G. H. (1989), *El Niño, La Niña, and the Southern Oscillation*, 662 pp., Academic, San Diego, Calif.
Philander, S. G. H., and R. Pacanowski (1980), The generation of equatorial currents, *J. Geophys. Res.*, *85*(C2), 1123–1136.
Picaut, J., and L. Sombardier (1993), Influence of density stratification and bottom depth on vertical mode structure functions in the tropical Pacific, *J. Geophys. Res.*, *98*(C8), 14,727–14,737, doi:10.1029/93JC00885.
Trenberth, K. E., G. W. Branstator, D. Karoly, A. Kumar, N. C. Lau, and C. Ropelewski (1998), Progress during TOGA in understanding and modeling global teleconnections associated with tropical sea surface temperatures, *J. Geophys. Res.*, *103*(C7), 14,291–14,324, doi:10.1029/97JC01444.
Yu, X., and M. J. McPhaden (1999), Seasonal variability in the equatorial pacific, *J. Phys. Oceanogr.*, *29*(5), 925–947.

3 Reconstructing Tropical Pacific Sea Level Variability for The Period 1961-2002 Using A Linear Multi-mode Model

In this chapter, the model built in Chapter 2 is applied to the pre-satellite era driven by ERA-40 and NCEP/NCAR monthly wind stress anomalies for comparison, since the latter was reported having spurious trends in the eastern Pacific. The westward shift in the pivot point over the period 1961-2014 is investigated and is attributed to an increase in zonal wind stress variance of the western equatorial Pacific over the same time period.

Citation: **Greatbatch, R. J., X. Zhu, and M. Claus (2018), Reconstructing tropical pacific sea level variability for the period 1961-2002 using a linear multi-mode model, Journal of Geophysical Research: Oceans, doi:10.1002/ 2017JC013652.**

The candidate's contribution to this publication are as below:

1. *Setting up and running of the model*
2. *Analysis of the model results*
3. *Preparing and analysis of the observational datasets*
4. *Production of all figures*
5. *Contributing to the ideas in the manuscript*
6. *Drafting the first version of the manuscript*

AGU PUBLICATIONS

JGR

Journal of Geophysical Research: Oceans

RESEARCH ARTICLE
10.1002/2017JC013652

Reconstructing Tropical Pacific Sea Level Variability for the Period 1961–2002 Using a Linear Multimode Model

Richard J. Greatbatch[1,2], Xiaoting Zhu[1], and Martin Claus[1,2]

[1]Ocean Circulation and Climate Dynamics, GEOMAR Helmholtz Centre for Ocean Research Kiel, Kiel, Germany, [2]Faculty of Mathematics and Natural Sciences, University of Kiel, Kiel, Germany

Key Points:
- A linear, multimode model driven by reanalysis wind stress products has skill at reproducing monthly mean sea level variability as measured by tide gauges in the presatellite era
- A spurious eastward trend in the zonal wind stress in the NCEP/NCAR product leads to a spurious upward trend in model-computed sea level in the eastern Pacific
- The pivot point at the equator was further west during 1993–2014 than earlier due to an upward trend in zonal wind stress variance in the western equatorial Pacific

Correspondence to:
R. J. Greatbatch,
rgreatbatch@geomar.de

Citation:
Greatbatch, R. J., Zhu, X., & Claus, M. (2018). Reconstructing tropical pacific sea level variability for the period 1961–2002 using a linear multimode model. *Journal of Geophysical Research: Oceans*, *123*. https://doi.org/10.1002/2017JC013652

Received 27 NOV 2017
Accepted 26 FEB 2018
Accepted article online 2 MAR 2018

Abstract Monthly mean sea level anomalies in the tropical Pacific for the period 1961–2002 are reconstructed using a linear, multimode model driven by monthly mean wind stress anomalies from the NCEP/NCAR and ERA-40 reanalysis products. Overall, the sea level anomalies reconstructed by both wind stress products agree well with the available tide gauge data, although with poor performance at Kanton Island in the western-central equatorial Pacific and reduced amplitude at Christmas Island. The reduced performance is related to model error in locating the pivot point in sea level variability associated with the so-called "tilt" mode. We present evidence that the pivot point was further west during the period 1993–2014 than during the period 1961–2002 and attribute this to a persistent upward trend in the zonal wind stress variance along the equator west of 160° W throughout the period 1961–2014. Experiments driven by the zonal component of the wind stress alone reproduce much of the trend in sea level found in the experiments driven by both components of the wind stress. The experiments show an upward trend in sea level in the eastern tropical Pacific over the period 1961–2002, but with a much stronger upward trend when using the NCEP/NCAR product. We argue that the latter is related to an overly strong eastward trend in zonal wind stress in the eastern-central Pacific that is believed to be a spurious feature of the NCEP/NCAR product.

1. Introduction

In the tropical Pacific, simplified ocean models (e.g., reduced-gravity, shallow water models) driven by estimates of the observed wind stress are able to reproduce sea level fluctuations not only on the interannual time scale (Qiu & Chen, 2012; Zhu et al., 2017) but also on decadal and multidecadal time scales (Qiu & Chen, 2012; Timmermann et al., 2010). However, before the satellite era, the only direct measurements of sea level are from tide gauges, mostly located on islands, resulting in a very sparse spatial coverage compared to that from the satellite altimeter, leading to uncertainty in the variability of sea level in the presatellite era on a range of time scales (Rhein et al., 2013). There are also uncertainties in simulated and projected sea level rise in climate models (Church et al., 2013), not least arising from uncertainties in the initial conditions used for future projections (Bordbar et al., 2015).

Given that a multimode linear model has considerable success at reproducing interannual sea level variability in the tropical Pacific as seen by the satellite altimeter (Zhu et al., 2017), one way to estimate sea level variability in the presatellite era is to run the same model using estimates of the surface wind stress from reanalysis, e.g., the 40 year European Centre for Medium-Range Weather Forecasts (ECMWF) Reanalysis (ERA-40) (Kalnay et al., 1996) and/or the National Center for Environmental Prediction/National Center for Atmospheric Research (NCEP/NCAR) Reanalysis (Uppala et al., 2005). However, these wind stress products are, themselves, subject to error that can, in turn, lead to errors in the simulated sea level variability. The problem is highlighted by a recent study using the Max Planck Institute Earth System Model (Pohlmann et al., 2017). These authors demonstrate that a large artificial trend in NCEP/NCAR-zonal wind stress in the eastern-central tropical Pacific reduces the hindcast prediction skill for sea surface temperature in the tropical Pacific when the NCEP/NCAR product is used as part of the initialization.

The objective of the present study is to reconstruct monthly sea level variability in the equatorial Pacific for the period 1961–2002 using the linear, multimode model of Zhu et al. (2017) driven by monthly mean wind stress fields from the NCEP/NCAR and ERA-40 reanalysis products. The multimodel of Zhu et al. (2017) has its origin in the early work by Busalacchi and O'Brien (1981) and Busalacchi et al. (1983). However, unlike

those early studies that consider only a single baroclinic normal mode, Zhu et al. (2017) consider the first five baroclinic normal modes. They also do not specify a vertical structure for the wind forcing term; rather, the vertical structure is derived by fitting model-computed sea level variability to that seen by satellite data along the equator. Nagura and McPhaden (2010) take a similar approach to modeling the equatorial Indian Ocean but restricting to long, equatorial waves (waves for which the zonal flow is in geostrophic balance along the equator) and using a method based on McCreary (1981) to project the wind forcing onto the different vertical modes. Likewise, Qiu and Chen (2012) have used a nonlinear, $1\frac{1}{2}$ layer model driven by observed wind stress to simulate tropical Pacific sea level variability over the period 1993–2009.

The paper is organized as follows. In section 2, the model setup and data are described. In section 3, we show the reconstructed sea level anomalies obtained using the linear, multimode model and validate the model performance against the available tide gauge and satellite data. We also examine the model-computed trends in sea level and the impact of the trend in the NCEP/NCAR reanalysis noted by Pohlmann et al. (2017) on the modeled sea level. The interannual variability is, not surprisingly, dominated by El Niño-Southern Oscillation (ENSO) events (Becker et al., 2012) and leads us into a discussion of the pivot point in the western-central Pacific that is a manifestation of the "tilt" mode of Clarke (2010) and the associated trends in zonal wind stress variance. Finally, section 4 provides a summary and discussion.

2. Methods

We adopt the linear, multimode model described in Zhu et al. (2017). This model is a linear combination of linear, shallow water models for the first five baroclinic vertical normal modes (see Gill (1982) and McCreary (1981) for a discussion of vertical normal modes). The weighting given to each mode is the same as used in Zhu et al. (2017) and was obtained by running the model using monthly mean wind stress anomalies from ERA-Interim and fitting the simulated sea level anomalies along the equator to those of the satellite altimeter measured sea level anomalies produced by Ssalto/Duacs and distributed by AVISO with support from Cnes (http://www.aviso.altimetry.fr/duacs/; hereafter, this data set is referred to as AVISO). Readers who are interested in the details are referred to Zhu et al. (2017).

In our experiments, except for the wind forcing, the model configuration is the same as in Zhu et al. (2017), including the model domain (12°S–18°N, 112°E–70°W), coastline (300 m isobath), horizontal resolution (0.5°×0.5°), boundary conditions (solid walls at the eastern/western boundaries, sponge layers applied to the momentum equations at the northern/southern boundaries with e-folding scale of 5° in latitude) and a horizontal eddy viscosity of 5,000 $m^2\ s^{-1}$.

Two standard experiments are, respectively, driven by monthly mean wind stress anomalies from the National Center for Environmental Prediction/National Center for Atmospheric Research (NCEP/NCAR hereafter) Reanalysis (Uppala et al., 2005) and the 40 year European Centre for Medium-Range Weather Forecasts (ECMWF) Reanalysis (ERA-40 hereafter) (Kalnay et al., 1996). Both model runs are carried out for the period from the 1 September 1957 to the 1 August 2002 and the analysis period is 1 January 1961 to 1 August 2002 to exclude the model spin-up.

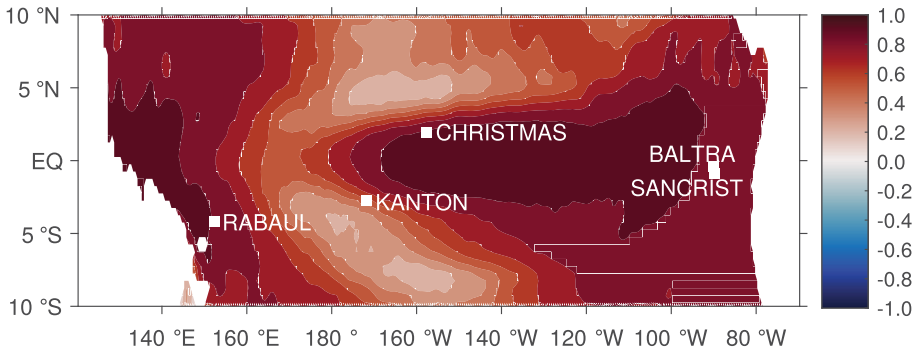

Figure 1. Locations of tide gauge stations (white squares): Rabaul in the western basin, Kanton Island and Christmas Island in the central basin, Baltra Island and Sancrist Island in the eastern basin. The contour shading denotes the correlation between monthly means of AVISO and model-computed sea level for the period 1993–2014 (using the same color scale as in Figure 6a of Zhu et al. (2017) and note that there are no negative correlations in the region shown).

The wind stress anomalies are referenced to the respective monthly mean wind stress climatologies from NCEP/NCAR and ERA-40 for the analysis period 1961–2002. These two standard experiments are called the NCEP/NCAR experiment and the ERA-40 experiment, respectively. In addition, we also conduct two sensitivity experiments forced only by zonal wind stress anomalies from the NCEP/NCAR and ERA-40 data sets; these experiments are called NCEP/NCAR-zonal and ERA-40-zonal, respectively. We also make use of the results from the standard experiment of Zhu et al. (2017) that is driven by monthly mean wind stress anomalies from the ERA-Interim reanalysis (Berrisford et al., 2009). In this experiment, the anomalies are referenced to the period 1993–2014.

To validate the model, we use sea level obtained from the tide gauge stations marked in Figure 1. The data were downloaded from the Permanent Service for Mean Sea Level (Holgate et al., 2013; PSMSL, 2016). We also use the satellite measured sea level anomalies from January 1993 to September 2014 from AVISO at $1/4^{\circ}$ resolution in latitude and longitude.

3. Results

3.1. The Model Performance

To gain an overview of the model performance, we first show Hovmoeller diagrams of the zonal wind stress and sea level anomalies along the equator from the NCEP/NCAR and ERA-40 experiments (Figure 2). Both

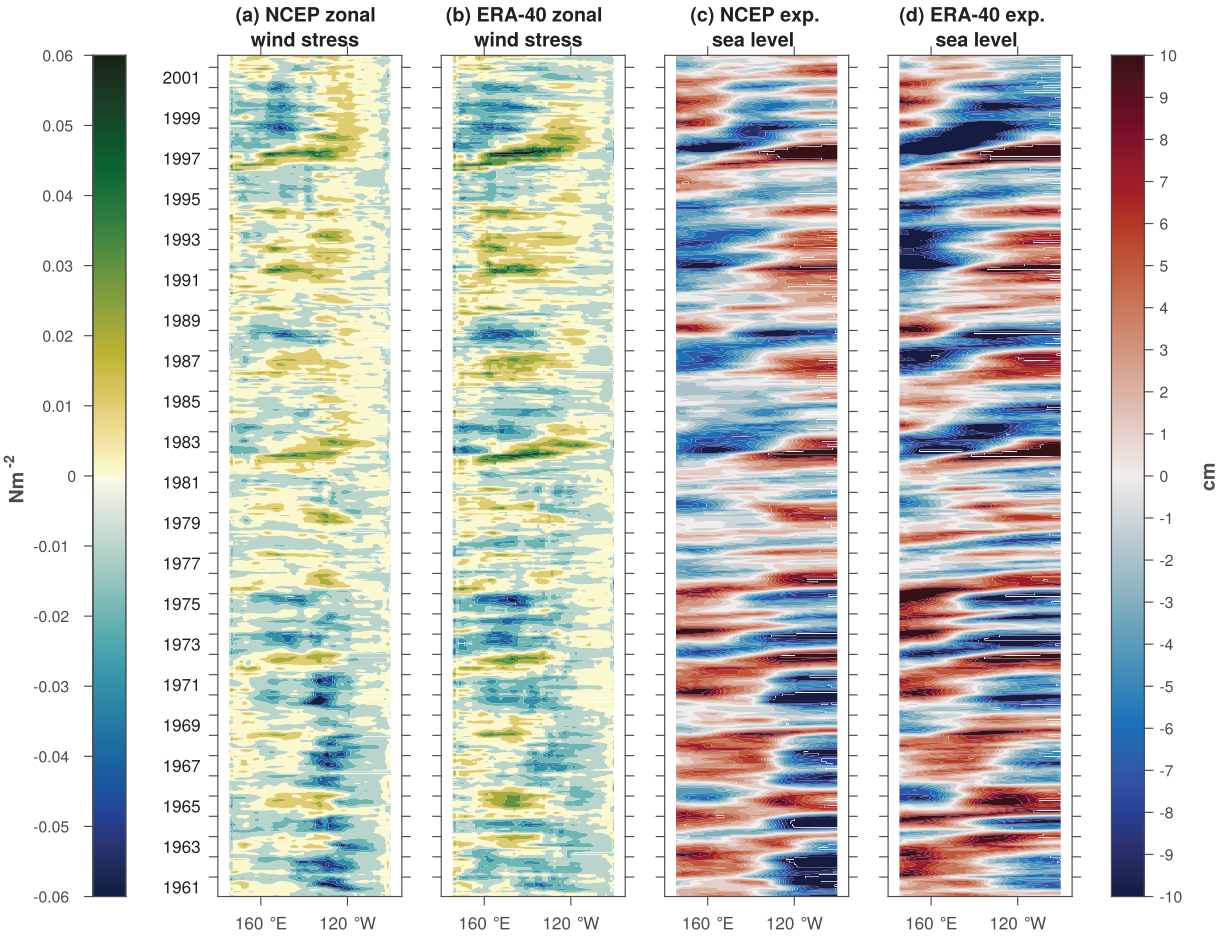

Figure 2. Hovmoeller diagrams along the equator, showing monthly means of zonal wind stress anomalies from (a) the NCEP/NCAR and (b) the ERA-40 products, and model-computed sea level anomalies from (c) the NCEP/NCAR experiment and (d) the ERA-40 experiment.

experiments reproduce the documented El Niño events (e.g., 65/66, 72/73, 82/83, 86/87, and 97/98 El Niños) and La Niña events (e.g., 64/65, 70/71, 84/85, 88/89, and 99/00 La Niñas) (Wang & Fiedler, 2006), where the 86/87 El Niño (Ashok et al., 2007) and the 88/89 La Niña (Capotondi et al., 2015) are examples of Modoki ENSO events. Comparing the two experiments, NCEP/NCAR-zonal wind stress anomalies (Figure 2a) experience a large eastward trend near 120°W during 1961–2002, which is missing from ERA-40 (Figure 2b), as reported by Pohlmann et al. (2017). There is a corresponding positive trend in sea level in the eastern equatorial Pacific basin in the case driven by NCEP/NCAR wind stress anomalies (Figure 2c) that, again, is missing from the ERA-40 experiment (Figure 2d) and which we discuss further in section 3.2. An interesting feature of the results of both experiments is the presence of a "pivot" point near the center of the basin about which the modeled sea level along the equator has a tendency to tip up and down, as in a see-saw. The presence of the pivot point is the manifestation of the "tilt" mode that has been discussed by Clarke (2010). The pivot point was noted by Zhu et al. (2017) in their model experiments and is also found in AVISO, a topic we discuss in more detail in section 3.3.

To evaluate the performance of the models in more detail, Figure 3 compares the sea level anomaly time series from the NCEP/NCAR and ERA-40 experiments with the tide gauge observations at the five tide gauge stations marked in Figure 1 (all data are monthly means). As a check, the tide gauge data are verified against AVISO, i.e., during the satellite era, in Figure 4, from which it is clear that there is good agreement. (Note the suggestion of a problem with the tide gauge at Rabaul between 1995 and 1998 given the offset

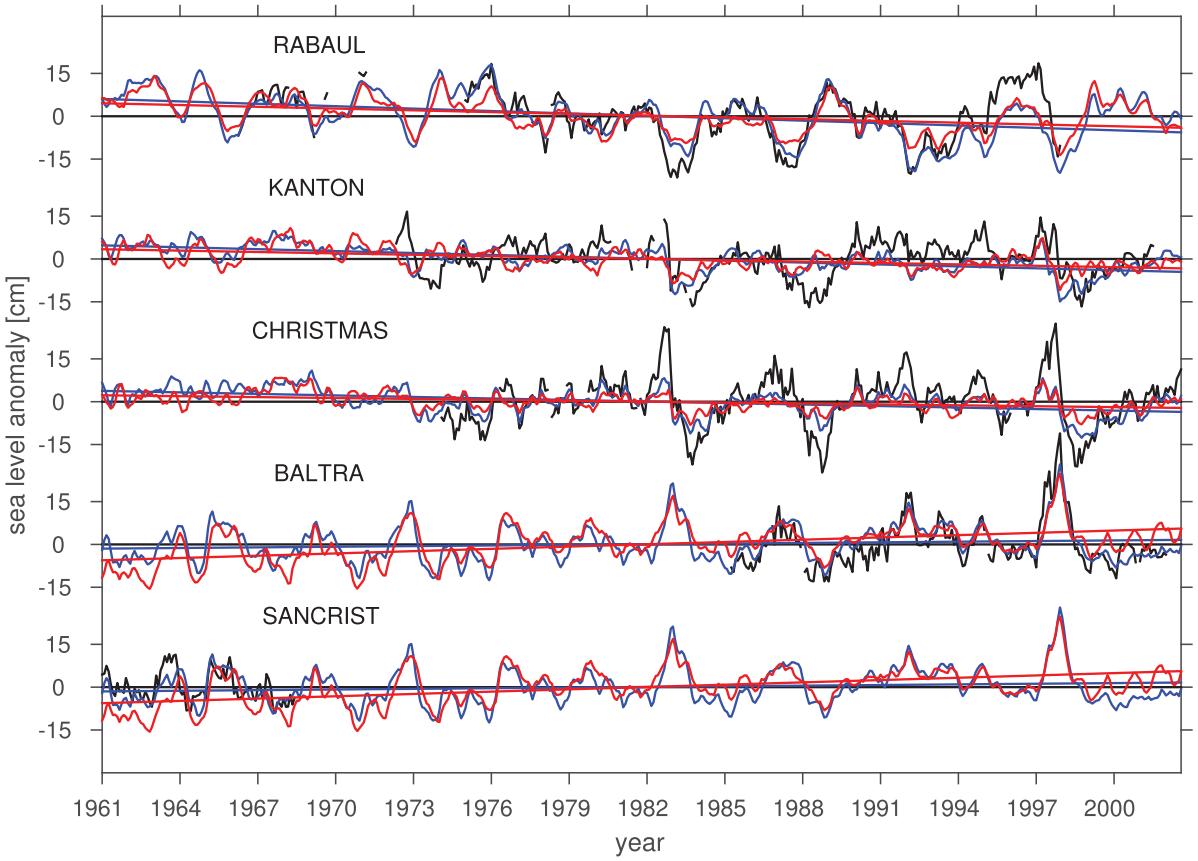

Figure 3. The time evolution of monthly mean sea level anomalies (in cm) from the tide gauge measurements (black lines), the NCEP/NCAR experiment (red lines), and the ERA-40 experiment (blue lines) at the tide gauge locations shown in Figure 1. Trends are shown by corresponding, colored straight lines. Here the labeling on the *x* axis refers to 1 January of each year. Note also that there is only a short time period, from 1961 to 1968, for which data are available from Sancrist.

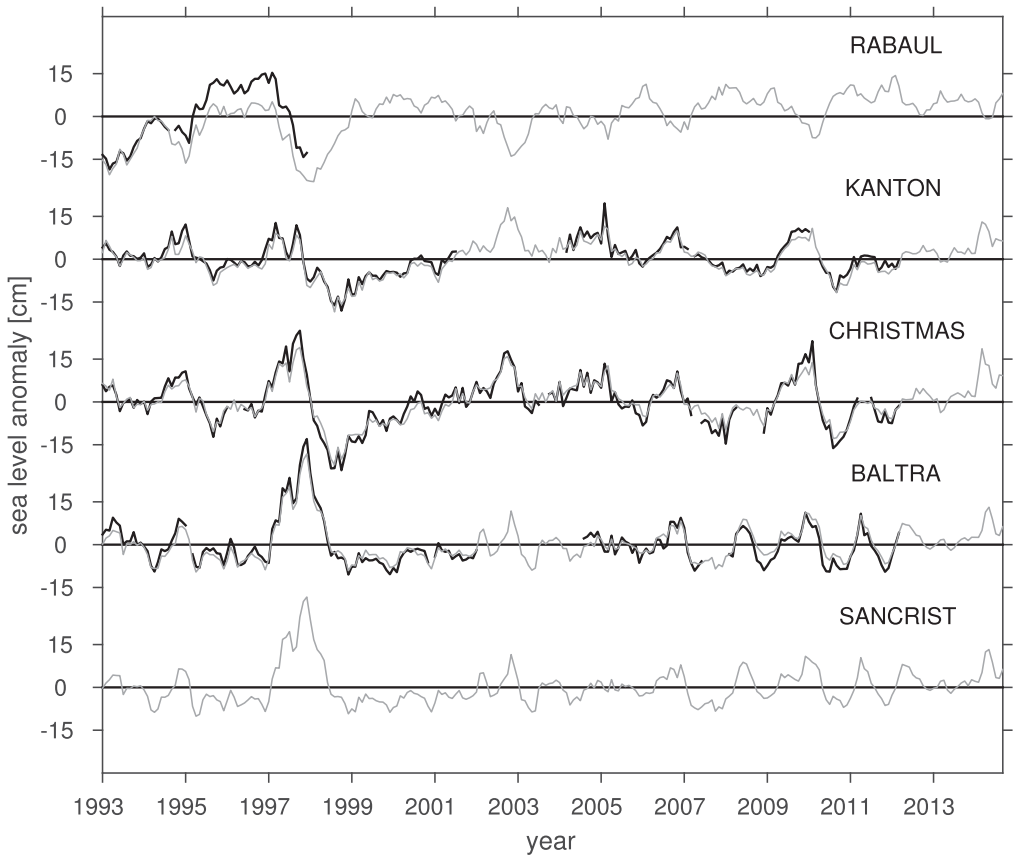

Figure 4. The time evolution of monthly mean sea level anomalies (in cm) from the tide gauge measurements (black) and satellite altimetry measurements (gray) at the tide gauge locations shown in Figure 1. As in Figure 3, the labeling on the *x* axis refers to 1 January of each year. Note also that no tide gauge data are available from Sancrist for the AVISO period.

from AVISO during this period, an offset that is not present before 1995.) Looking at Figure 3, we see that the model has skill at reproducing the interannual sea level variations. To quantify this, we compute the correlations between observed and reconstructed sea level at Rabaul (4.2°S, 152.2°E), Kanton (2.8°S, 171.7°W), Christmas (2.0°N, 157.5°W) and Baltra (0.4°S, 90.3°W) for the time period 1985–1997 for which we have almost continuous tide gauge records (any data gaps are filled by linear interpolation). During this 13 year long period, the correlations at Rabaul, Kanton, Christmas, and Baltra for the NCEP/NCAR (ERA-40) experiments are 0.85 (0.82), 0.09 (0.31), 0.68 (0.87), and 0.84 (0.84), respectively. Based on the method of Ebisuzaki (1997), these correlations are significantly different from zero at the 95% level with the exception of those at Kanton. The drop off in correlation at Kanton is consistent with the spatial pattern of correlation for the period 1993–2014 between AVISO and the model-computed sea level anomalies noted by Zhu et al. (2017) and shown by the color shading in Figure 1. The region of relatively low correlation near Kanton Island is, in turn, related with the misplacement of the pivot point in the model, a topic we return to in section 3.3. At Christmas Island, the model has skill at capturing events, especially in the ERA-40 experiment, but generally underestimates the amplitude, consistent with Figure 5 in Zhu et al. (2017) (in particular, compare their Figures 5a and 5b). Interestingly, the region of reduced correlation near Kanton Island is also the region in which Bunge and Clarke (2014) argue that the relationship between variations in sea surface height and the depth of the 20°C isotherm is obscured by the influence of rainfall. These authors note the importance of zonal advective processes in this region (see also Dewitte et al., 2013), processes that are missing from the

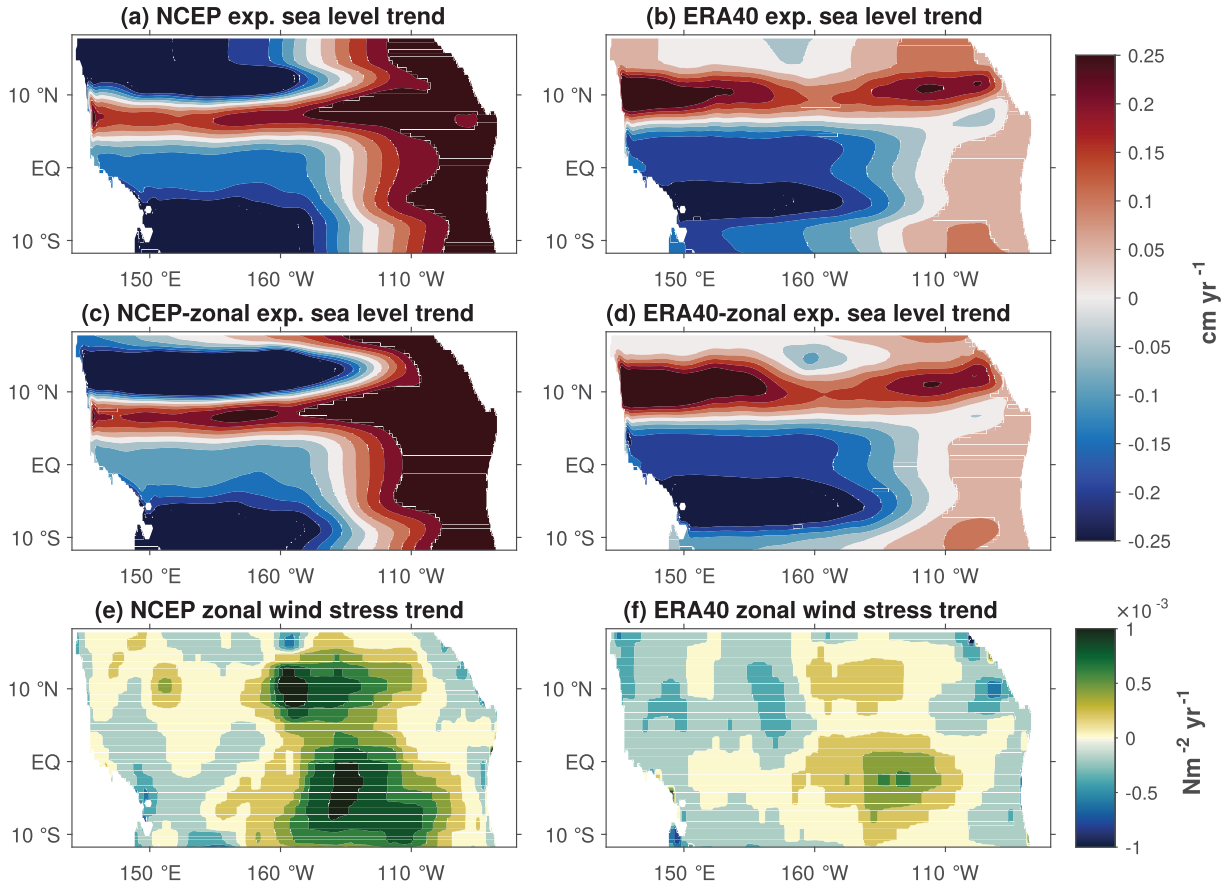

Figure 5. Spatial pattern of the trend in sea level over the period 1961–2002 (in cm yr^{-1}) in (a) the NCEP/NCAR experiment, (b) the ERA-40 experiment, (c) the NCEP/NCAR-zonal experiment, and (d) the ERA-40-zonal experiment, as well as the corresponding trend in the zonal wind stress anomalies (in N m^{-2} yr^{-1}) from (e) the NCEP/NCAR and (f) the ERA-40 products.

multimode model and which Zhu et al. (2017) argue contribute to the reduced performance of their model in this region.

3.2. The Trends in Model-Computed Sea Level

In addition to the interannual variability, Figure 3 also shows the trend in the model time series at the locations of the tide gauges. It is notable that the NCEP/NCAR experiments shows an upward trend at Sancrist and Baltra in the eastern equatorial Pacific that is much stronger than that found in the ERA-40 experiment. This difference in the trend between the two experiments in the eastern equatorial Pacific is clear when looking at Figures 5a and 5b. To determine the origin of the trend, we use the experiments driven by only the zonal wind stress: the NCEP/NCAR-zonal experiment and the ERA-40-zonal experiment. The spatial distribution of the sea level trend in these experiments is shown in Figures 5c and 5d and is very similar to that in Figures 5a and 5b. It follows that the zonal wind stress primarily determines the model-computed sea level trend in the tropical Pacific. Furthermore, it is clear that the large positive trend in sea level in the eastern tropical Pacific in the NCEP/NCAR experiment is associated with the large eastward trend in zonal wind stress in the NCEP/NCAR product (Figure 5e) that, in turn, has been attributed as spurious by Pohlmann et al. (2017). It follows that the large upward trend in sea level in the NCEP/NCAR experiment is almost certainly spurious and that the weaker upward trend in the ERA-40 experiment is more reliable. Indeed, both NCEP/NCAR and ERA-40-zonal wind stress anomalies exhibit an eastward trend, corresponding

to a weakening of the Walker circulation associated with the 1976–1977 climate shift (Trenberth et al., 1998), but this is much stronger in the NCEP/NCAR case. Qiu and Chen (2012), by considering the later period 1993–2009, noted the opposite trend in tropical Pacific sea level to that noted here, in both AVISO data and in a nonlinear 1½ layer, reduced gravity model driven by observed wind stress. These authors attribute the trend in this case to the strengthening of the Walker circulation after the transition of the Pacific Decadal Oscillation from a warm to a cold equatorial phase in the last 1990s (Minobe, 2002), consistent with our results.

3.3. Interannual Variability and the Pivot Point

As noted earlier, an interesting feature of equatorial sea level variability is the presence of a "pivot" point near the center of the basin about which the modeled sea level along the equator has a tendency to tip up and down, as in a see-saw. The "pivot" point is associated with the "tilt" mode of Clarke (2010). Along the equator, the gradient of sea level associated with the "tilt" mode is close to being in equilibrium with the zonal wind stress. In the simplest example, the anomalous (departure from the mean) zonal wind stress is uniform along the equator and the corresponding anomalous (departure from the mean) sea level associated with the "tilt" mode varies linearly along the equator, with a zero crossing near the center of the basin (see Figure 2e in Zhu et al. (2017) and the discussion thereon). The sea level variability associated with the "tilt" mode therefore tips up and down, as in a see-saw, about the zero crossing; what we refer to here as the "pivot" point. In reality, most of the variability in zonal wind stress along the equator is found in the western Pacific (see Figure 2a in Zhu et al., 2017) with the result that the "pivot point" moves westward, as

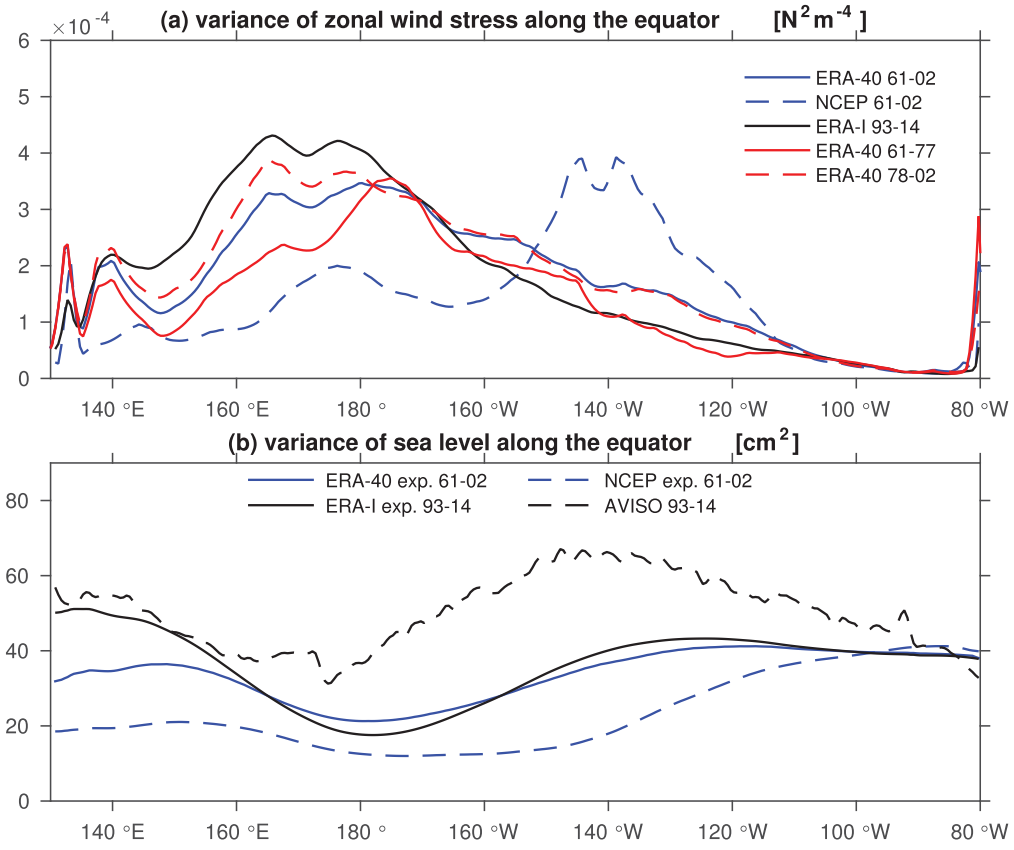

Figure 6. Variance in monthly means of (a) zonal wind stress anomalies from NCEP/NCAR, ERA-40 and ERA-Interim and (b) model-computed sea level anomalies along the equator from the NCEP/NCAR and ERA-40 experiments and the experiment in Zhu et al. (2017) driven by ERA-Interim monthly wind stress anomalies. Also shown is the variance of monthly mean sea level anomalies from AVISO.

can be seen by comparing Figures 2c and 2e in Zhu et al. (2017). It follows, as noted by Zhu et al. (2017), that the location of the pivot point is determined by the longitude range over which the zonal wind stress exhibits the largest temporal variability.

Figure 6 shows the variance of monthly zonal wind stress and sea level along the equator as a function of longitude in the different model experiments and also in AVISO. The peak in zonal wind stress variability from NCEP/NCAR near 140°W is associated with the spurious trend in this product noted in section 3.2. Apart from the peak, the variability in zonal wind stress tends to be less in the NCEP/NCAR than in the ERA-40 product and this is reflected in the lower variability in the model-computed sea level in this case shown in Figure 6b. The minimum in variance of sea surface height, reflecting the location of the pivot point, is also broader, less clearly defined and extends further to the east in the NCEP/NCAR than in the ERA-40 experiment. It is notable that all three model versions, including that discussed by Zhu et al. (2017), show generally lower variability in sea level than AVISO. This is similar to the finding of Nagura and McPhaden (2010) who compared sea level variability as seen by AVISO with sea level variability from a simple model for the Indian Ocean, a model with similarities to the one used here (see section 1). It is also notable that the minimum in sea level variance is shifted eastward in the model

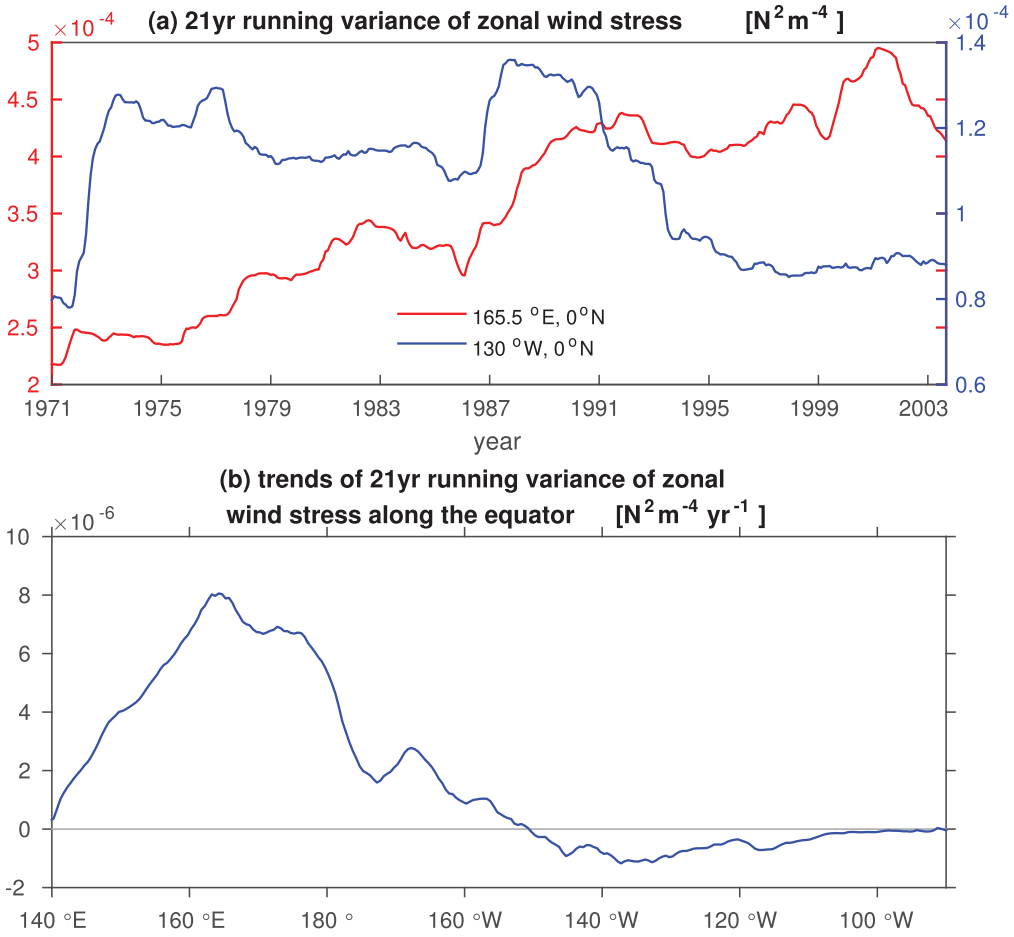

Figure 7. (a) Time series of the variance in monthly mean zonal wind stress at 165.5°E (red line) and 130°W (blue line) on the equator in 21 year running windows. (b) The trend in the time series of the variance of zonal wind stress in 21 year running windows plotted as a function of longitude along the equator and covering the time period 1961–2014. Note that the ERA-40 product is used from 1961 to 1992 and the ERA-Interim product from 1993 to 2014.

Table 1
The Percentage of Variance Explained by Each of the First Two EOFs for Sea Level Variability Along the Equator Computed From AVISO and in the Different Model Experiments (ERA-I Refers to the Standard Experiment in Zhu et al. (2017) *Covering the Period 1993–2014)*

	EOF1 (%)	EOF2 (%)	Correlation
AVISO	71	19	0.84 (0.39)
ERA-I	72	20	0.84 (0.42)
ERA-40 (61-02)	70	23	0.77 (0.30)
NCEP (61-02)	70	22	0.82 (0.30)

Note. Also shown is the correlation between the principal component time series of EOF1 and the zonal mean of the zonal wind stress along the equator (the 95% significance levels based on the method of Ebisuzaki (1997) are indicated in the brackets).

compared to AVISO. The eastward shift in the pivot point compared to AVISO was noted by Zhu et al. (2017) who attributed this error to the lack of zonal advection in the model (Dewitte et al., 2013), as noted earlier.

Also shown in Figure 6a is the variance of the zonal wind stress from ERA-40 in the subperiods 1961–1977 and 1978–2002, before and after the 1976–1977 climate shift (Trenberth et al., 1998). A notable increase and westward shift in zonal wind stress variance is found after the climate shift in the western equatorial Pacific in the ERA-40 product and there is a further increase in variance in the ERA-Interim product covering the period 1993–2014. By contrast, in the eastern tropical Pacific, the increase in zonal wind stress variance after the climate shift, i.e., for the 1978–2002 period, is not found in the ERA-Interim product covering 1993–2014. This issue is explored further in Figure 7a, where 21 year running windows are used to compute the zonal wind stress variance (the ERA-40 product is used from 1961 to 1992 and the ERA-Interim product from 1993 to 2014). The situation in the western equatorial Pacific is illustrated on the equator at 165.5°E, where there is a systematic increase in zonal wind variance throughout the study period, with no evidence of any influence from the 1976 to 1977 climate shift or, indeed, of the Pacific Decadal Oscillation which is known to have changed phase in both 1976–1977 and 1998–1999 (Minobe, 2002). Somewhat different behavior is seen further east on the equator at 130°W. Figure 7b shows the trend in zonal wind stress variance, again using 21 year running means over the period 1961–2002, but this time as a function of longitude along the equator. From this figure, one can see that the upward trend in zonal wind stress variance is found throughout the equatorial Pacific west of 160°W with very little trend in variance further east. The situation in the western equatorial Pacific is consistent with the westward shift in the region of zonal wind stress variability, especially after 1999, that has been noted by Lübbecke and McPhaden (2014). From what we show here, however, the increase in zonal wind stress variance in the western equatorial Pacific seems to be part of a much longer time scale trend than considered by these authors.

Comparing the model-computed sea level variability shown in Figure 2 for the period 1961–2002 with Figure 2 from Zhu et al. (2017) for the period 1993–2014 leaves the impression that the pivot point is located further west in the later period. This can be quantified by computing Empirical Orthogonal Functions (EOFs) from monthly mean sea level anomalies along the equator, for both the different model experiments and for AVISO. Doing this, one finds that the first EOF typically explains about 70% and the second mode around 20% of the variance, indicating their dominance (see Table 1). The spatial pattern and principal component (PC) time series associated with the first two EOFs computed from AVISO are shown in Figure 8. For AVISO, EOF1 explains 71% and EOF2 19% of the variance. The prominent El Niño events of 1997–1998 and 2009–2010 are clearly evident, especially in the PC times series for EOF1. EOF1 corresponds to what Clarke (2010) calls the "tilt" mode, for which the tilt in sea level along the equator is close to being in equilibrium with the zonal wind stress (Clarke, 2010). Indeed, the PC time series for EOF1 is highly correlated with the time series of the zonal mean of the zonal wind stress (0.84 in the case of AVISO and wind stress from ERA-Interim; see Table 1). In what follows, the longitude of the zero crossing in the spatial structure of EOF1 will be taken as the location of the pivot point.

EOF1 is shown in Figure 9a for AVISO, the two model runs, ERA-40 and NCEP/NCAR for the period 1961–2002, and the standard model run from Zhu et al. (2017) that is driven by wind stress anomalies from ERA-Interim for the period 1993–2014. It is clear that the zero crossing (and by implication the pivot point) is located further to the west in AVISO than in the model runs, consistent with the previous discussion. In the case of the NCEP/NCAR experiment, the zero crossing is located some 30° further east than in AVISO, a bias that has its origin in the spurious trend in the NCEP/NCAR wind stress product. Focusing on the more reliable ERA-40 experiment, we see a westward shift of almost 10° longitude in the zero crossing in the model experiment from Zhu et al. (2017) compared to the ERA-40 experiment discussed here. This is the shift we anticipated earlier and is a consequence of the increase and westward shift in the zonal wind stress variance along the equator in the western Pacific shown in Figures 6 and 7b.

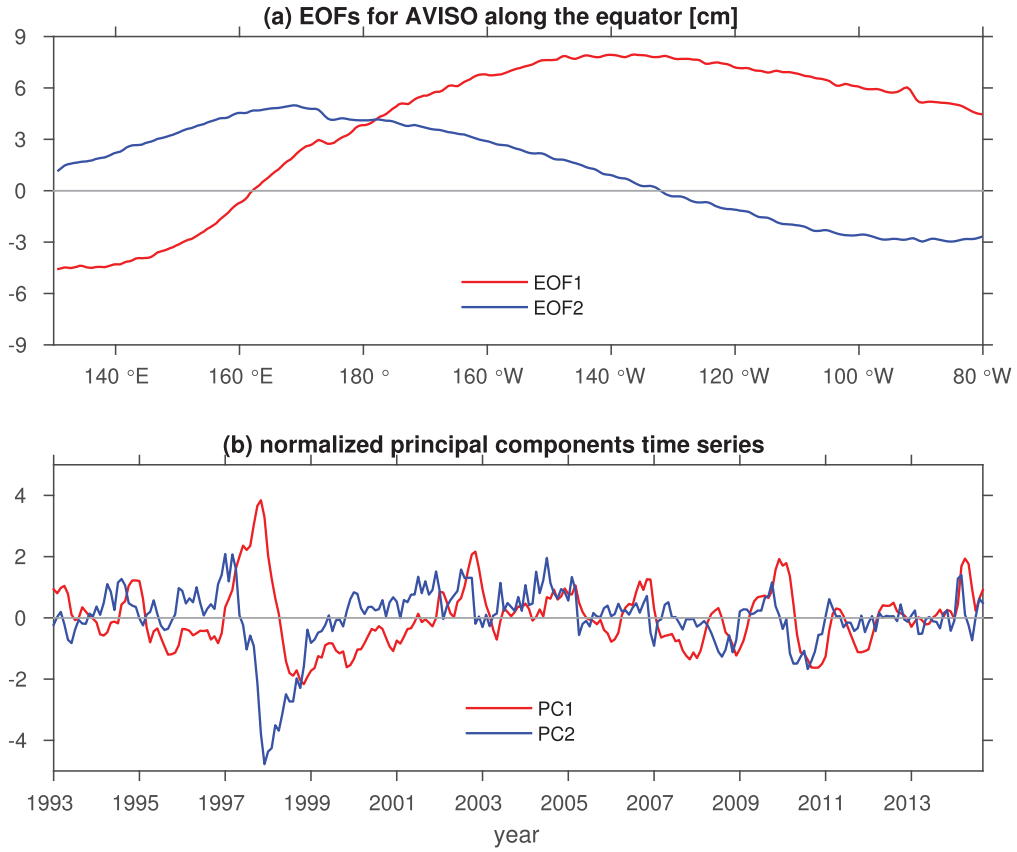

Figure 8. The (a) spatial structure and (b) principal component time series for the first two EOFs of sea level variability along the equator from AVISO (PC1: red line; PC2: blue line). The PC time series are normalized by their respective standard deviations.

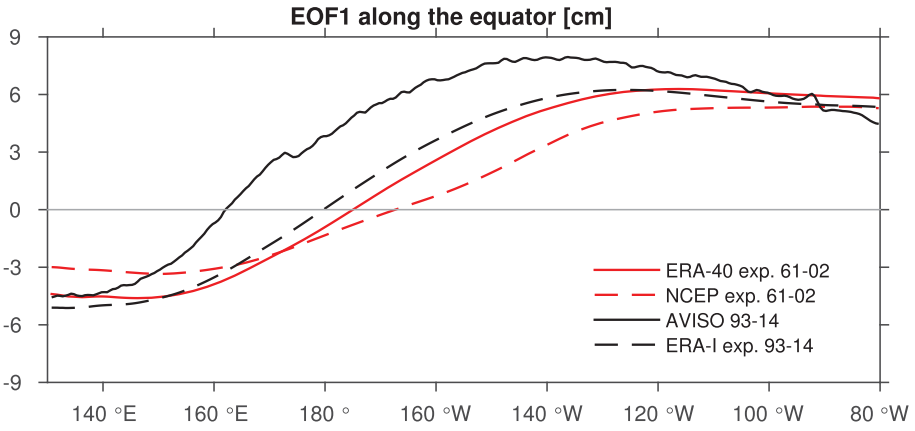

Figure 9. The first EOF of sea level variability along the equator from the full length of the model reconstructions and from AVISO.

4. Summary and Discussion

We have used the linear, multimode model of Zhu et al. (2017) to reconstruct monthly mean sea level variability in the tropical Pacific using monthly mean wind stress anomalies from the NCEP/NCAR and ERA-40 wind reanalysis. Zhu et al. (2017) noted that their model-computed sea level agrees well with the satellite-derived sea level provided by AVISO. Here the analysis period of 1961–2002 is mostly before the satellite era and includes the 1976–1977 climate shift (Trenberth et al., 1998). The simulated sea level anomalies capture the major ENSO events and generally compare well with the sea level anomalies measured by the available tide gauges shown in Figure 3, although the events in the modeled time series at Christmas Island have lower amplitude than observed. An exception is the tide gauge station at Kanton Island, which is located in the region with the lowest correlation between the model-computed sea level and AVISO (Zhu et al., 2017). The reduced correlation is due to the misplacement in the model of the pivot point along the equator associated with the "tilt" model of Clarke (2010)—see Zhu et al. (2017) for a detailed discussion.

The origin of the trend in sea level in both experiments is explored using sensitivity experiments driven by only the zonal wind stress anomalies from the NCEP/NCAR and ERA-40 products. In both cases, the spatial pattern of the sea level trend is well-captured in the sensitivity experiments compared to the experiments driven by both components of the wind stress, indicating the importance of the zonal wind stress for determining the trends in sea level in the tropical Pacific. Compared to ERA-40, NCEP/NCAR-zonal wind stress anomalies exhibit a much larger eastward trend in the eastern-central tropical Pacific that Pohlmann et al. (2017) conclude is spurious. It follows that the much larger upward trend in sea level in the eastern tropical Pacific in the NCEP/NCAR compared to the ERA-40 experiment is also, almost certainly, spurious.

We noted that the relatively poor model performance at Kanton Island is due to the presence of a pivot point along the equator about which sea level has a tendency to tip, as in a sea-saw. This behavior is the manifestation of the "tilt" mode that has been discussed by Clarke (2010) by which the tilt in sea level along the equator is close to being in equilibrium with the zonal wind stress. As noted by Zhu et al. (2017), the pivot point in the model is located to the east of the pivot point in the satellite data, i.e., AVISO, behavior that was attributed to the missing zonal advection in the model. A way to quantify the location of the pivot point is to identify its location with the zero crossing of the first EOF for sea level computed from data along the equator. The extreme eastward location of the pivot point in the experiment driven by the NCEP/NCAR wind stress product is another indication of the spurious trend in this wind stress product. The analysis also shows a more westward location in the pivot point during the period 1993–2014 than in the ERA-40 experiment. We attribute the westward shift in the pivot point to an increase and westward shift in zonal wind stress variance in the western equatorial Pacific throughout the period 1961–2002. This increase in zonal wind stress variance seems to be independent of the Pacific Decadal Oscillation and part of a much longer time scale mode of variability, possibility related to anthropogenic climate change, and requiring further study.

Acknowledgments
We thank two reviewers for their helpful comments. Xiaoting Zhu is grateful for funding from the China Scholarship Council (201306330071). This study has also been supported by the Deutsche Forschungsgemeinschaft as part of the Sonderforschungsbereich 754 "Climate-Biogeochemistry interactions in the Tropical Ocean," by the German Ministry for Education and Research (BMBF) through MiKlip2,subproject 01LP1517D (ATMOSMODINI) and SACUS (03G0837A), and by the European Union 7th Framework Programme (FP7 2007–2013) under grant agreement 603521 PREFACE project. R.J.G. is grateful to GEOMAR for continuing support. The data used in this study are available at data.geomar.de.

References

Ashok, K., Behera, S. K., Rao, S. A., Weng, H., & Yamagata, T. (2007). El Niño modoki and its possible teleconnection. *Journal of Geophysical Research*, *112*, C11007. https://doi.org/10.1029/2006JC003798

Becker, M., Meyssignac, B., Letetrel, C., Llovel, W., Cazenave, A., & Delcroix, T. (2012). Sea level variations at tropical pacific islands since 1950. *Global and Planetary Change*, *80*, 85–98.

Berrisford, P., Dee, D., Fielding, K., Fuentes, M., Kallberg, P., Kobayashi, S., et al. (2009). The ERA-interim archive. *ERA Report Series*, *1*, 1–16.

Bordbar, M. H., Martin, T., Latif, M., & Park, W. (2015). Effects of long-term variability on projections of twenty-first century dynamic sea level. *Nature Climate Change*, *5*(4), 343.

Bunge, L., & Clarke, A. J. (2014). On the warm water volume and its changing relationship with ENSO. *Journal of Physical Oceanography*, *44*(5), 1372–1385.

Busalacchi, A. J., & O'brien, J. J. (1981). Interannual variability of the equatorial Pacific in the 1960's. *Journal of Geophysical Research*, *86*(C11), 10901. https://doi.org/10.1029/JC086iC11p10901

Busalacchi, A. J., Takeuchi, K., & O'brien, J. J. (1983). Interannual variability of the equatorial Pacific Revisited. *Journal of Geophysical Research*, *88*(C12), 7551. https://doi.org/10.1029/JC088iC12p07551

Capotondi, A., Wittenberg, A. T., Newman, M., Di Lorenzo, E., Yu, J.-Y., Braconnot, P., et al. (2015). Understanding ENSO diversity. *Bulletin of the American Meteorological Society*, *96*(6), 921–938.

Church, J. A., Clark, P. U., Cazenave, A., Gregory, J. M., Jevrejeva, S., Levermann, A., et al. (2013). Sea level change. In *Climate change 2013: The physical science basis. Contribution of working group I to the fifth assessment report of the intergovernmental panel on climate change* (Technical report number 13). Cambridge, UK: Cambridge University Press.

Clarke, A. J. (2010). Analytical theory for the quasi-steady and low-frequency equatorial ocean response to wind forcing: The ''tilt'' and ''warm water volume'' modes. *Journal of Physical Oceanography*, *40*(1), 121–137.

Dewitte, B., Yeh, S.-W., & Thual, S. (2013). Reinterpreting the thermocline feedback in the western-central equatorial pacific and its relationship with the ENSO modulation. *Climate Dynamics*, *41*(3–4), 819–830.
Ebisuzaki, W. (1997). A method to estimate the statistical significance of a correlation when the data are serially correlated. *Journal of Climate*, *10*(9), 2147–2153.
Gill, A. E. (1982). *Atmosphere-ocean dynamics (International Geophysics Series)*. Cambridge, MA: Academic Press.
Holgate, S. J., Matthews, A., Woodworth, P. L., Rickards, L. J., Tamisiea, M. E., Bradshaw, E., et al. (2013). New data systems and products at the permanent service for mean sea level. *Journal of Coastal Research*, *29*(3), 493–504.
Kalnay, E., Kanamitsu, M., Kistler, R., Collins, W., Deaven, D., Gandin, L., et al. (1996). The NCEP/NCAR 40-year reanalysis project. *Bulletin of the American Meteorological Society*, *77*(3), 437–471.
Lübbecke, J. F., & McPhaden, M. J. (2014). Assessing the twenty-first-century shift in ENSO variability in terms of the Bjerknes stability index. *Journal of Climate*, *27*(7), 2577–2587.
McCreary, J. (1981). A linear stratified ocean model of the equatorial undercurrent. *Philosophical Transactions of the Royal Society of London A*, *298*(1444), 603–635.
Minobe, S. (2002). Interannual to interdecadal changes in the Bering Sea and concurrent 1998/99 changes over the north pacific. *Progress in Oceanography*, *55*(1), 45–64.
Nagura, M., & McPhaden, M. J. (2010). Dynamics of zonal current variations associated with the Indian Ocean dipole. *Journal of Geophysical Research*, *115*, C11026. https://doi.org/10.1029/2010JC006423
Pohlmann, H., Kröger, J., Greatbatch, R. J., & Müller, W. A. (2017). Initialization shock in decadal hindcasts due to errors in wind stress over the tropical pacific. *Climate Dynamics*, *49*(7), 2685–2693. https://doi.org/10.1007/s00382-016-3486-8.
PSMSL (2016). *Permanent Service for Mean Sea Level (PSMSL), "Tide gauge data"*. Retrieved from http://www.psmsl.org/data/obtaining/, accessed 23 November 2016
Qiu, B., & Chen, S. (2012). Multidecadal sea level and gyre circulation variability in the northwestern tropical pacific ocean. *Journal of Physical Oceanography*, *42*(1), 193–206.
Rhein, M., Rintoul, S., Aoki, S., Campos, E., Chambers, D., Feely, R., et al. (2013). Observations: Ocean. In *Climate change 2013: The physical science basis. Contribution of working group I to the fifth assessment report of the intergovernmental panel on climate change* (Technical report number 3). Cambridge, UK: Cambridge University Press.
Timmermann, A., McGregor, S., & Jin, F.-F. (2010). Wind effects on past and future regional sea level trends in the southern indo-pacific*. *Journal of Climate*, *23*(16), 4429–4437.
Trenberth, K. E., Branstator, G. W., Karoly, D., Kumar, A., Lau, N.-C., & Ropelewski, C. (1998). Progress during toga in understanding and modeling global teleconnections associated with tropical sea surface temperatures. *Journal of Geophysical Research*, *103*(C7), 14291–14324. https://doi.org/10.1029/97JC01444
Uppala, S. M., Kållberg, P., Simmons, A., Andrae, U., Bechtold, V., Fiorino, M., et al. (2005). The era-40 re-analysis. *Quarterly Journal of the Royal Meteorological Society*, *131*(612), 2961–3012.
Wang, C., & Fiedler, P. C. (2006). ENSO variability and the eastern tropical pacific: A review. *Progress in Oceanography*, *69*(2), 239–266.
Zhu, X., Greatbatch, R. J., & Claus, M. (2017). Interannual variability of tropical pacific sea level from 1993 to 2014. *Journal of Geophysical Research: Oceans*, *122*, 602–616. https://doi.org/10.1002/2016JC012347

4 ENSO Diversity and Thermocline Feedback for The Period 1961-2014 Assessed Using A Linear Multi-mode Model

Whether or not EOF1 and EOF2 of SSTa over the tropical Pacific can represent EP ENSO and CP ENSO is under debate. Besides, the change of thermocline feedback responsible for the emergence of CP ENSO is uncertain. Chapter 3 shows that the westward shift of sea level pivot point is associated with the increasing variability in zonal wind stress, motivating the exploration of the possible mechanism for emergence of CP ENSO. All these issues are addressed in this chapter.

Citation: **Zhu, X., R. J. Greatbatch, and M. Claus (2018), ENSO diversity and thermocline feedback for the period 1961-2014 assessed using a linear multi-mode model, Climate Dynamics, under review.**

The candidate's contribution to this publication are as below:

1. *Initiated the study*
2. *Analysis of the model results*
3. *Preparing and analysis of the observational datasets*
4. *Production of all figures*
5. *Contributing to the ideas in the manuscript*
6. *Drafting the first version of the manuscript*

Climate Dynamics

ENSO diversity and thermocline feedback for the period 1961-2014 assessed using a linear multi-mode model

--Manuscript Draft--

Manuscript Number:	
Full Title:	ENSO diversity and thermocline feedback for the period 1961-2014 assessed using a linear multi-mode model
Article Type:	S.I. : ENSO Diversity
Keywords:	ENSO diversity; Thermocline feedback; Bjerknes feedback; Pivot point; Shallow water model
Corresponding Author:	Xiaoting Zhu Helmholtz-Zentrum fur Ozeanforschung Kiel GERMANY
Corresponding Author Secondary Information:	
Corresponding Author's Institution:	Helmholtz-Zentrum fur Ozeanforschung Kiel
Corresponding Author's Secondary Institution:	
First Author:	Xiaoting Zhu
First Author Secondary Information:	
Order of Authors:	Xiaoting Zhu
	Richard John Greatbatch
	Martin Claus
Order of Authors Secondary Information:	
Funding Information:	China Scholarship Council (201306330071) — Ms Xiaoting Zhu
	Deutsche Forschungsgemeinschaft (DE) (01LP1517D, 03G0837A) — Prof. Dr. Richard John Greatbatch
	European Union 7th Framework Programme (603521) — Prof. Dr. Richard John Greatbatch
Abstract:	Monthly mean sea level variations computed using a linear, multi-mode model are combined with satellite measurements to assess ENSO diversity and thermocline feedback in the equatorial Pacific for the period 1961-2014. We find little evidence for the occurrence of Central Pacific (CP) events before the 1976/77 climate shift. After the climate shift, thermocline feedback in the CP (Nino4 region) is found to increase strongly. At the same time, the Bjerknes feedback mechanism is shown to increase in strength in the Nino4 region, concurrent with the increased occurrence of CP events. An important point is that the emergence of the thermocline feedback in the Nino4 region can be related to changes in the wind field over the equatorial Pacific; in particular, the westward shift of the pivot point for sea level (and hence thermocline) variations associated with the increase in zonal wind stress variance in the western equatorial Pacific, the latter in turn being related to the increased frequency of CP events due to the Bjerknes feedback. As the pivot point shifts westward, the Nino4 region is found increasingly to the east of the pivot point enabling the thermocline feedback to operate there. These arguments imply a positive feedback in which CP events are self-maintaining and suggest that they may be part of the natural variability of the climate system and could occur episodically without the need for changes in external forcing.
Suggested Reviewers:	Michael McPhaden NOAA Pacific Marine Environmental Laboratory Michael.J.Mcphaden@noaa.gov

	Chunzai Wang South China Sea Institute of Oceanology Chinese Academy of Sciences cwang@scsio.ac.cn
	Jay McCreary University of Hawai'i at Manoa jay@hawaii.edu
	Ping Chang Texas A&M University College of Geosciences ping@tamu.edu

Dear Editor,

We are submitting the following manuscript entitled “ENSO diversity and thermocline feedback for the period 1961-2014 assessed using a linear multi-mode model” for publication in Climate Dynamics.

Best regards,
Xiaoting Zhu, Richard Greatbatch, Martin Claus

ENSO diversity and thermocline feedback for the period 1961-2014 assessed using a linear multi-mode model

Xiaoting Zhu[1a], Richard J. Greatbatch[a,b], and Martin Claus[a,b]

[a]Ocean Circulation and Climate Dynamics, GEOMAR Helmholtz Centre for Ocean Research Kiel, Germany

[b]Faculty of Mathematics and Natural Sciences, University of Kiel, Kiel, Germany

January 10, 2018

[1]xzhu@geomar.de

Abstract

Monthly mean sea level variations computed using a linear, multi-mode model are combined with satellite measurements to assess ENSO diversity and thermocline feedback in the equatorial Pacific for the period 1961-2014. We find little evidence for the occurrence of Central Pacific (CP) events before the 1976/77 climate shift. After the climate shift, thermocline feedback in the CP (Nino4 region) is found to increase strongly. At the same time, the Bjerknes feedback mechanism is shown to increase in strength in the Nino4 region, concurrent with the increased occurrence of CP events. An important point is that the emergence of the thermocline feedback in the Nino4 region can be related to changes in the wind field over the equatorial Pacific; in particular, the westward shift of the pivot point for sea level (and hence thermocline) variations associated with the increase in zonal wind stress variance in the western equatorial Pacific, the latter in turn being related to the increased frequency of CP events due to the Bjerknes feedback. As the pivot point shifts westward, the Nino4 region is found increasingly to the east of the pivot point enabling the thermocline feedback to operate there. These arguments imply a positive feedback in which CP events are self-maintaining and suggest that they may be part of the natural variability of the climate system and could occur episodically without the need for changes in external forcing.

Keywords: ENSO diversity; Thermocline feedback; Bjerknes feedback; Pivot point; Shallow water model

1 Introduction

El Niño Southern Oscillation (ENSO) is the dominant mode of interannual variability in the coupled ocean-atmosphere system in the tropical Pacific (Becker et al., 2012). In recent decades, observational studies reveal the occurrence of El Niño events with the largest Sea Surface Temperature (SST) anomalies in the central equatorial Pacific (e.g. Ashok et al., 2007; Lee and McPhaden, 2010; McPhaden, 2004), contrasting with "typical" El Niño events for which the largest SST anomalies occur in the eastern Pacific (e.g. McPhaden, 1999). These different SST patterns are associated with different anomalous atmospheric convection patterns and lead to significantly different global impacts from those associated with the conventional El Niño events (Ashok and Yamagata, 2009).

Given the different flavours of ENSO, the scientific community has sought to classify ENSO diversity based on various methods (Capotondi et al., 2015). For example, Ashok et al., (2007) argue that the first and second Empirical Orthogonal Functions (EOFs) for SST in the tropical Pacific represent the canonical Eastern Pacific ENSO events (EOF1) and the Central Pacific (what they call "Modoki") ENSO events (EOF2), respectively. They propose the El Niño Modoki Index (EMI), using SST in three different boxes, as a measure for Central Pacific ENSO events. The EMI and the principle component (PC) time series for EOF2 are highly correlated (0.91) during their study period of 1979-2005. The EMI is derived from the contrast between the spatially-averaged SST in the central Pacific and the spatially-averaged SST in the western and eastern Pacific, and is related to the Trans-Nino Index (TNI) of Trenberth and Stepaniak, (2001) (correlation with the EMI of -0.87 over the period 1979-2005). Takahashi et al., (2011) and Dommenget et al., (2013) point out, however, that ENSO in fact, exhibits quite nonlinear behaviour. Dommenget et al., (2013) note that strong warm and weak cold events tend to have maximum amplitude in the eastern tropical Pacific whereas weak warm and strong cold events are, instead, focussed on the central tropical Pacific. Takahashi et al., (2011) further argue that ENSO events are best described by E and C indices, the axes of which are rotated anticlockwise in PC1-PC2 space by 45° from the standard PC1 and PC2 axes, and that El Niño Modoki events are a part of the C regime. To define their EOFs, Takahashi et al., (2011) use the period 1979-2009 and project data from the much longer period 1870-2010 onto these EOFs to create their PC time series. Likewise, the EOFs used by Ashok et al., (2007) to define ENSO Modoki are based only on the period 1979-2005. Indeed, Ashok et al., (2007) show that EOF2 has a very different character before than after the 1976/77 climate shift (Trenberth et al., 2002) (see Section 4 of Ashok et al., (2007)), a topic we investigate further here. Interpreting Takahashi et al., (2011) is therefore complicated by the change in the spatial pattern of the EOFs (especially EOF2) in different epochs, for example, before and after the

1976/77 climate shift(note, however, that these authors claim that using a spatial domain to compute EOFs that is more confined to equator than that used by Ashok et al., (2007) reduces the sensitivity of the EOFs to the time period used for their computation). In the following, we follow the terminology of Yeh et al., (2009) and refer to Central Pacific (CP) events (corresponding to ENSO Modoki) and Eastern Pacific (EP) events, and study the period 1961-2014.

A number of studies have pointed out that the relative importance of thermocline feedback and zonal advective feedback, the most prominent two physical processes among those responsible for the evolution of ENSO (Jin et al., 2006), is critical for understanding ENSO diversity (e.g. Belmadani et al., 2010; Capotondi, 2013; Dewitte et al., 2013; Lübbecke and McPhaden, 2014). In terms of what causes the increasing occurrence of CP El Niño events during recent decades, Yeh et al., (2009) suggest that the flattening and strengthening of the thermocline along the equator in the central Pacific after the 1976/77 climate shift led to a more important role for thermocline feedback there, a change Yeh et al., (2009) attribute to global warming. They argue that with a flatter, stronger thermocline, cold subsurface water can more easily influence SST through mean vertical advection. This seems to be supported by Dewitte et al., (2013) who argue that thermocline feedback has, indeed, become more important in the central equatorial Pacific since the 1976/77 climate shift. On the other hand, McPhaden et al., (2011) find a systematic shift from the 1980-1999 to the 2000-2010 periods in which the trade winds strengthened, the thermocline steepened and the prevailing ENSO flavor converted from EP El Niño to CP El Niño . These results appear to contradict Yeh et al., (2009), particularly concerning whether a flatter or steeper thermocline slope along the equator favours the occurrence of CP events. McPhaden et al., (2011) further conclude that the change in ENSO characteristics from 1980-1999 to 2000-2019 occurred naturally rather than being forced by global warming, as claimed by Yeh et al., (2009). In addition, Lübbecke and McPhaden, (2014) argue that the cooler background state during 2000-2010 in the central-eastern tropical Pacific led to a westward shift in the ascending branch of the Walker circulation and smaller zonal wind fetch, which is favorable for CP El Niño events and weakens the thermocline feedback in the central-eastern Pacific. Thus, the dynamics governing ENSO diversity and the role of thermocline feedback remains unclear.

In two recent studies, we have shown that a linear, multi-mode model driven by surface wind stress anomalies taken from reanalysis has considerable success at reproducing monthly mean sea level variability in the equatorial Pacific for the periods 1961-2002 (Greatbatch et al., 2017, submitted to Journal of Geophysical Research Oceans; hereafter G17) and 1993-2014 (Zhu et al., 2017). Here, we use these simulations together with COBE2 SST data (Hirahara et al., 2014) to (i) revisit the relationship between EOFs of SST in the tropical Pacific and ENSO diversity before and after the 1976/77 climate shift and (ii) analyse and interpret the change of

thermocline feedback associated with ENSO diversity during the analysis period of 1961-2014. In section 2, we introduce the model simulations and datasets employed. In section 3, we analyse how EOF1 and EOF2 of SST relate to ENSO diversity before and after the 1976/77 climate shift (section 3.1). Additionally, the changing strength of the thermocline feedback in the equatorial Pacific is analyzed and its relationship with ENSO diversity is discussed (section 3.2). Finally, we provide a summary and discussion in section 4.

2 Data

For Empirical Orthogonal Function (EOF) analysis of SST anomalies over the tropical Pacific, we employ the COBE2 SST dataset (Hirahara et al., 2014) for the period 1961-2014. The results based on COBE2 SST are consistent (not shown) with those from HadISST (Rayner et al., 2003) frequently used in previous studies. Additionally, different SST indices for ENSO, as mentioned in section 1, are used, in particular the El Niño Modoki Index (EMI) and the Nino3 and Nino4 indices. EMI, obtained from http://www.jamstec.go.jp/, is defined by Ashok et al., (2007) as the SST averaged over the central Pacific (165°E - 140°W, 10°S - 10°N) minus SST averaged over the western Pacific (125° - 145°E, 10°S - 20°N) and eastern Pacific (110° - 70°W, 15°S - 5°N). The Nino3 or Nino4 indices, obtained from https://www.esrl.noaa.gov/psd, refer to the area-averaged SST anomalies over the Nino3 (150°W - 90°W, 5°S - 5°N) or Nino4 regions (160°E - 150°W, 5°S - 5°N) respectively (the exact time period used to reference the anomalies varies according to context and is given in the text). Moreover, sea level indices for the Nino3 and Nino4 regions, denoted SLA[Nino3] and SLA[Nino4] respectively, are calculated by replacing SST anomalies in the definition formulae for the indices by sea level anomalies (SLA's), either from AVISO or from the model with, in the case of Nino4, some adjustment in the location used for the averaging, as explained later. Following Rebert et al., (1985), these sea level indices are used as a proxy for anomalies in the depth of the thermocline.

SLA's for the period of 1993-2014 and 1961-2002 are taken from the standard experiment in Zhu et al., (2017) and the ERA-40 experiment described in G17, respectively. The former experiment uses a linear, multi-mode ocean model driven by ERA-Interim monthly mean wind stress anomalies from 1979 to 2014, relative to the climatological monthly mean for each month for the period of 1993-2012, and provided by the European Centre for Medium-Range Weather Forecasts (ECWMF) (Berrisford et al., 2009). The multi-mode model is the sum of five linear shallow water models, one for each of the first five baroclinic modes, over the model domain (112°E - 70°W, 12°S - 18°N). The projection coefficients of wind stress for the five modes are derived by fitting time variations of sea level along the equator from the model to the satellite measured time variations of sea level from 1993 to

2014 provided by Ssalto/Duacs and distributed by AVISO with support from Cnes (http://www.aviso.altimetry.fr/duacs/) (hereafter referred to as AVISO). The resultant multi-mode model is further applied in the ERA-40 experiment to reconstruct the sea level variations during the pre-satellite era. Here, the model is driven by the 40-yr ECMWF Re-analysis (ERA-40) (Kalnay et al., 1996) monthly mean wind stress anomalies from 1957 to 2002 relative to the climatological monthly mean for each month for the period 1961-2002. The SLA's from the experiments were validated using AVISO observations and tide gauge measurements from the Permanent Service for Mean Sea Level (Holgate et al., 2013) (see Zhu et al., (2017) and G17 for the details). To clarify the difference between the thermocline feedback in our study and Dewitte et al., (2013), the sea surface height for the period 1961-2009 from the SODA reanalysis dataset (version 2.2.4, Giese and Ray, (2011)), which is applied in Dewitte et al., (2013), is also used in the analysis.

3 Results

3.1 ENSO diversity from 1961 to 2014

In this section, we explore the relationship between ENSO diversity and EOFs of SST over the tropical Pacific (112°E - 70°W, 12°S - 18°N)[1] before and after the 1976/77 climate shift. We begin with the study period 1961-2002, limited by the ERA-40 experiment in G17 where the linear, multi-mode model is driven by the ERA-40 wind stress anomalies from 1957 to 2002. The subperiods of 1961-1977 and 1978-2002 correspond to before and after the 1976/77 climate shift, respectively. Later we examine the period 1993-2014 using AVISO satellite data and the model results of Zhu et al., (2017).

In Ashok et al., (2007), the EP and CP events are identified with the variability associated with the first two EOFs of SST in the tropical Pacific. We therefore begin by showing the spatial patterns and principal components of the first and second EOFs of SST in the tropical Pacific before and after the 1976/77 climate shift in Figures 1 and 2. The time series of Nino3 and EMI (Ashok et al., 2007) are also plotted in comparison with the principal component time series PC1 and PC2, respectively. Together, these first two EOFs account for almost 60% of the variance in monthly mean SST in both time periods and are well-separated both from each other and from the third EOF according to the criterion of North et al., (1982). The spatial patterns of the first EOF are almost the same both before and after the climate shift (Figure 1a and 1b), and the PC time series are well correlated with the Nino3 SST index (Figure 1c and 1d) in both time periods. It follows that EOF1 provides a good representation for the traditional EP events both before and after the 1976/77 climate

[1]The domain used to compute the EOFs is the same as the model domain used by Zhu et al., (2017)

shift. By contrast, for the second EOF, the spatial patterns differ markedly before and after the climate shift (compare Figures 2a,b), having the appearance of being shifted eastward in the later period when there is also the emergence of anomalies in the western Pacific of the same sign as those found in the eastern Pacific. Indeed, it was the tripole structure of EOF2 after the 1976/77 climate shift that motivated the definition of the EMI proposed by Ashok et al., (2007) in which SST averaged over boxes in the eastern and western Pacific is subtracted from SST averaged over a box in the central Pacific and, furthermore, the spatial pattern of EOF2 in the later period (Figure 2b) resembles the spatial pattern of SST usually associated with CP events. On the other hand, the spatial pattern of EOF2 in the earlier period resembles more a modification of the conventional EP ENSO events represented by EOF1, as point that is already noted in Section 4 of Ashok et al., (2007). Given how the EMI is defined, it is not surprising that it is highly correlated with PC2 in the later period (Figure 2c). In the earlier period, however, before the 1976/77 climate shift (Figure 2d), the correlation between the EMI and PC2 is considerably reduced and the relevance of the EMI as an independent index during this time period is called into question. It is notable that Ashok et al., (2007) could not identify CP ENSO amongst the EOFs of SST before the 1976/77 climate shift, only after. They point out that CP events were, at best, very weak before the climate shift. These results also question the statement in Takahashi et al., (2011) that the spatial pattern of EOF2, admittedly computed in a slightly smaller spatial domain, is not sensitive to the time domain. From our analysis, it is difficult to identify any evidence for the existence of CP events before the 1976/77 climate shift.

Given that the EMI is not a good substitute for PC2 before the 1976/77 climate shift , we use PC1 and PC2 instead of Nino3 and EMI for the further analysis in this section. Figure 3 and 4 show the regression of SLA's from the ERA-40 experiment in G17 onto PC1 and PC2, respectively, for the two time periods. Also shown are the corresponding regressions of monthly mean zonal wind stress, TAUX, on PC1 and PC2. In the case of EOF1 (Figure 3), the spatial patterns of both regressed sea level and TAUX are very similar either side of the 1976/77 climate shift as expected: in the warm phase of ENSO, strong westerly wind anomalies are evident west of 120°W (Figure 3c and 3d), and sea level is higher than normal in the east while lower in the west (Figure 3a and 3b), corresponding to the so-called tilt mode (Clarke, 2010), and in agreement with the Bjerknes feedback hypothesis (Bjerknes, 1969) for the EP events. In the case of EOF2 (Figure 4), however, the spatial patterns of both regressed sea level and TAUX experience a significant change following the 1976/77 climate shift. Before the 1976/77 climate shift (Figure 4a), the pattern of SLA associated with EOF2 looks like a propagating Rossby wave, suggesting that it is somehow related to the ENSO adjustment process, whereas after the 1976/77 climate shift (Figure 4b), the sea level has positive anomalies on the equator (rather than negative there, as in

the earlier period), although there is still some suggestion of Rossby wave propagation off the equator. The regressed TAUX in the pre-climate shift period (Figure 4c) has weak easterly anomalies along the equator, suggesting the decaying phase of ENSO when PC2 is in its positive phase. In the post-climate shift period (Figure 4d), the spatial pattern of regressed TAUX looks quite different with westerly anomalies now appearing west of the date line along the equator. Indeed, along the equator, the pattern of regressed TAUX now looks somewhat similar, but westward shifted, to that associated with EOF1 (Figure 3d), and similar to the scenario described in Lübbecke and McPhaden, (2014) that is favorable for CP events. Likewise, after the 1976/77 climate shift , we see the emergence of strong easterly wind anomalies east of the date line. These anomalous zonal wind patterns agree with those during CP events in observational studies (see Figure 5b in McPhaden, (2004)) and are consistent with the emergence of CP events after the 1976/77 climate shift. On the other hand, before the 1976/77 climate shift, the behaviour of EOF2 is very different from that associated with CP events.

To further understand the change in the sea level and TAUX regressions associated with EOF2, we look at the lagged correlation of PC1 and PC2 before and after the 1976/77 climate shift (Figure 5). We see that before the 1976/77 climate shift, PC2 lags PC1 with the maximum correlation (0.57, above the 95% significant level) occurring at the lag of 10 months, consistent with the suggestion above that EOF2 reflects the decaying phase of ENSO before the 1976/77 climate shift(see also Section 4 of Ashok et al., (2007) where the same lag correlation is noted). On the other hand, after the 1976/77 climate shift, PC2 leads PC1 with a maximum correlation of 0.52 (above the 95% significant level) about 12 months before the peak in PC1. The relatively long lead time indicates that PC2 is not always linked to the onset phase of EP ENSO. Takahashi et al., (2011) raise concern that the extreme 1982/83 and 1997/98 El Niño events can distort conclusions drawn concerning changes associated with the 1976/77 climate shift, in particular regarding the change in the relationship between the TNI index and the Nino3.4 index for SST before and after the climate shift that was noted by Trenberth and Stepaniak, (2001). To determine whether these extreme EP El Niño events influence our conclusions, we set the PC1 and PC2 to zero during the extreme warm events (1982/83 and 1997/98 El Niño events) and repeat the analysis used to produce Figures 4 and 5. The results show no significant change (not shown).

Finally in this section, we show figures corresponding to Figures 3 and 4 but for the period 1993-2014 for which we have satellite-derived sea level data from AVISO. The spatial patterns shown in Figure 6b,c for EOF1 are very similar to those shown in Figure 3 and confirm the robustness of the EP events, as represented by EOF1 of SST, beyond 2002. Comparing the regression of PC1 on the AVISO satellite data (Figure 6a) with that from the multi-mode model (here the standard run in Zhu et

al., (2017)), we see the eastward shift in the modelled sea level compared to AVISO that was noted by Zhu et al., (2017). Looking at Figure 7 for EOF2, we again see the eastward shift when comparing Figure 7a,b, but also basically the same picture that we see in Figure 4b,d, i.e. for the post-climate shift period 1978-2002, that was discussed above. If anything, the Rossby wave-type structure in the sea level regression is more prominent here than in Figure 4b, with the sea level regression pattern looking rather like a mixture of that before and after the climate shift in Figure 4. On the other hand, the regression of the zonal wind stress, TAUX, looks very similar to that in Figure 4d with westerly wind anomalies in the western equatorial Pacific when PC2 is in its positive phase.

3.2 Thermocline feedback in the eastern and central Pacific during the period from 1961 to 2014

In this section, we explore changes in thermocline feedback in the eastern and central tropical Pacific, one of the key ingredients for understanding ENSO diversity. Here the study period spans 1961-2014: SLA's for the period 1993-2014 come from the standard experiment in Zhu et al., (2017) and for the period 1961-1992 from the ERA-40 experiment in G17. It should be noted that the multi-mode model was driven by the monthly mean wind stress climatologies for the separate periods of 1961-2002 and 1993-2012 in order to adjust the reference state so that all anomalies are now referenced to the monthly mean climatology for the period 1961-2014. Of particular interest here are changes in thermocline feedback in the Nino3 and Nino4 regions in the eastern and central equatorial Pacific, respectively. Dewitte et al., (2013) have shown evidence using the SODA ocean reanalysis of Giese and Ray, (2011) that the role of thermocline feedback has increased in the Nino4 region since the 1976/77 climate shift , a topic we investigate further here.

3.2.1 Adjusting the model-computed sea level to correspond to the Nino4 region

We noted at the end of the Section 3.1 that model-computed sea level is shifted to the east compared to AVISO in the western-central equatorial Pacific. The eastward shift can be clearly seen in the Hovmoeller diagram shown in Figure 2 of Zhu et al., (2017) when comparing model and AVISO and is related to the too eastward position of the pivot point associated with the "tilt" mode in the model compared to AVISO, leading to relatively low model skill in the western-central Pacific (see Zhu et al., (2017) and G17). These authors attribute this displacement to the lack of zonal advection in the model. It therefore makes sense to shift the box used for model-computed sea level in the Nino4 region eastward from that used for SST. To do this, we use the standard experiment from Zhu et al., (2017)) and shift the box eastward along the equator

from the standard Nino4 box until the correlation over the period 1993-2014 between detrended AVISO, averaged over the standard Nino4 region, and detrended modelled sea level, averaged over the shifted box, reaches a maximum. In fact the maximum correlation is 0.91 when the box is shifted eastward by 17°. The shifted box is shown using solid yellow lines in Figure 7b. From this figure, it can be seen that the spatial structures of the regressed sea level anomaly on PC2, as seen by AVISO in the Nino4 box (solid yellow lines) in Figure 7a are also seen in the model in the shifted box (solid yellow lines) in Figure 7b, giving us confidence in the use of the shifted box.

3.2.2 Change in thermocline feedback

In order to assess the importance of thermocline feedback, we use the correlation between the variations in sea level and those of SST. Variations in sea level are here being used as a proxy for variations in thermocline depth. The link between sea level variations and thermocline depth anomalies in the equatorial oceans is well known (Rebert et al., 1985) and is implicit in the multi-mode model since we use only the first five baroclinic modes to model sea level, with no contribution from the barotropic model. In fact, the model response to the imposed wind forcing is dominated by the second baroclinic mode (Zhu et al., 2017). It is also well-known that the thermocline feedback is not as effective in the central Pacific as in the eastern Pacific. Indeed, Dewitte et al., (2013), using SODA data, find a negative correlation between anomalous SST and thermocline depth in the Nino4 region over the period 1950-2008 (see their Figure 2) and especially before the 1976/77 climate shift (their Figure 3).

Figure 8 shows the spatial distribution of the correlation between SST and sea level variations from both AVISO and the ERA-Interim experiment from Zhu et al., (2017) for the period 1993-2014. Using AVISO (Figure 8a), we see that the equatorial Pacific is covered by positive correlations with values over 0.80 in the eastern Pacific (Nino3 region) and mostly over 0.60 in the central Pacific (Nino4 region), indicating very strong thermocline feedback in the eastern Pacific and even quite strong thermocline feedback in the Nino4 region. Using sea level taken from the linear model (Figure 8b), the strength of thermocline feedback is well reproduced in the Nino3 region but deviates from AVISO over and to the west of the standard Nino4 region (dashed yellow lines). As noted above, this is where the model error in placing the pivot point for the "tilt" mode occurs. This problem is fixed by shifting the Nino4 box used for the modelled sea level to that shown by the solid yellow lines, as discussed above, for which the resultant strength of the thermocline feedback from the linear model experiment is comparable to that from AVISO in the Nino4 region.

Now we combine the two experiments, i.e. the ERA-40 experiment (1961-1992) and the ERA-Interim experiment (1993-2014), as described above, in order to investigate the changes in the thermocline feedback over the period 1961 to 2014 in

the eastern Pacific (Nino3 region) and the central Pacific (Nino4 region). Figure 9 shows the 15-year running correlations between SST and sea surface height, both from AVISO and the linear model experiments, averaged over the Nino3 or Nino4 regions (the reason for using 15 year running means is to ensure some meaningful overlap with the AVISO period; the results do not differ in any substantive way if 21 year running windows are used). The time series are detrended within each 15-year running window before calculating the correlations. Note that the correlations from the model experiments for both the Nino3 and Nino4 regions agree well with those derived from AVISO during the period of overlap. In contrast with the eastern Pacific where the implied thermocline feedback is continuously strong (> 0.8) over the analysis period, the implied thermocline feedback in the central Pacific undergoes a dramatic increase, with the correlation increasing from about 0.4 to over 0.7, comparable to that in the eastern Pacific in the most recent 15 year period. This result is consistent with the increase in thermocline feedback in the Nino4 region noted by Dewitte et al., (2013), although their correlations (see their Figure 3) are consistently lower than we find here. Dewitte et al., (2013) correlated SST with the depth of the 20°C isotherm, the latter being calculated from SODA ocean reanalysis data (Giese and Ray, 2011). As a check, we have computed the 11-year running correlation between SST and sea level variations in the Nino4 region using sea level data from SODA, the model-computed sea level and AVISO, shown in Figure 10. It is clear that when using sea level from SODA (dashed blue line), there is generally good agreement with the model (solid blue line), showing that the difference from Dewitte et al., (2013) arises from their use of the depth of the 20°C isotherm to compute the correlation and our use of sea level. The use of an 11 year running window here is because the SODA data only runs to 2009 and we wanted to show some overlap with AVISO. It is notable that many of the variations in the running correlation are found when using both sea level from SODA and sea level from the model. This suggests that these variations have their origin in the variations in the wind forcing since the model is forced only by wind stress. Generally speaking the correlation between SST and sea level from SODA tends to higher/lower than when using model sea level early/later in the analysis period with excellent agreement between with AVISO during the overlap period.

We next note that G17 found a large increasing trend in the 21-yr running variance of zonal wind stress, TAUX, in the western equatorial Pacific over the period 1961 to 2014, with the largest increase occurring near 165.5°E on the equator (see their Figure 7). Figure 11 shows the 21-yr running variance of TAUX at 165.5°E, 0°N and the 21-yr running correlations between SST and sea level variations, as computed from our model and averaged over the Nino4 region, for the period 1961 to 2014. Note that all the time series have been detrended within the each 21-yr window (detrending was not applied by G17). Both time series show a similar upward trend, even showing a jump centred around 1990, suggesting that the wind at 165.5°E, 0°N is active in improving

the thermocline feedback in the Nino4 region. G17 also noted that one consequence of the upward trend in zonal wind stress variance in the western equatorial Pacific is the westward shift of the pivot point of sea level (and hence the thermocline) associated with the "tilt" mode. A westward shift in the pivot point puts the Nino4 region more clearly to the east of the pivot point suggesting the possibility that the Bjerknes feedback can operate there, exactly as it does in the Nino3 region further east, consistent with the emergence of CP ENSO events in recent decades. In fact, as can be seen from Figure 9 in G17, based on AVISO data, the pivot point was located near 160°E on the equator during the period 1993-2014, right at the western edge of the standard Nino4 box and, furthermore, was almost certainly located further to the east before that time, as argued there.

3.2.3 Assessing the Bjerknes feedback for the Nino4 region

The next step in the argument is to show that Bjerknes feedback does indeed operate in the central Pacific and, more importantly, that the strength of this feedback has increased during the analysis period, a factor that could explain the increased occurrence of CP events. To do this, we use the approach taken by Dippe et al., (2017) (see their Section 6) and look for a relationship between three key variables: SST anomalies and sea level anomalies in the Nino4 region as in the previous analysis, and zonal wind stress anomalies in the region 5°S - 5°N, 150°E - 180°E (hereafter the CPwest region), indicated by the solid-line-edged boxes in Figure 7a,b,c. The longitudinal range of the CPwest region is chosen based on Figure 7b in G17, and is such that within the box, the trend in the 21yr running variance of zonal wind stress for the period 1961-2002 exceeds half of the maximum trend ($\sim 8 \times 10^{-6} N^2 m^{-4} yr^{-1}$) that is found at 165.5°E, 0°N. Figure 12 shows the correlations in the 21 year running window from 1961 to 2014 between pairs of the three variables: SST anomalies in the standard Nino4 box, sea level anomalies in the shifted Nino4 box from the linear model experiments, and zonal wind stress anomalies in the CPwest region. The higher these correlations, the stronger is the implied Bjerknes feedback centred on the Nino4 region. It is clear that all three correlations have an upward trend during the analysis period. Furthermore, remembering that we are using a 21 year running window here, the upward shift in the correlations, which starts in the late 1980's, coincides with the first of the 21 year windows to sit entirely in the post-1976/77 climate shift period. Of particular importance in closing the Bjerknes feedback loop is the increase in thermocline feedback, indicated by the SST/sea level correlation, that was already noted in the previous paragraph. What these results indicate is that: (i) SST anomalies in the Nino4 region lead to zonal wind stress anomalies in the CPwest region (black); (ii) zonal wind stress anomalies in the CPwest region drive sea level anomalies (i.e. thermocline depth anomalies) in the Nino4 region, presumably through equatorial Kelvin waves (red curve); and (iii) thermocline depth (here sea level) anomalies in

the Nino4 region influence SST anomalies through thermocline feedback (blue curve), hence closing the Bjerknes feedback loop. Furthermore, the strength of this loop has increased during the time period that CP events have become more common, in particular since the 1976/77 climate shift.

Following on from the previous paragraphs, we envisage the following scenario. Variations in zonal wind stress to the west of the Nino4 region excite equatorial Kelvin waves that propagate eastwards and lead to variations in the thermocline depth in the Nino4 region. Furthermore, because of the westward shift in the pivot point, these thermocline depth variations are analogous to variations in thermocline depth in the Nino3 region, further east, that are traditionally associated with ENSO events. These thermocline variations have the potential to influence SST in the Nino4 region through the thermocline feedback and, indeed, we have presented evidence for an increase in the thermocline feedback in the Nino4 region in recent decades. The resulting SST variations manifest themselves in an increased occurrence of CP events (Lee and McPhaden, 2010), the SST variability in turn, through the Bjerknes feedback, leading to the increased variance in zonal wind stress west of the Nino4 region which, in turn, acts to maintain the westward shift in the pivot point. In effect, the Bjerknes feedback mechanism operates further west than during EP events, an effect that is facilitated by the westward shift of the pivot point for thermocline variations. The above analysis suggests that episodes of CP events could occur naturally as part of a positive feedback process involving the westward shift of the pivot point. It is known that come coupled models exhibit episodes in which CP events become prominent (Capotondi et al., 2015), perhaps associated with the positive feedback noted here.

4 Summary and discussion

We began by revisiting the relationship between ENSO diversity and EOFs of SST over the tropical Pacific (112°E - 70°W, 12°S - 18°N), here utilizing sea level for the tropical Pacific computed using a linear, multi-mode model for the period 1961-2014, together with AVISO satellite data that is available from 1993 onwards . Ashok et al., (2007) used the second EOF of SST (EOF2) to identify Central Pacific (CP) events (what they called ENSO Modoki events) and introduced the EMI index (ENSO Modoki Index), based in the spatial pattern of EOF2, as a means of measuring these events. Their analysis, however, was confined to the time period after the 1976/77 climate shift and they had difficulty identifying CP events before the 1976/77 climate shift. The existence of CP events is actually quite controversial. Indeed, Takahashi et al., (2011) and Dommenget et al., (2013) have argued that ENSO is fundamentally nonlinear and that a linear EOF analysis leads to the misleading interpretation that CP events, associated with EOF2, operate independently from the East Pacific (EP) events, captured by EOF1. Here, we found that the spatial pattern of EOF1 to be

quite robust either side of the 1976/77 climate shift and well represents the traditional EP events. By contrast, EOF2 is shifted to the west before the 1976/77 climate shift and shows the emergence of anomalies in the western Pacific of the same sign as those found in the eastern Pacific, consistent with the SST pattern usually associated with CP events, after the 1976/77 climate shift. Consistently, the regression of sea level and zonal wind stress onto the principal component time series, PC1 and PC2, show a significant difference in their spatial patterns either side of the 1976/77 climate shift in the case of PC2. The sea level associated with EOF2 in the earlier period looks like a propagating Rossby wave and the zonal wind stress has weak easterly anomalies along the equator, suggesting the decaying phase of ENSO. The regression in the later period, on the other hand, not only shows the characteristics of CP El Niño events in the observational studies (e.g. McPhaden, 2004) but also shows similarities to the regression patterns obtained using PC1, be they westward shifted. In particular, for the positive phase of EOF2, a region of westerly wind stress anomaly along the equator is now found in the western equatorial Pacific. These results support the view that CP events emerged after the 1976/77 climate shift and, furthermore, that they have many of the characteristics usually associated with ENSO.

We then set out to assess and interpret the change in the thermocline feedback in the Nino3 and Nino4 regions associated with ENSO over the period 1961-2014. The thermocline feedback is measured by the correlation between SST anomalies and sea level anomalies (a proxy for thermocline depth anomalies). Dewitte et al., (2013) show evidence, using the SODA ocean reanalysis, that the role of thermocline feedback has increased in the Nino4 region and attribute it to the increased stratification in the western-central tropical Pacific. Our results also show that the thermocline feedback in the Nino4 region underwent a dramatic increase, with the correlation between SST and sea level increasing from about 0.4 to over 0.7 in recent decades. We argue that this change is rooted in changes in the wind field over the equatorial Pacific, especially the western equatorial Pacific, where there was a strong increase in the variance of the zonal wind stress throughout our analysis period of 1961-2014.

As noted above, Dewitte et al., 2013 argue that the increase in thermocline feedback in the Nino4 region was a consequence of the change the strength of the thermocline following the 1976/77 climate shift. It is an interesting point that changes in stratification are not considered by the linear multi-mode model we have used to compute sea level, since it uses a fixed set of vertical normal modes, derived as described in Zhu et al., (2017) from World Ocean Atlas data (Locarnini et al., 2013). Furthermore, the wind projection coefficients for each vertical mode are fixed throughout the analysis period. It follows that the vertical movement of the thermocline that, in turn, can influence SST through the thermocline feedback, is not influenced by changes in stratification in our analysis. While this does not preclude the possibility that changes in stratification can change the SST, it does place emphasis on the role of

the wind field in the dynamics of the changing thermocline feedback. It is also worth pointing out that CP events occur not only when the thermocline is anomalously flat along the equator, as in the years after the 1976/77 climate shift (Yeh et al., 2009), but also when the thermocline is anomalously steep, as in the early years of the 21st century (Lübbecke and McPhaden, 2014; McPhaden et al., 2011). This also points to an important role for the wind field in the dynamics of ENSO diversity.

The concurrence of increasing thermocline feedback in the Nino4 region, increasing zonal wind stress variability to the west of the Nino4 region, and the increased occurrence of CP events, led us to investigate the Bjerknes feedback (Bjerknes, 1969) , as it applies to the Nino4 region. To do this, we followed the approach used in Section 6 of Dippe et al., (2017) and work with three key variables: SST and sea level anomalies in the Nino4 region and zonal wind stress anomalies in the region of 5°S - 5°N, 150°E - 180°E (called CPwest region) immediately to the west of the Nino4 region. CPwest is the region associated with the increasing trend in zonal wind stress variance (see Greatbatch et al., submitted; G17). The correlations between the pairs of the three variables all exhibit an upward trend during the analysis period, indicating that the Bjerknes feedback loop is closed and has been strengthening. Of particular importance for closing the loop is the increase in the thermocline feedback in the Nino4 region. Moreover, G17 have pointed out that one consequence of the increasing zonal wind stress variance in the western Pacific is to shift the pivot point associated with the "tilt" mode of Clarke, (2010) to the west. This, in turn, helps to increase the thermocline feedback in the Nino4 region, in turn facilitating the emergence of the Bjerknes feedback in the Nino4 region, favorable for the occurrence of the CP events. Furthermore, an increase in the occurrence of CP events increases the variance of the zonal wind stress to the west through the Bjerknes feedback. The analysis suggests that episodes of CP events could occur naturally as part of a positive feedback process involving the westward shift of the pivot point, a topic for further investigation.

Acknowledgements

Xiaoting Zhu is grateful for funding from the China Scholarship Council (201306330071). This study has also been supported by the Deutsche Forschungsgemeinschaft as part of the Sonderforschungsbereich 754 "Climate-Biogeochemistry interactions in the Tropical Ocean", through the German Ministry for Education and Research (BMBF) through MiKlip2, subproject 01LP1517D (ATMOS-MODINI) and SACUS (03G0837A), and by the European Union 7th Framework Programme (FP7 2007-2013) under grant agreement 603521 PREFACE project. The data used in this study can be obtained from data.geomar.de.

References

Ashok, K. and T. Yamagata (2009). "Climate change: The El Niño with a difference". In: *Nature* 461.7263, pp. 481–484.

Ashok, K., S. K. Behera, S. A. Rao, H. Weng, and T. Yamagata (2007). "El Niño Modoki and its possible teleconnection". In: *Journal of Geophysical Research: Oceans* 112.C11.

Becker, M., B. Meyssignac, C. Letetrel, W. Llovel, A. Cazenave, and T. Delcroix (2012). "Sea level variations at tropical Pacific islands since 1950". In: *Glob. Planet. Change* 80, pp. 85–98.

Belmadani, A., B. Dewitte, and S.-I. An (2010). "ENSO feedbacks and associated time scales of variability in a multimodel ensemble". In: *Journal of Climate* 23.12, pp. 3181–3204.

Berrisford, P., D Dee, K Fielding, M Fuentes, P Kallberg, S Kobayashi, and S Uppala (2009). "The ERA-Interim Archive". In: *ERA Rep. Ser.* 1.1, pp. 1–16.

Bjerknes, J. (1969). "Atmospheric teleconnections from the equatorial Pacific". In: *Monthly Weather Review* 97.3, pp. 163–172.

Capotondi, A. (2013). "ENSO diversity in the NCAR CCSM4 climate model". In: *Journal of Geophysical Research: Oceans* 118.10, pp. 4755–4770.

Capotondi, A., A. T. Wittenberg, M. Newman, E. Di Lorenzo, J.-Y. Yu, P. Braconnot, J. Cole, B. Dewitte, B. Giese, E. Guilyardi, et al. (2015). "Understanding ENSO diversity". In: *Bulletin of the American Meteorological Society* 96.6, pp. 921–938.

Clarke, A. J. (2010). "Analytical theory for the quasi-steady and low-frequency equatorial ocean response to wind forcing: The "tilt" and "warm water volume" modes". In: *Journal of Physical Oceanography* 40.1, pp. 121–137.

Dewitte, B., S.-W. Yeh, and S. Thual (2013). "Reinterpreting the thermocline feedback in the western-central equatorial Pacific and its relationship with the ENSO modulation". In: *Climate dynamics* 41.3-4, pp. 819–830.

Dippe, T., R. J. Greatbatch, and H. Ding (2017). "On the relationship between Atlantic Niño variability and ocean dynamics". In: *Climate Dynamics*. DOI: 10.1007/s00382-017-3943-z.

Dommenget, D., T. Bayr, and C. Frauen (2013). "Analysis of the non-linearity in the pattern and time evolution of El Niño southern oscillation". In: *Climate dynamics* 40.11-12, pp. 2825–2847.

Ebisuzaki, W. (1997). "A method to estimate the statistical significance of a correlation when the data are serially correlated". In: *Journal of Climate* 10.9, pp. 2147–2153.

Giese, B. S. and S. Ray (2011). "El Niño variability in simple ocean data assimilation (SODA), 1871–2008". In: *Journal of Geophysical Research: Oceans* 116.C2.

Hirahara, S., M. Ishii, and Y. Fukuda (2014). "Centennial-scale sea surface temperature analysis and its uncertainty". In: *Journal of Climate* 27.1, pp. 57–75.

Holgate, S. J., A. Matthews, P. L. Woodworth, L. J. Rickards, M. E. Tamisiea, E. Bradshaw, P. R. Foden, K. M. Gordon, S. Jevrejeva, and J. Pugh (2013). "New data systems and products at the permanent service for mean sea level". In: *Journal of Coastal Research* 29.3, pp. 493–504.

Jin, F.-F., S. T. Kim, and L. Bejarano (2006). "A coupled-stability index for ENSO". In: *Geophysical research letters* 33.23.

Kalnay, E., M. Kanamitsu, R. Kistler, W. Collins, D. Deaven, L. Gandin, M. Iredell, S. Saha, G. White, J. Woollen, et al. (1996). "The NCEP/NCAR 40-year reanalysis project". In: *Bull. Amer. Meteor. Soc.,* 77.3, pp. 437–471.

Lee, T. and M. J. McPhaden (2010). "Increasing intensity of El Niño in the central-equatorial Pacific". In: *Geophysical Research Letters* 37.14.

Locarnini, R. A., A. V. Mishonov, J. I. Antonov, T. P. Boyer, H. E. Garcia, O. K. Baranova, M. M. Zweng, C. R. Paver, J. R. Reagan, D. R. Johnson, M. Hamilton, and D. Seidov (2013). "World Ocean Atlas 2013. Vol. 1: Temperature." In: *S. Levitus, Ed.; A. Mishonov, Tech. Ed.; NOAA Atlas NESDIS* 73.September, p. 40. DOI: 10.1182/blood-2011-06-357442.

Lübbecke, J. F. and M. J. McPhaden (2014). "Assessing the twenty-first-century shift in ENSO variability in terms of the Bjerknes stability index". In: *Journal of Climate* 27.7, pp. 2577–2587.

McPhaden, M., T Lee, and D McClurg (2011). "El Niño and its relationship to changing background conditions in the tropical Pacific Ocean". In: *Geophysical Research Letters* 38.15.

McPhaden, M. J. (1999). "Genesis and evolution of the 1997-98 El Niño". In: *Science* 283.5404, pp. 950–954.

— (2004). "Evolution of the 2002/03 El Niño". In: *Bulletin of the American Meteorological Society* 85.5, pp. 677–695.

North, G. R., T. L. Bell, R. F. Cahalan, and F. J. Moeng (1982). "Sampling errors in the estimation of empirical orthogonal functions". In: *Monthly Weather Review* 110.7, pp. 699–706.

Rayner, N., D. E. Parker, E. Horton, C. Folland, L. Alexander, D. Rowell, E. Kent, and A Kaplan (2003). "Global analyses of sea surface temperature, sea ice, and night marine air temperature since the late nineteenth century". In: *Journal of Geophysical Research: Atmospheres* 108.D14.

Rebert, J.-P., J.-R. Donguy, G. Eldin, and K Wyrtki (1985). "Relations between sea level, thermocline depth, heat content, and dynamic height in the tropical Pacific Ocean". In: *Journal of Geophysical Research: Oceans* 90.C6, pp. 11719–11725.

Takahashi, K, A Montecinos, K Goubanova, and B. Dewitte (2011). "ENSO regimes: Reinterpreting the canonical and Modoki El Niño". In: *Geophysical Research Letters* 38.10.

Trenberth, K. E. and D. P. Stepaniak (2001). "Indices of el Niño evolution". In: *Journal of Climate* 14.8, pp. 1697–1701.

Trenberth, K. E., J. M. Caron, D. P. Stepaniak, and S. Worley (2002). "Evolution of El Niño–Southern Oscillation and global atmospheric surface temperatures". In: *Journal of Geophysical Research: Atmospheres* 107.D8.

Yeh, S.-W., J.-S. Kug, B. Dewitte, M.-H. Kwon, B. P. Kirtman, and F.-F. Jin (2009). "El Niño in a changing climate". In: *Nature* 461.7263, pp. 511–514.

Zhu, X., R. J. Greatbatch, and M. Claus (2017). "Interannual variability of tropical Pacific sea level from 1993 to 2014". In: *Journal of Geophysical Research: Oceans* 122.1, pp. 602–616. DOI: 10.1002/2016JC012347.

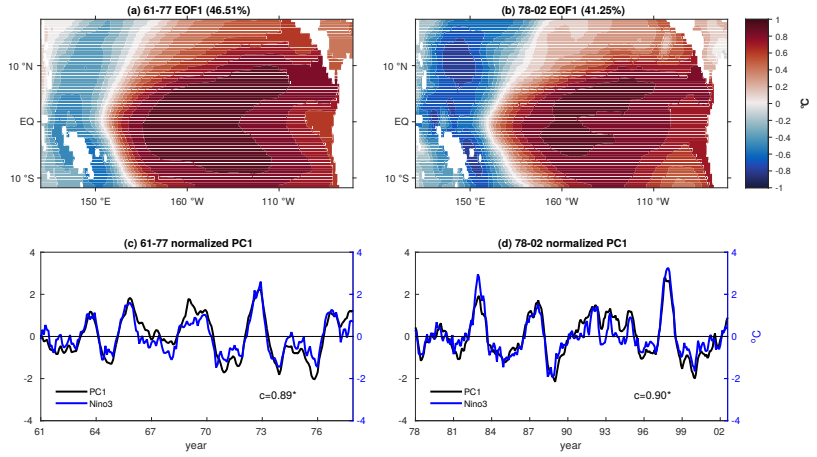

Figure 1: *Dimensional spatial pattern of the first Empirical Orthogonal Function (EOF1) of COBE2 SST anomalies for the period of* ***(a)*** *1961-1977 and* ***(b)*** *1978-2002. Explained variance is denoted in the bracket.* ***(c, d)*** *Normalized time series of the principal component (PC1) corresponding to (a) and (b) respectively, with the contemporary Nino3 index superimposed. The correlation between PC1 and the Nino3 index is indicated in each panel. The star subscript refers to correlations above 95% significance level based on the method of Ebisuzaki, (1997).*

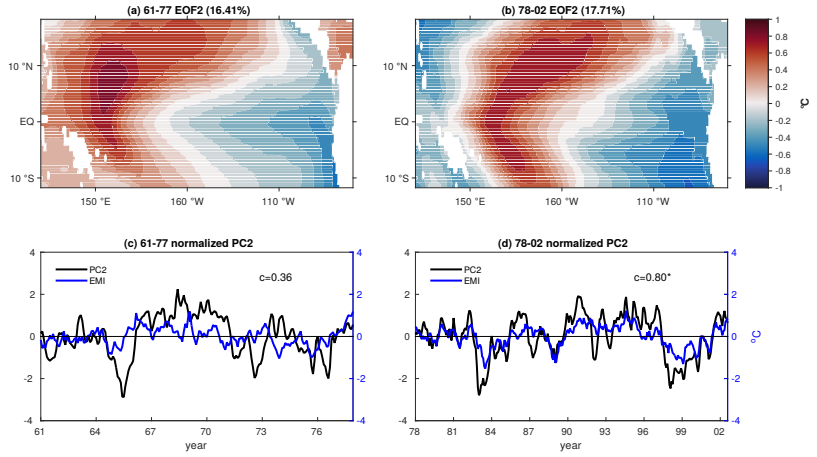

Figure 2: *Same as Figure 1, but for EOF2 and with the El Niño Modoki Index (EMI) substituted for the Nino3 index.*

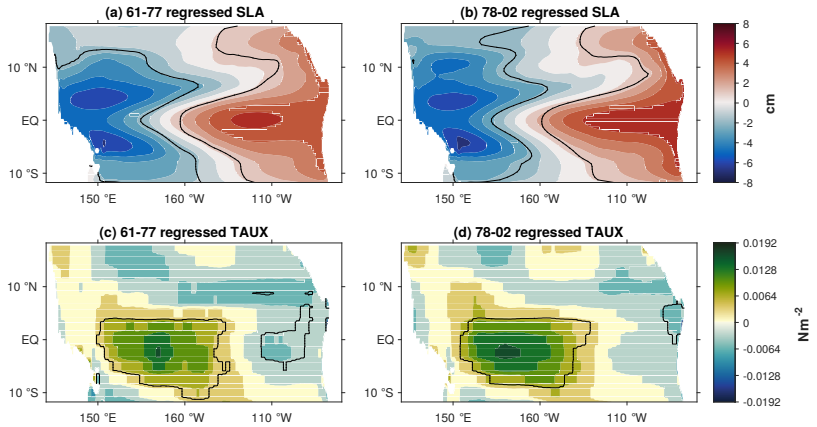

Figure 3: *Spatial patterns of* ***(a)*** *sea level anomalies (SLA) from the ERA-40 experiment in G17 driven by ERA-40 monthly wind stress anomalies and* ***(c)*** *ERA-40 zonal wind stress anomalies (TAUX) regressed onto PC1 for COBE2 SST anomalies at zero lag for the period of 1961-1977.* ***(b, d)*** *Same as (a) and (c) respectively, but for the period of 1978-2002. The superimposed black contour lines denote the* 95% *significance level based on the method of Ebisuzaki, (1997).*

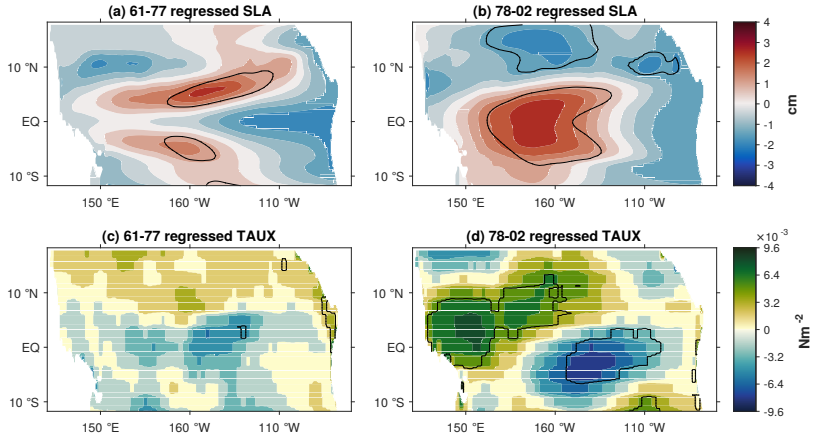

Figure 4: *Same as figure 3, but regressed onto PC2 for SST anomalies.*

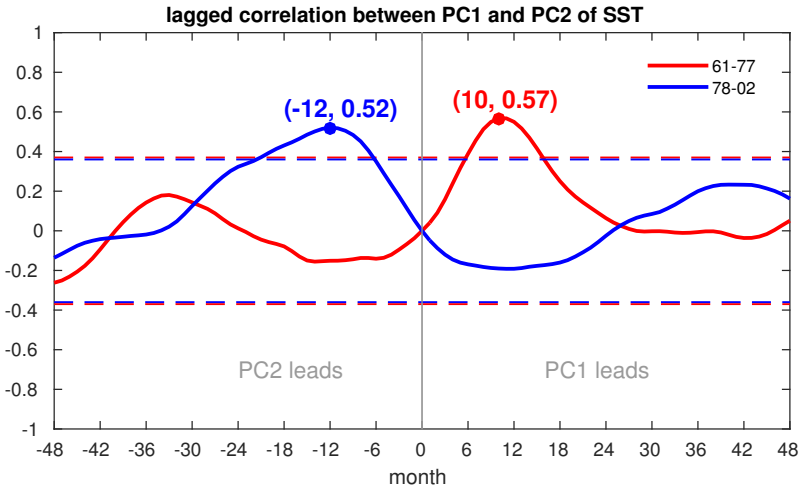

Figure 5: *Lagged correlations between PC1 and PC2 of COBE2 SST for the period of 1961-1977 (red curve) and 1978-2002 (blue curve). The corresponding 95% significance levels based on the method of Ebisuzaki, (1997) are denoted by the horizontal dashed colored lines, and the coordinates of maximum correlations are highlighted by the colored dots and text. Positive (negative) lag means PC1 leads (lags) PC2.*

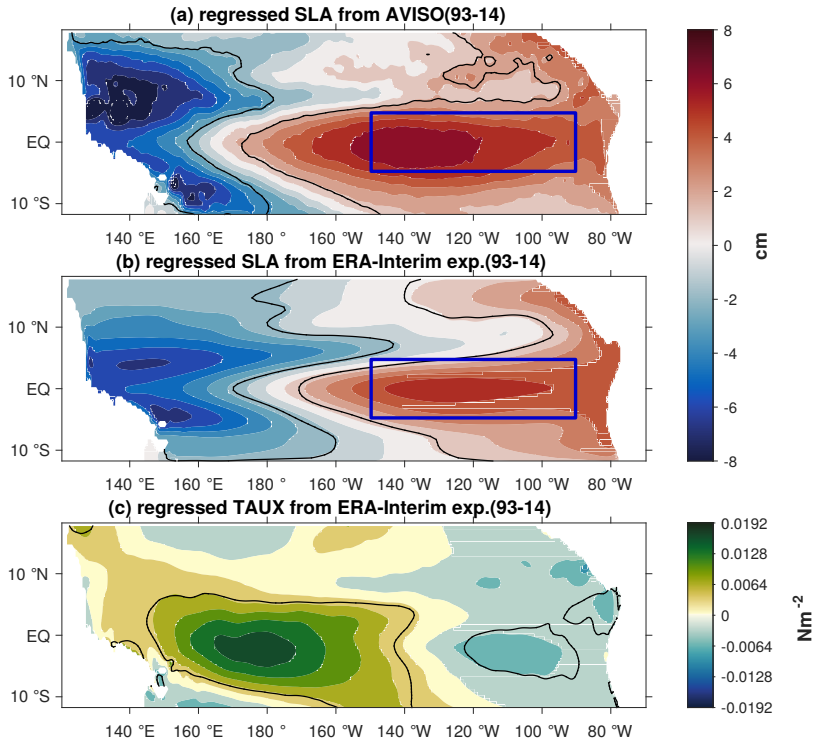

Figure 6: *Spatial patterns of* ***(a)*** *AVISO SLA,* ***(b)*** *SLA from the standard ERA-Interim experiment in Zhu et al., (2017) and* ***(c)*** *ERA-Interim TAUX regressed onto PC1 for COBE2 SST anomalies at zero lag for the period of 1993-2014. The superimposed black contour lines denote the* 95% *significance level based on the method of Ebisuzaki, (1997). The rectangle boxes in (a) and (b) indicate the Nino3 box.*

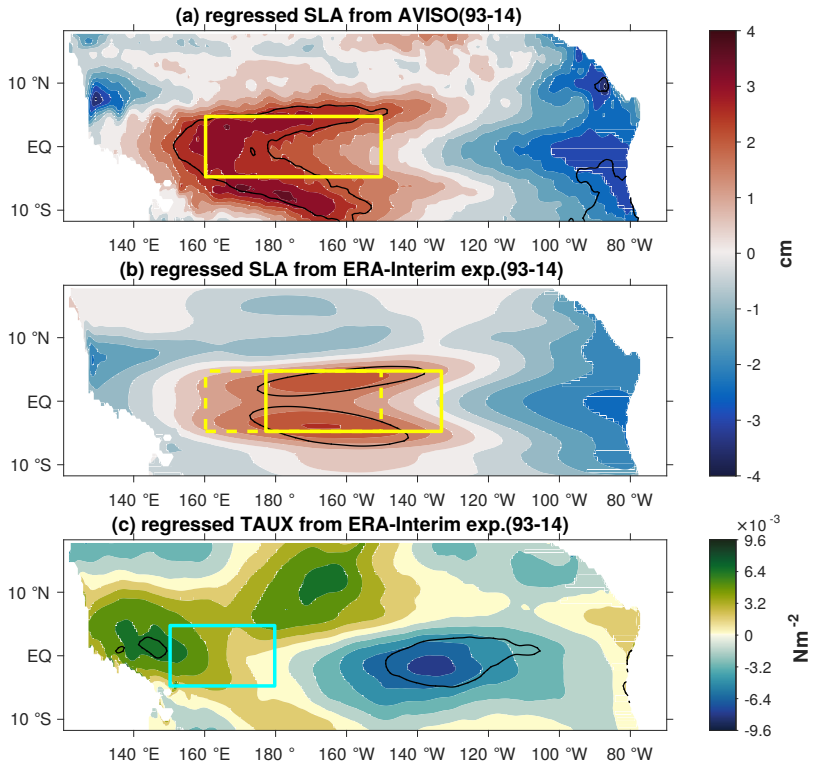

Figure 7: *Same as figure 6, but regressed onto PC2. The yellow boxes indicate the Nino4 boxes used for the analysis. In* ***(b)****, this is shifted to the east from the standard Nino4 box (shown using dashed lines yellow lines). The cyan box shows the CPwest region used for assessing the strength of the Bjerknes feedback (see text for details).*

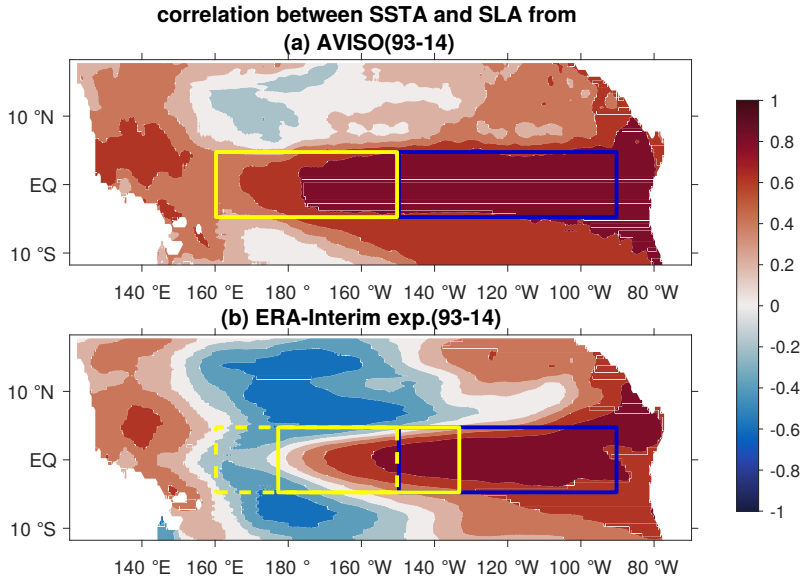

Figure 8: ***(a)*** *Spatial distribution of correlations between COBE2 SST anomalies and SLA from satellite observations (AVISO) for the period 1993-2014. The rectangular boxes show the Nino3 (blue) and Nino4 (yellow) regions used for computing the sea level indices SLA[Nino3] and SLA[Nino4] from AVISO, respectively.* ***(b)*** *Same as (a), but for SLA from the standard experiment driven by ERA-Interim monthly wind stress anomalies in Zhu et al., (2017). The regions for computing SLA[index] from the model experiments are shown as in (a). Note that for the Nino4 region, this is shifted to the east from the standard Nino4 box (shown by dashed yellow lines).*

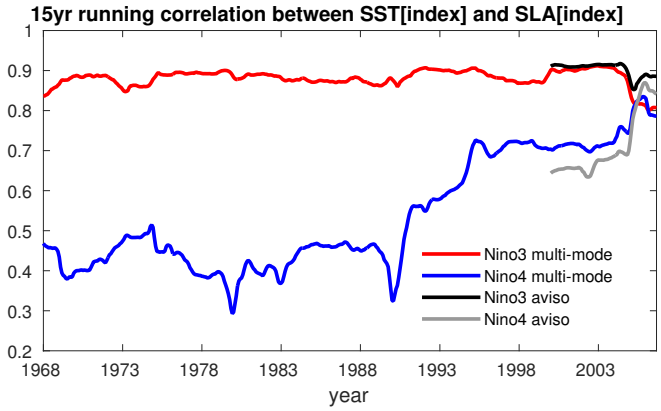

Figure 9: *15-yr running correlation from 1961 to 2014 between Nino3 and SLA[Nino3] (red solid curve), Nino4 and SLA[Nino4] (blue solid curve), indicating the strength of the thermocline feedback in the Nino3 and Nino4 regions. The SLA[index] is computed from the ERA-40 experiment for the period of 1961-1992 and from the ERA-Interim experiment for the period of 1993-2014, as explained in the text. The corresponding running correlations using AVISO sea level are shown by the black (grey) line for the Nino3 (Nino4) regions, respectively.*

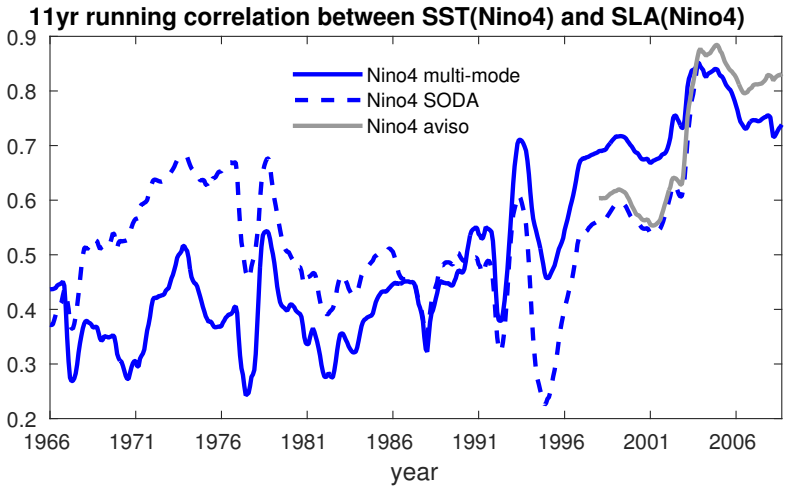

Figure 10: *11-yr running correlation between SST and SLA[Nino4] for the Nino4 regions from the multi-mode model experiments (1961-2014), SODA (1961-2009) and AVISO (1993-2014).*

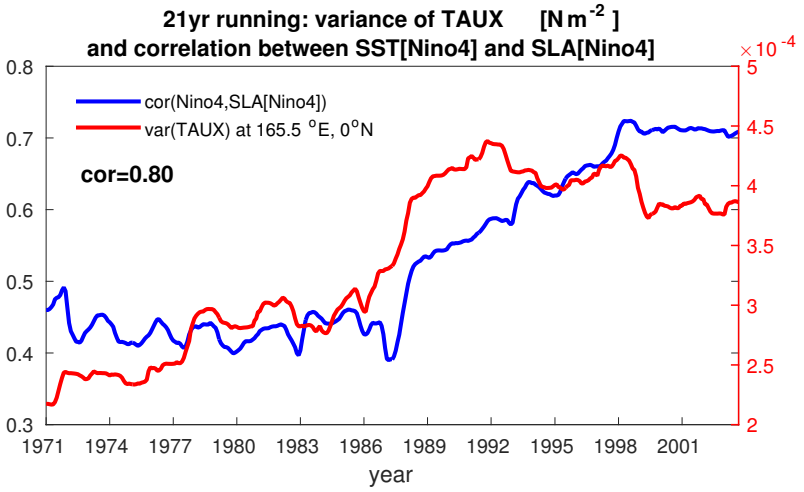

Figure 11: *21-yr running variance from 1961 to 2014 of zonal wind stress, TAUX, at 160° E, 0° N (red curve-right scale) and 21-yr running correlation from 1961 to 2014 between Nino4 and SLA[Nino4] (blue curve-left scale). The correlation is shown. SLA's are same as those used in Figure 9. Similarly, TAUX is the combination of ERA-40 for the period of 1961-1992 and ERA-Interim for the period of 1993-2014.*

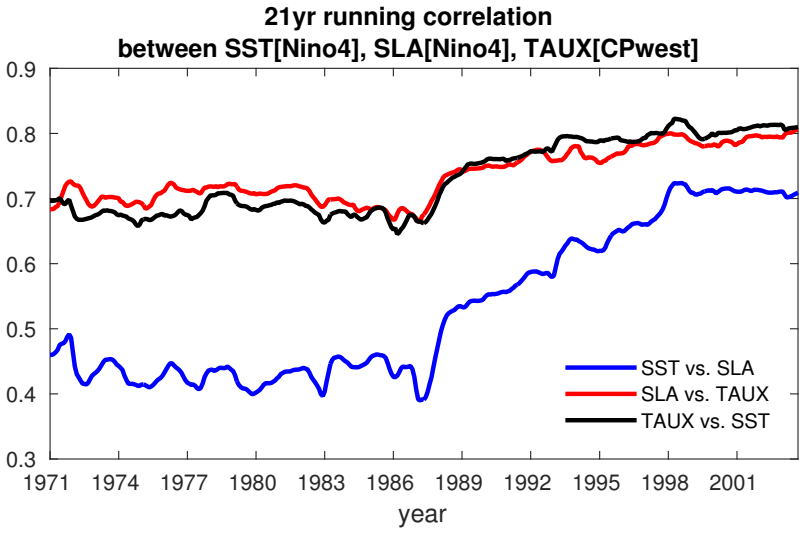

Figure 12: *21-yr running correlations for the period 1961-2014 pairs of the variables SST (for the Nino4 region), SLA[Nino4] and spatially averaged zonal wind stress over the box CPwest (5° S - 5° N, 150° E - 180° E), representing the three components of the Bjerknes feedback. The Nino4 and CPwest boxes are shown by the yellow and cyan boxes in Figure 7b and Figure 7c, respectively.*

5 Summary

In this thesis, the interannual sea level variations in the tropical Pacific over the time span 1961-2014 are simulated to investigate the dynamics of ENSO using a linear multi-mode model, given the good agreement of the ENSO-related sea level variations with the linear wave dynamics. A special focus is the dynamics of the increasing occurrence of the Central Pacific ENSO (CP ENSO) contrasting with the classical Eastern Pacific ENSO (EP ENSO), termed with respect to the locations of maximum Sea Surface Temperature anomalies (SSTa) during the mature phase, which posts new challenges to the prediction of ENSO in recent two decades.

The previous three chapters give the answers to the scientific questions raised in Chapter 1.5 as follows.

- **Which vertical baroclinic modes are important for ENSO-related sea level variations in the tropical Pacific? Does the model capture the characteristics of ENSO (e.g. the pivot point of sea level)? Is the Sverdrup transport fundamental to the recharge/discharge oscillator (RDO) mechanism for EP ENSO?** (Chapter 2)

  $\rightarrow$ In the linear multi-mode model for the tropical Pacific (112°E - 70°W, 12°S - 18°N) built in this thesis, the weighting given to each mode was assigned by fitting the modelled sea level anomalies (SLA) forced by ERA-Interim monthly wind stress anomalies (named ERA-I exp.) to the AVISO SLA along the equator over the period 1993-2014. The signal associated with modes higher than mode 6 (with approximately zero amplitude) cannot be extracted from the AVISO data. Thus the model includes the first five vertical modes. Mode 2 is dominant, although with some role particularly in the western equatorial Pacific for mode 1, the eastern equatorial Pacific for mode 5, and both regions for mode 3.

  The model successfully captures the ENSO events of various strengths and flavors. An interesting feature is the presence of a pivot point in the western Pacific on the equator that seems to depend mainly on the fact that most variations in zonal wind stress occur in the western basin, although there is also a signature from the RDO

in which eastward/westward zonal mean zonal wind stress anomalies are associated with a downward/upward displacement of the zonal mean thermocline along the equator at zero lag.

It is also shown that the recharge/discharge of the warm water volume (WWV) does not depend on the spatial structure of the wind forcing and, in particular, on the Sverdrup transport as in the original RDO theory, although the spatial structure of the wind forcing has a role to play in determining the amplitude of the WWV along the equator.

- **Which wind forcing dataset is more reliable? What are the changes in the characteristics of ENSO-related sea level variations and their causes, particularly regarding the pivot point of sea level?** (Chapter 3)
  → SLA for the period 1961-2002 are reconstructed with the NCEP/NCAR and ERA-40 wind forcing (named NCEP/NCAR exp. and ERA-40 exp. respectively) validated by tide gauge records. The ERA-40 wind product is more reliable than the NCEP/NCAR product with higher correlations between modelled sea level and tide gauge data. Besides, the sensitivity experiments driven by only the zonal component of the two wind stress products suggest that a large increasing trend in sea level found in the NCEP/NCAR exp. but not in the ERA-40 exp. is related to a spurious eastward trend in NCEP/NCAR zonal wind stress in the eastern-central Pacific.

  A way to quantify the location of the pivot point is to identify its location with the zero crossing of the EOF1 for sea level along the equator. The analysis also shows a more westward location in the pivot point during the period 1993–2014 than 1961-2002. It is attributed to a persistent upward trend in the zonal stress variance along the equator west of 160°W throughout the period 1961-2014.

- **Do the EOF1 and EOF2 of SSTa in the tropical Pacific represent EP ENSO and CP ENSO? What is the role of the thermocline feedback in, and what is the underlying mechanism for, the emergence of CP ENSO?** (Chapter 4)
  → The regression of sea level from ERA-I exp. and ERA-40 exp. onto the principal component (PC) of EOF2 of SSTa show significantly different spatial patterns either side of the 1976/77 climate shift, whereas those of EOF1 remain quite robust throughout the climate shift. The sea level associated with EOF2 in the earlier period looks like a propagating Rossby wave suggesting the decaying phase of ENSO, whereas that in the later period shows the characteristics of CP ENSO

in the observations. Consistently, PC1 leads (lags) PC2 before (after) the 1976/77 climate shift. These results support the view that EOF1 and EOF2 can represent EP ENSO and CP ENSO after the climate shift, but little evidence for the occurrence of Central Pacific (CP) events before the 1976/77 climate shift is found.

After the climate shift, the thermocline feedback in the CP (Nino4 region) is found to increase strongly. At the same time, the Bjerknes feedback mechanism is shown to increase in strength in the CP, concurrent with the increased occurrence of CP events. An important point is that the emergence of the thermocline feedback in the Nino4 region can be related to the westward shift of the pivot point for sea level (and hence thermocline) variations associated with the increase in zonal wind stress variance in the western equatorial Pacific, the latter in turn being related to the increased frequency of CP events due to the increasing Bjerknes feedback. As the pivot point shifts westward, the Nino4 region is found increasingly to the east of the pivot point enabling the thermocline feedback to operate there. These arguments imply a positive feedback in which CP events are self-maintaining and suggest that they may be part of the natural variability of the climate system and could occur episodically without the need for changes in external forcing.

All results presented in this thesis are based on the linear multi-mode model and thus rely on the assumption that the basic dynamics of ENSO phenomenon is mainly controlled by the linear wave dynamics. Unlike in previous studies, the vertical profile for the wind forcing in the ocean is not set a prior but determined by the fitting coefficients for the first five modes and thus is more realistic. Due to the lack of zonal advection in the model, the pivot point for sea level is displaced systematically to the east of the pivot point in AVISO leading to reduced correlations between model results and AVISO data in the region near the pivot point. While this should not influence the relative westward shift of the pivot point in the period 1993-2014 compared to 1961-2002 found in Chapter 3, this has to be considered in Chapter 4 when assessing the changes in thermocline feedback in the central Pacific (Nino4 region) including/near the pivot point. The method is to shift the Nino4 region for the modelled SLA eastward to the location where the correlation between the modelled SLA averaged over the shifted region and the AVISO SLA averaged over the normal Nino4 region reaches the maximum. Note that the changes in the stratification associated with the 1976/77 climate shift, which is attributed to the increase of thermocline feedback in the Nino4 region by *Dewitte et al.* (2013), is not included in the linear multi-mode model because both the vertical structure of vertical modes and of the wind forcing profile remains unchanged either side of the 1976/77 climate shift. Therefore, the mechanism for the emergence of CP ENSO in terms of the linear wave dynamics

proposed in this thesis provides a novel insight for understanding ENSO diversity.

5.1 Outlook

In the mechanism proposed in this thesis for the emergence of CP ENSO in recent two decades, the location of the pivot point for sea level (hence thermocline) plays the key role. The westward shift of pivot point leads to increased thermocline feedback and thus increasing Bjerknes feedback in the central Pacific (Nino4 region). As illustrated in Figure 1.2 from *Dewitte et al.* (2013), the pivot point of thermocline depth on the equator corresponds to the zero skewness of SST. The cold SST asymmetry in the western equatorial Pacific is associated with the dominance of zonal advective feedback as noted by *Belmadani et al.* (2010). These authors also point out that the biases in the advection terms are to a large extent induced by the biases in the mean surface circulation. Thus, modifying the linear multi-mode model linearized about a state of rest used in this thesis into a multi-mode model linearized about a realistic mean flow, by extending the method employed in *Claus et al.* (2014) from using barotropic mean flow to using baroclinic mean flow, is of interest for the influence of mean flow on the characteristics of CP ENSO.

Current state-of-the-art climate models, i.e. coupled general circulation models, still have problems in simulating the important features of ENSO or the strength of feedbacks, and there is uncertainty in the future projection for ENSO (*Collins et al.*, 2010; *Capotondi et al.*, 2015, and references therein). A recent study by *Bayr et al.* (2017) on the influence of the mean state of the Pacific on the atmospheric feedback shows that the cold bias (La Niña-like mean state) in the Nino4 region, a common problem in current climate models, leads to the rising branch of the Walker Circulation locating in the far west and a weak convective response, which causes different ENSO dynamics than in observations. The mean state of the Walker circulation is important for the Bjerknes feedback, which is a main concept in this thesis to explain the CP ENSO. Besides, they suggest that the mean state SST is a major source of ENSO diversity. Given that the equatorial cold bias and its consequences are common in climate models, they suggest to use only one climate model to reduce possible other causes in further relevant investigations. Motivated by their results, it is important to look at the proposed mechanism of dependence of the Bjerknes feedbacks in this thesis on the pivot point in a climate model especially in terms of the oceanic physical processes (see Section 1.2.2), in particular the relative importance of thermocline feedback and zonal advective feedback (*Belmadani et al.*, 2010; *Lübbecke and McPhaden*, 2014). The relative importance of these feedbacks is of particular interest for deep understanding of ENSO diversity

and leading oscillator mechanism (see Section 1.2.3) for CP ENSO, for which the RDO is not thought to be important (*Capotondi*, 2013).

The Atlantic Nino (e.g. *Lübbecke and McPhaden*, 2017; *Dippe et al.*, 2017), a counterpart of Pacific ENSO in the Atlantic Ocean, is another possible direction for future work based on the method of a linear multi-mode model in this thesis. However, the smaller basin of the Atlantic compared to the Pacific, and the associated basin mode resonances (*Brandt et al.*, 2016), may influence the accuracy of the relative importance of vertical modes from this model.

List of Figures

Bibliography

An, S.-I., and B. Wang (2000), Interdecadal change of the structure of the enso mode and its impact on the enso frequency, *Journal of Climate*, *13*(12), 2044–2055.

Ashok, K., and T. Yamagata (2009), Climate change: The el niño with a difference, *Nature*, *461*(7263), 481–484.

Ashok, K., S. K. Behera, S. A. Rao, H. Weng, and T. Yamagata (2007), El niño modoki and its possible teleconnection, *Journal of Geophysical Research: Oceans*, *112*(C11).

Bayr, T., M. Latif, D. Dommenget, C. Wengel, J. Harlaß, and W. Park (2017), Mean-state dependence of enso atmospheric feedbacks in climate models, *Climate Dynamics*, pp. 1–24.

Becker, M., B. Meyssignac, C. Letetrel, W. Llovel, A. Cazenave, and T. Delcroix (2012), Sea level variations at tropical pacific islands since 1950, *Glob. Planet. Change*, *80*, 85–98.

Belmadani, A., B. Dewitte, and S.-I. An (2010), Enso feedbacks and associated time scales of variability in a multimodel ensemble, *Journal of Climate*, *23*(12), 3181–3204.

Berrisford, P., D. Dee, K. Fielding, M. Fuentes, P. Kallberg, S. Kobayashi, and S. Uppala (2009), The ERA-Interim Archive, *ERA Rep. Ser.*, *1*(1), 1–16.

Bjerknes, J. (1969), Atmospheric teleconnections from the equatorial pacific, *Monthly Weather Review*, *97*(3), 163–172.

Bosc, C., and T. Delcroix (2008), Observed equatorial rossby waves and enso-related warm water volume changes in the equatorial pacific ocean, *Journal of Geophysical Research: Oceans*, *113*(C6).

Brandt, P., M. Claus, R. J. Greatbatch, R. Kopte, J. M. Toole, W. E. Johns, and C. W. Böning (2016), Annual and semiannual cycle of equatorial atlantic circulation associated with basin-mode resonance, *Journal of Physical Oceanography*, *46*(10), 3011–3029.

Busalacchi, A. J., and M. A. Cane (1985), Hindcasts of sea level variations during the 1982–83 el niño, *Journal of physical oceanography*, *15*(2), 213–221.

Busalacchi, A. J., and J. J. O'Brien (1981), Interannual variability of the equatorial pacific in the 1960's, *Journal of Geophysical Research: Oceans*, *86*(C11), 10,901, doi: 10.1029/JC086iC11p10901.

Busalacchi, A. J., K. Takeuchi, and J. J. O'Brien (1983), Interannual variability of the equatorial pacific—revisited, *Journal of Geophysical Research: Oceans*, *88*(C12), 7551–7562.

Cane, M. A., and E. S. Sarachik (1981), The response of a linear baroclinic equatorial ocean to periodic forcing, *Journal of Marine Research*, *39*, 651–693.

Capotondi, A. (2013), Enso diversity in the ncar ccsm4 climate model, *Journal of Geophysical Research: Oceans*, *118*(10), 4755–4770.

Capotondi, A., A. T. Wittenberg, M. Newman, E. Di Lorenzo, J.-Y. Yu, P. Braconnot, J. Cole, B. Dewitte, B. Giese, E. Guilyardi, et al. (2015), Understanding enso diversity, *Bulletin of the American Meteorological Society*, *96*(6), 921–938.

Cazenave, A., and F. Remy (2011), Sea level and climate: measurements and causes of changes, *Wiley Interdisciplinary Reviews: Climate Change*, *2*(5), 647–662.

Chelton, D. B., and M. G. Schlax (1996), Global observations of oceanic rossby waves, *Science*, *272*(5259), 234–238.

Chen, N., and A. J. Majda (2017), Simple stochastic dynamical models capturing the statistical diversity of el niño southern oscillation, *Proceedings of the National Academy of Sciences*, p. 201620766.

Clarke, A. J. (2010), Analytical theory for the quasi-steady and low-frequency equatorial ocean response to wind forcing: The "tilt" and "warm water volume" modes, *Journal of Physical Oceanography*, *40*(1), 121–137.

Claus, M., R. J. Greatbatch, and P. Brandt (2014), Influence of the barotropic mean flow on the width and the structure of the atlantic equatorial deep jets, *Journal of Physical Oceanography*, *44*(9), 2485–2497.

Collins, M., S.-I. An, W. Cai, A. Ganachaud, E. Guilyardi, F.-F. Jin, M. Jochum, M. Lengaigne, S. Power, A. Timmermann, et al. (2010), The impact of global warming on the tropical pacific ocean and el niño, *Nature Geoscience*, *3*(6), 391.

Delcroix, T. (1998), Observed surface oceanic and atmospheric variability in the tropical pacific at seasonal and enso timescales: A tentative overview, *Journal of Geophysical Research: Oceans*, *103*(C9), 18,611–18,633.

Dewitte, B., S.-W. Yeh, and S. Thual (2013), Reinterpreting the thermocline feedback in the western-central equatorial pacific and its relationship with the enso modulation, *Climate dynamics*, *41*(3-4), 819–830.

Dippe, T., R. J. Greatbatch, and H. Ding (2017), On the relationship between atlantic niño variability and ocean dynamics, *Climate Dynamics*, pp. 1–16.

Dommenget, D., T. Bayr, and C. Frauen (2013), Analysis of the non-linearity in the pattern and time evolution of el niño southern oscillation, *Climate dynamics*, *40*(11-12), 2825–2847.

Forget, G., and R. M. Ponte (2015), The partition of regional sea level variability, *Prog. Oceanogr.*, *137, Part*, 173 – 195, doi:10.1016/j.pocean.2015.06.002.

Gill, A., and A. Clarke (1974), Wind-induced upwelling, coastal currents and sea-level changes, in *Deep Sea Research and Oceanographic Abstracts*, vol. 21, pp. 325–345, Elsevier.

Gill, A. E. (1982), *Atmosphere-ocean Dynamics*, 662 pp., Academic press, san diego, california.

Han, W., G. A. Meehl, A. Hu, M. A. Alexander, T. Yamagata, D. Yuan, M. Ishii, P. Pegion, J. Zheng, B. D. Hamlington, et al. (2014), Intensification of decadal and multi-decadal sea level variability in the western tropical pacific during recent decades, *Clim. Dyn.*, *43*(5-6), 1357–1379.

Hirst, A. C. (1986), Unstable and damped equatorial modes in simple coupled ocean-atmosphere models, *Journal of the atmospheric sciences*, *43*(6), 606–632.

Hu, Z.-Z., A. Kumar, H.-L. Ren, H. Wang, M. L'Heureux, and F.-F. Jin (2013), Weakened interannual variability in the tropical pacific ocean since 2000, *Journal of Climate*, *26*(8), 2601–2613.

Im, S.-H., S.-I. An, S. T. Kim, and F.-F. Jin (2015), Feedback processes responsible for el niño-la niña amplitude asymmetry, *Geophysical Research Letters*, *42*(13), 5556–5563.

Imada, Y., H. Tatebe, M. Watanabe, M. Ishii, and M. Kimoto (2016), South pacific influence on the termination of el niño in 2014, *Scientific reports*, *6*, 30,341.

Jin, F.-F. (1997a), An equatorial ocean recharge paradigm for enso. part i: Conceptual model, *Journal of the atmospheric sciences*, *54*(7), 811–829.

Jin, F.-F. (1997b), An equatorial ocean recharge paradigm for enso. part i: Conceptual model, *Journal of the atmospheric sciences*, *54*(7), 811–829.

Jin, F.-F., and J. D. Neelin (1993), Modes of interannual tropical ocean–atmosphere interaction—a unified view. part i: Numerical results, *Journal of the atmospheric sciences*, *50*(21), 3477–3503.

Jin, F.-F., S. T. Kim, and L. Bejarano (2006), A coupled-stability index for enso, *Geophysical Research Letters*, *33*(23).

Kalnay, E., M. Kanamitsu, R. Kistler, W. Collins, D. Deaven, L. Gandin, M. Iredell, S. Saha, G. White, J. Woollen, et al. (1996), The ncep/ncar 40-year reanalysis project, *Bull. Amer. Meteor. Soc.,*, *77*(3), 437–471.

Kang, I.-S., J.-S. Kug, S.-I. An, and F.-F. Jin (2004), A near-annual pacific ocean basin mode, *Journal of climate*, *17*(12), 2478–2488.

Kessler, W. S. (1990), Observations of long rossby waves in the northern tropical pacific, *Journal of Geophysical Research: Oceans*, *95*(C4), 5183–5217.

Kim, S. T., and F.-F. Jin (2011), An enso stability analysis. part i: results from a hybrid coupled model, *Climate dynamics*, *36*(7-8), 1593–1607.

Li, B., and A. J. Clarke (1994), An examination of some enso mechanisms using interannual sea level at the eastern and western equatorial boundaries and the zonally averaged equatorial wind, *Journal of physical oceanography*, *24*(3), 681–690.

Liu, Z. (2012), Dynamics of interdecadal climate variability: A historical perspective, *Journal of Climate*, *25*(6), 1963–1995.

Lübbecke, J. F., and M. J. McPhaden (2014), Assessing the twenty-first-century shift in enso variability in terms of the bjerknes stability index, *Journal of Climate*, *27*(7), 2577–2587.

Lübbecke, J. F., and M. J. McPhaden (2017), Symmetry of the atlantic niño mode, *Geophysical Research Letters*, *44*(2), 965–973.

McCreary, J. (1981), A linear stratified ocean model of the equatorial undercurrent, *Phil. Trans. R. Soc. Lond. A*, *298*(1444), 603–635.

McGregor, S., A. Timmermann, F.-F. Jin, and W. S. Kessler (2016), Charging el niño with off-equatorial westerly wind events, *Climate dynamics*, *47*(3-4), 1111–1125.

McPhaden, M., T. Lee, and D. McClurg (2011), El niño and its relationship to changing background conditions in the tropical pacific ocean, *Geophysical Research Letters*, *38*(15).

McPhaden, M. J. (1999), Genesis and evolution of the 1997-98 el niño, *Science*, *283*(5404), 950–954.

McPhaden, M. J. (2004), Evolution of the 2002/03 el niño, *Bulletin of the American Meteorological Society*, *85*(5), 677–695.

McPhaden, M. J., A. J. Busalacchi, R. Cheney, J.-R. Donguy, K. S. Gage, D. Halpern, M. Ji, P. Julian, G. Meyers, G. T. Mitchum, et al. (1998), The tropical ocean-global atmosphere observing system: A decade of progress, *Journal of Geophysical Research: Oceans*, *103*(C7), 14,169–14,240.

Meinen, C. S., and M. J. McPhaden (2000), Observations of warm water volume changes in the equatorial pacific and their relationship to el niño and la niña, *Journal of Climate*, *13*(20), 3551–3559.

Meinen, C. S., and M. J. McPhaden (2001), Interannual variability in warm water volume transports in the equatorial pacific during 1993–99, *Journal of physical oceanography*, *31*(5), 1324–1345.

Merrifield, M. A. (2011), A shift in western tropical pacific sea level trends during the 1990s, *Journal of Climate*, *24*(15), 4126–4138.

Meyssignac, B., and A. Cazenave (2012), Sea level: a review of present-day and recent-past changes and variability, *Journal of Geodynamics*, *58*, 96–109.

Meyssignac, B., D. S. y Melia, M. Becker, W. Llovel, and A. Cazenave (2012), Tropical pacific spatial trend patterns in observed sea level: internal variability and/or anthropogenic signature?, *Climate of the Past*, *8*(2), 787.

Moon, B.-K., S.-W. Yeh, B. Dewitte, J.-G. Jhun, I.-S. Kang, and B. P. Kirtman (2004), Vertical structure variability in the equatorial pacific before and after the pacific climate shift of the 1970s, *Geophysical Research Letters*, *31*(3).

Neelin, J. D., D. S. Battisti, A. C. Hirst, F.-F. Jin, Y. Wakata, T. Yamagata, and S. E. Zebiak (1998), Enso theory, *Journal of Geophysical Research: Oceans*, *103*(C7), 14,261–14,290.

Philander, S. G. (1989), *El Niño, La Niña, and the Southern Oscillation*, 662 pp., Academic press, san diego, california.

Picaut, J., F. Masia, and Y. Du Penhoat (1997), An advective-reflective conceptual model for the oscillatory nature of the enso, *Science*, *277*(5326), 663–666.

Qiu, B., and S. Chen (2012), Multidecadal sea level and gyre circulation variability in the northwestern tropical pacific ocean, *Journal of Physical Oceanography*, *42*(1), 193–206.

Rebert, J.-P., J.-R. Donguy, G. Eldin, and K. Wyrtki (1985), Relations between sea level, thermocline depth, heat content, and dynamic height in the tropical pacific ocean, *Journal of Geophysical Research: Oceans*, *90*(C6), 11,719–11,725.

Rhein, M., S. Rintoul, S. Aoki, E. Campos, D. Chambers, R. Feely, S. Gulev, G. Johnson, S. Josey, A. Kostianoy, et al. (2013), Observations: Ocean. in: Climate change 2013: The physical science basis. contribution of working group i to the fifth assessment report of the intergovernmental panel on climate change, *Tech. rep.*, PM Cambridge University Press, Cambridge, United Kingdom and New York, NY, USA.

Roden, G. I. (1963), On sea level, temperature, and salinity variations in the central tropical pacific and on pacific ocean islands, *Journal of Geophysical Research*, *68*(2), 455–472.

Suarez, M. J., and P. S. Schopf (1988), A delayed action oscillator for enso, *Journal of the atmospheric Sciences*, *45*(21), 3283–3287.

Takahashi, K., A. Montecinos, K. Goubanova, and B. Dewitte (2011), Enso regimes: Reinterpreting the canonical and modoki el niño, *Geophysical Research Letters*, *38*(10).

Timmermann, A., S. McGregor, and F.-F. Jin (2010), Wind effects on past and future regional sea level trends in the southern indo-pacific*, *J. Clim.*, *23*(16), 4429–4437.

Trenberth, K. E. (1997), The definition of el nino, *Bulletin of the American Meteorological Society*, *78*(12), 2771–2777.

Trenberth, K. E., and D. P. Stepaniak (2001), Indices of el niño evolution, *Journal of Climate*, *14*(8), 1697–1701.

Trenberth, K. E., G. W. Branstator, D. Karoly, A. Kumar, N.-C. Lau, and C. Ropelewski (1998), Progress during toga in understanding and modeling global teleconnections associated with tropical sea surface temperatures, *Journal of Geophysical Research: Oceans*, *103*(C7), 14,291–14,324.

Uppala, S. M., P. Kållberg, A. Simmons, U. Andrae, V. Bechtold, M. Fiorino, J. Gibson, J. Haseler, A. Hernandez, G. Kelly, et al. (2005), The era-40 re-analysis, *Quarterly Journal of the Royal Meteorological Society*, *131*(612), 2961–3012.

Walker, G. T. (1923), Correlation in seasonal variations of weather, viii: A preliminary study of world weather, *Mem. Indian Meteor. Dept.*, *24*, 75–131.

Weisberg, R. H., and C. Wang (1997), A western pacific oscillator paradigm for the el niño-southern oscillation, *Geophysical research letters*, *24*(7), 779–782.

Wengel, C., M. Latif, W. Park, J. Harlaß, and T. Bayr (2017), Seasonal enso phase locking in the kiel climate model: The importance of the equatorial cold sea surface temperature bias, *Climate Dynamics*, pp. 1–19.

White, W., N. Graham, and C. Tai (1990), Reflection of annual rossby waves at the maritime western boundary of the tropical pacific, *J. Geophys. Res., to appear*.

Wright, P. B. (1977), *The Southern Oscillation-patterns and mechanisms of the teleconnections and the persistence*, vol. 77, Hawaii Institute of Geophysics, University of Hawaii.

Wyrtki, K. (1975), El niño—the dynamic response of the equatorial pacific oceanto atmospheric forcing, *Journal of Physical Oceanography*, *5*(4), 572–584.

Wyrtki, K. (1979), Sea level variations: Monitoring the breath of the pacific, *Eos, Transactions American Geophysical Union*, *60*(3), 25–27.

Wyrtki, K. (1985), Water displacements in the pacific and the genesis of el niño cycles, *Journal of Geophysical Research: Oceans*, *90*(C4), 7129–7132.

Yeh, S.-W., J.-S. Kug, B. Dewitte, M.-H. Kwon, B. P. Kirtman, and F.-F. Jin (2009), El niño in a changing climate, *Nature*, *461*(7263), 511–514.

Zebiak, S. E., and M. A. Cane (1987), A model el niñ–southern oscillation, *Monthly Weather Review*, *115*(10), 2262–2278.

Zhang, X., and J. A. Church (2012), Sea level trends, interannual and decadal variability in the pacific ocean, *Geophysical Research Letters*, *39*(21).

Own Publications

Zhu, X., R. J. Greatbatch, and M. Claus (2017), Interannual variability of tropical pacific sea level from 1993 to 2014, *Journal of Geophysical Research: Oceans*, *122*(1), 602–616.

Greatbatch, R. J., **X. Zhu**, and M. Claus (2018), Reconstructing tropical pacific sea level variability for the period 1961-2002 using a linear multi-mode model, *Journal of Geophysical Research: Oceans*, doi:10.1002/2017JC013652.

Zhu, X., R. J. Greatbatch, and M. Claus (2018), ENSO diversity and thermocline feedback for the period 1961-2014 assessed using a linear multi-mode model, *Climate Dynamics*, under review.

Acknowledgements

I would like to thank my supervisor Prof. Dr. Richard J. Greatbatch for the outstanding supervision during my PhD study. I have learnt from you not only how to do the scientific research but also how to be a nice person. Thank you for countless discussion and suggestions, insightful explanations for the results, support for my ideas and endeavors in improving my writing! Thank you for being responsible, patient and humorous all the time. By these, you walk me into the wonderful world of science. Thank you also for initiating many social activities such as the party at your house, annual trip to Lübecker and meeting in Wubbke.

I also want to thank Prof. Dr. Martin Claus for the impressive input to this work. Every time discuss (talk) with you about scientific questions (general view of science) I feel inspired. Also thank you for the shallow water model!

Thanks to the computing centers at both GEOMAR and University of Kiel for the numerical experiments, softwares for data analysis and plotting and technical support. Also thanks to Willi for the introduction of useful softwares as well as technical support.

I appreciate a lot the kind and cooperative working atmosphere at GEOMAR, particularly the Department of Theory and Modeling. Thank you Sabine and Nikole for kind assistance throughout my stay at GEOMAR. Special thanks go to Gereon, Tina, Annika (R), Annika (D) and Christian for not only being good friends but also the discussion on the scientific problems.

Thank you Sandra and Sibylle for inviting me to your homes for Christmas holidays which were very wonderful and impressive. Thank you Diyu and Xinyu for being faithful friends all the time. Thank you Feifei, Yaping, Xuewei, Zhaoyang, Qingyang, Xiangxin, Guokun, Eike, Rafael, Mirriam, Bernhard, Bettina, Yanyan, Di, Shi etc. for being warm and kind friends.

In the end, I would like to thank my families who are always behind me. Thank you mom and dad for your hard working, teaching me and understanding me because you care about me the most. Thank you Xiaoyan for being generous, simple, kind and thus making me tender. Thank you others for being a mirror which makes me realize my flaws. Thank you little nieces Yizhi and Huilin for bringing endless happiness to me and bringing out the huge potential positive energy inside of me.

Declaration of Independence

I hereby declare in lieu of oath that, apart from the guidance of my supervisor Prof. Dr. Richard J. Greatbatch, the thesis is completed by myself without any other external assistance and does not include the content from other sources without specifying them. This work has not been submitted, either partially or wholly as part of a doctoral degree, to any other examining board. It was created in compliance with the Rules of Good Scientific Practice of the German Research Foundation.

Kiel, March 2018